Use of thermoplastic starch in poly(lactic acid)/poly(butylene adipate-co-terephthalate) based nanocomposites for bio-based food packaging

by

Pavan Harshit Manepalli

B.Tech, Indian Institute of Technology, Kharagpur, 2012

M.S., Kansas State University, 2014

AN ABSTRACT OF A DISSERTATION

submitted in partial fulfillment of the requirements for the degree

DOCTOR OF PHILOSOPHY

Department of Grain Science and Industry
College of Agriculture

KANSAS STATE UNIVERSITY
Manhattan, Kansas

2019

Abstract

Poly(lactic acid) (PLA) is the most common bio-based & compostable polymer available commercially that is cost competitive and combines a range of desirable properties like melt processability, high strength and modulus. The films made from this aliphatic polyester tend to be brittle which can be overcome by blending PLA with another bio-based polymer with high flexibility poly(butylene adipate-co-terephthalate) (PBAT), but the resultant blend is only biodegradable in composting conditions. The primary focus of this study was incorporation of thermoplastic starch (TPS) in PLA/PBAT blends to increase the rate of biodegradability and decrease the cost. In the first part of this study, as a preliminary step only PLA/PBAT blends were investigated along with nanofiller nanocrystalline cellulose (NCC) as a nanofiller for enhancing mechanical and barrier properties. Melt extrusion was used for preparation of nanocomposites and 200 microns thick films were formed by melt pressing. PBAT enhanced elongation but NCC did not have any positive impact on the mechanical and barrier properties of the nanocomposites as NCC was aggregated in the polymer matrix due to the difference in polarity based on the hydrophilic nature of the nanofiller and hydrophobic nature of the polymer matrix.

In the second part of study, up to 40%TPS was blended along with the PLA/PBAT/NCC nanocomposites. Joncryl (0.5%) was used as a compatibilizer. TPS addition decreased the mechanical and barrier properties (Tensile strength (TS) = 15- 30 MPa, Elongation at break (EB) = 6-12%, Water vapor permeability (WVP) = 1.6-8.3 g.mm/kPa.h.m^2), although addition of NCC helped in increasing the TS and decreasing the WVP. Dispersion of NCC improved with the addition of hydrophilic TPS. Analytical techniques including transmission electron microscopy,

fourier-transform infrared spectroscopy, differential scanning calorimetry were used to study the polymer-polymer and polymer-nanofiller interactions.

Optimization study of PLA/PBAT/TPS/NCC nanocomposites was done using mixture response surface methods. Quadratic models with good predicted R^2 (between 84.3% and 97.59%) were developed for all the responses. Optimization study was done that could yield films with optimum properties comparable to commercial plastics and maximizing the level of TPS. Films with optimum properties (TS = 29.5 MPa, EB = 12%, WVP = 1.99 g.mm/kPa.h.m^2) were predicted at levels of 64.3% PLA, 14.5% PBAT, 18% TPS and 2.6% NCC along with 0.5% Joncryl. The improved mechanical and barrier performance suggested that PLA/PBAT/TPS/NCC nanocomposites have potential use in food packaging applications.

In the final phase of study, mathematical modeling was used to understand the influence of nanofiller (NCC) on the mechanical and barrier properties of the nanocomposites. The modified Halpin-Tsai equation was used to model the elastic modulus of the nanocomposites, while the modified Nielsen equation was used to model the WVP as a function of nanofiller content, geometry, strength and interactions with polymer matrix. The experimental results in both cases were close to the theoretical predictions by the models. The models predicted an increase in mechanical and barrier properties with increase in aspect ratio and surface interactions of nanofiller with polymer matrix.

Use of thermoplastic starch in poly(lactic acid)/poly(butylene adipate-co-terephthalate) based nanocomposites for bio-based food packaging

by

Pavan Harshit Manepalli

B.Tech, Indian Institute of Technology, Kharagpur, 2012

M.S., Kansas State University, 2014

A DISSERTATION

submitted in partial fulfillment of the requirements for the degree

DOCTOR OF PHILOSOPHY

Department of Grain Science and Industry
College of Agriculture

KANSAS STATE UNIVERSITY
Manhattan, Kansas

2019

Approved by:
Major Professor
Dr. Sajid Alavi

Abstract

Poly(lactic acid) (PLA) is the most common bio-based & compostable polymer available commercially that is cost competitive and combines a range of desirable properties like melt processability, high strength and modulus. The films made from this aliphatic polyester tend to be brittle which can be overcome by blending PLA with another bio-based polymer with high flexibility poly(butylene adipate-co-terephthalate) (PBAT), but the resultant blend is only biodegradable in composting conditions. The primary focus of this study was incorporation of thermoplastic starch (TPS) in PLA/PBAT blends to increase the rate of biodegradability and decrease the cost. In the first part of this study, as a preliminary step only PLA/PBAT blends were investigated along with nanofiller nanocrystalline cellulose (NCC) as a nanofiller for enhancing mechanical and barrier properties. Melt extrusion was used for preparation of nanocomposites and 200 microns thick films were formed by melt pressing. PBAT enhanced elongation but NCC did not have any positive impact on the mechanical and barrier properties of the nanocomposites as NCC was aggregated in the polymer matrix due to the difference in polarity based on the hydrophilic nature of the nanofiller and hydrophobic nature of the polymer matrix.

In the second part of study, up to 40%TPS was blended along with the PLA/PBAT/NCC nanocomposites. Joncryl (0.5%) was used as a compatibilizer. TPS addition decreased the mechanical and barrier properties (Tensile strength (TS) = 15- 30 MPa, Elongation at break (EB) = 6-12%, Water vapor permeability (WVP) = 1.6-8.3 g.mm/kPa.h.m^2), although addition of NCC helped in increasing the TS and decreasing the WVP. Dispersion of NCC improved with the addition of hydrophilic TPS. Analytical techniques including transmission electron microscopy,

fourier-transform infrared spectroscopy, differential scanning calorimetry were used to study the polymer-polymer and polymer-nanofiller interactions.

Optimization study of PLA/PBAT/TPS/NCC nanocomposites was done using mixture response surface methods. Quadratic models with good predicted R^2 (between 84.3% and 97.59%) were developed for all the responses. Optimization study was done that could yield films with optimum properties comparable to commercial plastics and maximizing the level of TPS. Films with optimum properties (TS = 29.5 MPa, EB = 12%, WVP = 1.99 g.mm/kPa.h.m^2) were predicted at levels of 64.3% PLA, 14.5% PBAT, 18% TPS and 2.6% NCC along with 0.5% Joncryl. The improved mechanical and barrier performance suggested that PLA/PBAT/TPS/NCC nanocomposites have potential use in food packaging applications.

In the final phase of study, mathematical modeling was used to understand the influence of nanofiller (NCC) on the mechanical and barrier properties of the nanocomposites. The modified Halpin-Tsai equation was used to model the elastic modulus of the nanocomposites, while the modified Nielsen equation was used to model the WVP as a function of nanofiller content, geometry, strength and interactions with polymer matrix. The experimental results in both cases were close to the theoretical predictions by the models. The models predicted an increase in mechanical and barrier properties with increase in aspect ratio and surface interactions of nanofiller with polymer matrix.

Table of Contents

List of Figures

List of Tables

Acknowledgements

I am very grateful to Dr. Sajid Alavi for giving me this opportunity for pursuing Ph.D. at Kansas State University. He has been my mentor and his motivation and guidance has boosted my thirst for knowledge. I am very much influenced by his scientific knowledge and dedication.

I would like to thank Dr. Xiuzhi Sun for providing support whenever I ask for any help and providing ideas that set directions of focus throughout my project. I am very thankful to Dr. Sri Narayan-Sarathy and Dr. Yong-Cheng Shi for their valuable suggestions and insightful comments. I am grateful for their encouragement which helped me in achieving my research goals. I would also like to thank Dr. Christopher M. Sorensen for giving me an opportunity to work with him and learn fundamentals of graphene which was very useful for my grant writing experience.

I would like to express my deep gratitude to my co-workers in our group especially Michael Joseph and Eric Maichel for their support and guidance during my research.

I would also like to thank my friends – Bharath, Kaushik, Anirudh, Ankith, Prudhvi, Aditya, Karthik, Swathi, Soumya, Apoorva, Tejitha, Tarangini, Priyanka, Kali, Anisha, Swapna, Deepthi, Sagar, Sekhar, Navya, Sravya, Sowmya, Shravan, Vyas, Nikitha, Anamika, Poojitha, Sneha, Sharmila, Pruthvi, Raja, Sudesh, Rahul, Sindhu, Teju, Nithin, Sravani for their love and encouragement without which nothing could have been possible.

Dedication

This thesis is dedicated to my parents, Muralidhar and Lakshmi Manepalli and my brother, Raja Manepalli for their endless support, love and encouragement. I am eternally grateful for everything they taught me.

Chapter 1 - Introduction

1.1 Food packaging

The major role of food packaging is to prevent the spoilage of food through external influences – chemical (moisture, gases, light), biological (microorganisms), physical (mechanical damage) (Marsh & Bugusu, 2007). Packaging is essential to provide effective distribution, storage efficiency and preservation of food (Mihindukulasuriya & Lim, 2014). It should satisfy the requirements of the industry and the consumers (product characteristics, marketing and environmental issues) in a cost-effective way. The use of petroleum-based plastics in food packaging is widely increasing due to the low cost and desirable mechanical and barrier properties of the material (Marsh & Bugusu, 2007).

However, petroleum-based plastic packaging also has some disadvantages as it contributes to waste disposal problems and environmental toxicity. These petroleum-based resources are also non-renewable. In 2013, 78 million metric tons of plastic packaging was produced around the world (The New Plastics Economy, 2016). Only 14% of the plastic packaging is collected for recycling and then reuse. The rest of the plastic packaging which are not recycled cause a serious ecological problem and gets ended up in landfill and ocean at some point. By 2050, the weight of plastic could be more than fish in the ocean based on the current trend of increasing usage of plastic.

1.2 Bio-based plastics

Renewable and bio-based plastics can be used to replace non-renewable petroleum-based resources. The term “Bio-based plastics” refers to the plastics made from renewable resources. Currently, bioplastic packaging production is about 1.6 million metric tons in 2015 and is

expected to grow to 6.1 million metric tons by 2020 (Global markets and technologies for bioplastics, 2016). Among the bioplastics, poly(lactic acid) (PLA) is a promising material and one of the widely growing sector in the market of bioplastics in 2016 (Global bioplastics market, 2017). PLA is an aliphatic thermoplastic polyester with a range of desirable properties including biodegradability in composting conditions, cost competitiveness with petroleum-based plastics, melt process ability, high strength and high modulus (Wacharawichanant et al., 2017).

Table 1.1 Properties of polymers

Material	Cost[a]	WVP[b]	Tensile strength[c]	Elongation at break[d]	Reference
PET	Moderate	Good	Good	Good	Auras et al., 2005
PP	Moderate	Good	Moderate	Good	Ismail, 2002
PE	Moderate	Moderate	Moderate	Good	Zhong et al., 2007
PS	High	Moderate	Moderate	Poor	Nair et al., 1996
PVC	Moderate	Good	Good	Good	Zheng et al., 2007
PA	High	Moderate	Good	Good	Yang et al., 1998
PVDC	Moderate	Good	Good	Moderate	Shiku et al., 2004
PLA	Moderate	Moderate	Good	Poor	Oksman et al., 2003

[a]Cost	[b]Test conditions:23^{o}C, 85% RH	[c]Tensile strength	[d]Elongation at break
Low: <5$/kg	Poor: 10-100 g*mm/m^2*day*kPa	Poor: <10 MPa	Poor: <10%
Moderate: 5-10$/kg	Moderate: 1-10 g*mm/m^2*day*kPa	Moderate: 10-50 MPa	Moderate: 10-50%
High: >10$/kg	Good: 0.1-1 g*mm/m^2*day*kPa	Good: >50 MPa	Good: >50%

PET=Poly(ethylene terephthalate), PP=Polypropylene, PE= Polyethylene, PS=Polystyrene, PVC=Poly(vinyl chloride), PA=polyamide, PVDC=Poly(vinylidene chloride)

The ideal food packaging material should have important characteristics, which includes good mechanical properties such as tensile strength and % elongation at break, along with low barrier properties such as water vapor permeability. The properties of some of the polymers

commonly used in packaging is shown in Table 1.1 (Krochta & De-Mulder-Johnston, 1997; Lange & Wyser, 2003). Polymers such as PET and PVC display good mechanical and barrier properties as can be seen from Table 1. However, these polymers have poor biodegradability and cause environmental concern. Compared to these polymers, PLA is biodegradable in composting conditions. However, PLA based films are brittle (low % elongation at break).

To improve the elongation of PLA, it can be blended with other flexible polymers such as poly (caprolactone) (PCL), poly (butylene succinate) (PBS), poly (butylene adipate-co-terephthalate) (PBAT) (Kumar et al., 2010; Wang et al., 1998; Zhao et al., 2010). PBAT, a fully biodegradable aliphatic-aromatic copolyester is a good candidate to decrease the brittleness of PLA and is selected in our study. Due to high cost of polymers of PLA and PBAT, it can be blended with starch to make it cost-effective. Starch is a widely available and naturally occurring biodegradable polymer and hence can be considered as an economically viable alternative (Ayana et al., 2014).

The melting temperature of native starch (T_m = 220–250^o C) is high and is close to its degradation temperature (~220^o C) (Ayana et al., 2014). Plasticizers can be used to decrease the melting temperature of starch as they form a hydrogen bond with the starch (i.e. amylose) molecules and decrease the inter-molecular hydrogen bonding sites in the crystalline parts of starch. Hence, native starch can be converted into thermoplastic starch (TPS) using thermo-mechanical treatment in the presence of plasticizers such as water, glycerol, sorbitol etc. (Wiedmann & Strobel, 1991). Addition of TPS also increases the rate of biodegradation of PLA in all conditions (Akrami et al., 2016; Iovino et al., 2008) as the various microorganisms can easily use starch as an energy source. However, TPS based packaging have some limitations due

to its high hydrophilic nature and weak mechanical properties (Babaee et al., 2015; Rico et al., 2016; Teixeira et al., 2009).

As it can be seen, the use of above methods is clearly not enough to improve the mechanical and barrier properties of the bio-based packaging. Hence, the need to explore innovative techniques to meet the challenges of developing high quality bioplastic films for food packaging is significant.

1.3 Use of nanofillers in food packaging

One of the promising and innovative methods is the use of nanofillers to improve the mechanical properties of bioplastics (Fortunati et al., 2012). The materials that contain components with at least one dimension less than 100 nm are referred to as nanofillers (Duncan, 2011). The properties of the materials vary a lot at nanoscale level when compared to the properties of the same material at macroscale. The use of nanofillers in reinforcing the polymers are referred to as polymer nanocomposites. The use of polymer nanocomposites was first implemented by Toyota researchers in 1986 (Kawasumi, 2004). The incorporation of nanofillers into various natural and synthetic polymers such as polystyrene, polyamide, poly(ethylene terephthalate, poly(lactic acid), poly(vinyl chloride), thermoplastic starch etc. were widely reported over the past 30 years (Joon Choi et al., 2006; Nazarenko et al., 2007; Park et al., 2003; Pereira et al., 2009; Ray et al., 2003; Sanchez-Garcia et al., 2007; Thellen et al., 2005).

The interaction between the polymer and nanofiller is influenced by chemistry of the nanofiller as it contributes to the enthalpic interaction of the nanofiller with the chains of polymer. These interactions can either be van der Waals interactions between the filler and polymer chains or specific interactions such as covalent bonds. The morphology of the

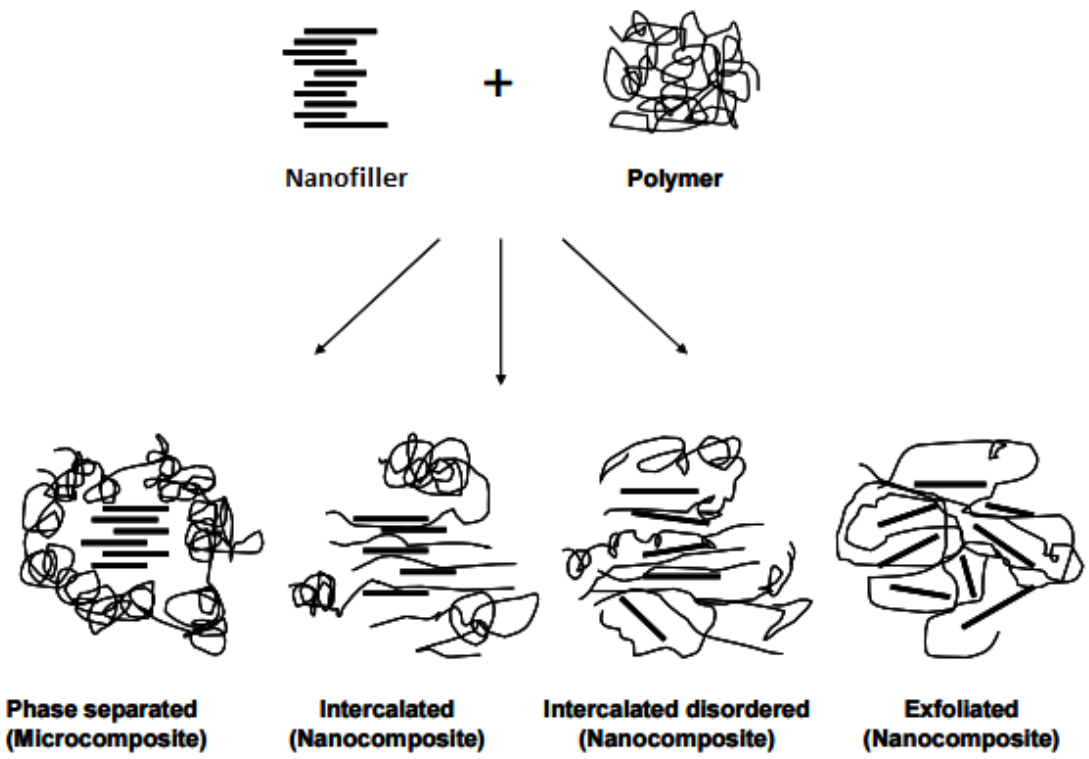

Figure 1.1 Schematic representation of possible nanocomposite structures (Tang, 2008)

nanocomposites is strongly influenced by the strength of these interactions. The interactions between the fillers become significant at high fraction of fillers in the nanocomposites and in the strength of the filler aggregates. The domains rich in nanofillers and poor in polymers can be formed where nanofillers form a separate phase. The filler aggregate will behave as a large filler particle instead of individual nanofillers if the interactions between the nanofillers are high. Hence, polymer-nanofiller interactions produce various kinds of structures ranging from intercalated to exfoliated structures (Figure 1.1).

In exfoliated structures, the nanofillers are dispersed homogeneously in the polymer matrix. In intercalated structures, the filler aggregates are dispersed throughout the matrix and a small amount of polymer penetrates the layers of nanofillers. Intercalated and exfoliated structures are only formed if the polymers and nanofillers are miscible. If they are immiscible,

nanofillers exist as agglomerates or tactoids (Tang, 2008). The nanofillers also have a high surface area which is useful for interfacial interactions with the polymer matrix. The complete dispersion of nanofillers in the polymer matrix facilitate the increased number of reinforcing elements available for the carrying the applied stress and deflecting cracks which indirectly leads to increase in mechanical properties.

The nanofillers used in this study are nanocrystalline cellulose (NCC) and graphene. NCC has various properties such as durability and high biodegradability (Brinchi et al., 2013). The structure of NCC is generally rod-shaped of about 5-10 nm in width and 100-200 nm in length (Fortunati et al., 2012). They have a very high aspect ratio (length/diameter) and a large surface area (Matos Ruiz et al., 2000). NCC have a very high tendency to form strong hydrogen bonds within themselves due to high amount of hydroxyl groups on the surface (Favier et al., 1995).

The complete dispersion of the nanofillers in the polymer matrix also helps in increasing the barrier properties of the nanocomposites as the diffusion pathway of the permeant (water vapor, gas etc.) through the nanocomposites is hindered and it must traverse a tortuous pathway

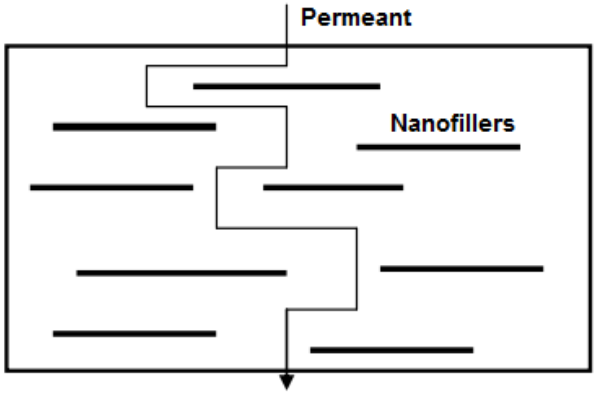

Figure 1.2 Schematic representation of a tortuous pathway of permeant in the nanocomposites (Yano et al., 1993)

thereby increasing the effective length of diffusion (Figure 1.2), which indirectly contributes to higher shelf life of the food. The gas permeability can be reduced by even 500 times at low levels of nanofillers in ideal conditions (Choudalakis & Gotsis, 2009). The degree of reduction is greatly dependent on the geometrical characteristics of the nanofillers i.e. shape, aspect ratio (length to thickness ratio), orientation of nanofiller in polymer nanocomposites etc. Hence, there have been several attempts to estimate the properties of the nanocomposites using mathematical models and compare them to the experimental results (Alavi et al., 2014; DeRocher et al., 2005; Picard et al., 2007; Swannack et al., 2005; Takahashi et al., 2006).

1.4 Objectives

The overall objective of this study is to develop a fundamental understanding of interactions between various components such as synthetic polymers (PLA, PBAT), natural polymer (corn starch), and nanofiller (NCC) and use these materials to develop biodegradable packaging films with enhanced mechanical and barrier properties for commercial production and application.

Chapter 2 deals with the synthesis of polymer-based nanocomposites using melt extrusion and study the fundamental interactions between polymers PLA, PBAT and nanofiller NCC. Mechanical, barrier, morphological, rheological and thermal properties of the nanocomposites were characterized using Instron, water vapor permeability (WVP), capillary rheometer, x-ray diffraction (XRD), transmission electron microscope (TEM), differential scanning calorimetry (DSC) and fourier-transform infrared spectroscopy (FTIR).

Chapter 3 studies the effect of incorporation of starch into PLA/PBAT blends, synthesize multi-component nanocomposites from polymer-starch-nanofiller blends and study the effect on dispersion of NCC due to addition of hydrophilic starch.

Chapter 4 deals with the optimization of PLA/PBAT/TPS/NCC nanocomposites using mixture response surface methods and investigate the effect of levels of the components on the film mechanical properties such as tensile strength and elongation at break and barrier properties such as water vapor permeability. These models can help in indirectly quantifying the properties of the films.

Chapter 5 presents the use of mathematical modeling in understanding the effect of NCC on the mechanical and barrier properties of the polymer matrix and providing direction for future research in studying the influence of more effective fillers.

Chapter 6 provides a summary of the conclusions and future work.

1.5 References

Akrami, M., Ghasemi, I., Azizi, H., Karrabi, M., & Seyedabadi, M. (2016). A new approach in compatibilization of the poly (lactic acid)/thermoplastic starch (PLA/TPS) blends. Carbohydrate polymers, 144, 254-262.

Alavi, S., Thomas, S., Sandeep, K. P., Kalarikkal, N., Varghese, J., & Yaragalla, S. (Eds.). (2014). Polymers for packaging applications. CRC Press.

Auras, R. A., Singh, S. P., & Singh, J. J. (2005). Evaluation of oriented poly (lactide) polymers vs. existing PET and oriented PS for fresh food service containers. Packaging technology and science, 18(4), 207-216.

Ayana, B., Suin, S., & Khatua, B. B. (2014). Highly exfoliated eco-friendly thermoplastic starch (TPS)/poly (lactic acid)(PLA)/clay nanocomposites using unmodified nanoclay. Carbohydrate polymers, 110, 430-439.

Babaee, M., Jonoobi, M., Hamzeh, Y., & Ashori, A. (2015). Biodegradability and mechanical properties of reinforced starch nanocomposites using cellulose nanofibers. Carbohydrate polymers, 132, 1-8.

Brinchi, L., Cotana, F., Fortunati, E., & Kenny, J. M. (2013). Production of nanocrystalline cellulose from lignocellulosic biomass: Technology and applications. Carbohydrate Polymers, 94(1), 154–169.

Choudalakis, G. & Gotsis, A. D. (2009). Permeability of polymer/clay nanocomposites: a review. European Polymer Journal, 45(4), 967-984.

DeRocher, J. P., Gettelfinger, B. T., Wang, J., Nuxoll, E. E., & Cussler, E. L. (2005). Barrier membranes with different sizes of aligned flakes. Journal of membrane science, 254(1-2), 21-30.

Duncan, T. V. (2011). Applications of nanotechnology in food packaging and food safety: barrier materials, antimicrobials and sensors. Journal of colloid and interface science, 363(1), 1-24.

Favier V., Chanzy H. & Cavaille J.Y. (1995). Polymer nanocomposites reinforced by cellulose whiskers. Macromolecules, 28(18), 6365–6367.

Fortunati, E., Armentano, I., Zhou, Q., Iannoni, A., Saino, E., Visai, L., Berglund, L. A., & Kenny, J. M. (2012). Multifunctional bionanocomposite films of poly(lactic acid),cellulose nanocrystals and silver nanoparticles. Carbohydrate Polymers, 87(2), 1596–1605.

Global bio plastics market to be driven by demand from packaging in North America, 2017. Retrieved from: http://www.plastemart.com/plastic-technical-articles/global-bio-plastics-market-to-be-driven-by-demand-from-packaging-in-north-america/2350

Global Markets and Technologies for Bioplastics, 2016. Retrieved from: https://www.bccresearch.com/market-research/plastics/bioplastics-technologies-markets-report-pls050d.html

Iovino, R., Zullo, R., Rao, M. A., Cassar, L., & Gianfreda, L. (2008). Biodegradation of poly (lactic acid)/starch/coir biocomposites under controlled composting conditions. Polymer Degradation and Stability, 93(1), 147-157.

Ismail, H. (2002). Thermoplastic elastomers based on polypropylene/natural rubber and polypropylene/recycle rubber blends. Polymer Testing, 21(4), 389-395.

Joon Choi, W., Kim, H. J., Han Yoon, K., Hyeong Kwon, O., & Ik Hwang, C. (2006). Preparation and barrier property of poly (ethylene terephthalate)/clay nanocomposite using clay-supported catalyst. Journal of Applied Polymer Science, 100(6), 4875-4879.

Kawasumi, M. (2004). The discovery of polymer-clay hybrids. Journal of Polymer Science Part A: Polymer Chemistry, 42(4), 819-824.

Krochta, J.M., and De Mulder-Johnston, C., 1997. Edible and biodegradable polymer films: challenges and opportunities. Food Technology. 51(2): 61-74.

Kumar, M., Mohanty, S., Nayak, S. K., & Parvaiz, M. R. (2010). Effect of glycidyl methacrylate (GMA) on the thermal, mechanical and morphological property of biodegradable PLA/PBAT blend and its nanocomposites. Bioresource technology, 101(21), 8406-8415.

Lange, J., & Wyser, Y. (2003). Recent innovations in barrier technologies for plastic packaging - a review. Packaging Technology and Science, 16(4), 149-158.

Marsh, K. & Bugusu, B. (2007). Food packaging - Roles, materials, and environmental issues. Journal of Food Science, 72(3), R39-R55.

Matos Ruiz, M., Cavaille, J. Y., Dufresne, A., Gerard, J. F. & Graillat, C. (2000). Processing and characterization of new thermoset nanocomposites based on cellulose whiskers. Composite Interfaces, 7(2), 117-131.

Mihindukulasuriya, S.D.F. & Lim, L.T. (2014). Nanotechnology development in food packaging: A review. Trends in Food Science & Technology, 40(2), 149-167.

Müller, R. J. (2005). Biodegradability of polymers: regulations and methods for testing. Biopolymers Online.

Nair, K. C., Diwan, S. M., & Thomas, S. (1996). Tensile properties of short sisal fiber reinforced polystyrene composites. Journal of applied polymer science, 60(9), 1483-1497.

Nazarenko, S., Meneghetti, P., Julmon, P., Olson, B. G., & Qutubuddin, S. (2007). Gas barrier of polystyrene montmorillonite clay nanocomposites: effect of mineral layer aggregation. Journal of Polymer Science Part B: Polymer Physics, 45(13), 1733-1753.

Oksman, K., Skrifvars, M., & Selin, J. F. (2003). Natural fibres as reinforcement in polylactic acid (PLA) composites. Composites science and technology, 63(9), 1317-1324.

Park, H. M., Lee, W. K., Park, C. Y., Cho, W. J., & Ha, C. S. (2003). Environmentally friendly polymer hybrids Part I Mechanical, thermal, and barrier properties of thermoplastic starch/clay nanocomposites. Journal of Materials Science, 38(5), 909-915.

Picard, E., Vermogen, A., Gérard, J. F., & Espuche, E. (2007). Barrier properties of nylon 6-montmorillonite nanocomposite membranes prepared by melt blending: influence of the clay content and dispersion state: consequences on modelling. Journal of Membrane Science, 292(1-2), 133-144.

Pereira, D., Losada, P. P., Angulo, I., Greaves, W., & Cruz, J. M. (2009). Development of a polyamide nanocomposite for food industry: morphological structure, processing, and properties. Polymer Composites, 30(4), 436-444.

Ray, S. S., Yamada, K., Okamoto, M., Fujimoto, Y., Ogami, A., & Ueda, K. (2003). New polylactide/layered silicate nanocomposites. 5. Designing of materials with desired properties. Polymer, 44(21), 6633-6646.

Rico, M., Rodríguez-Llamazares, S., Barral, L., Bouza, R., & Montero, B. (2016). Processing and characterization of polyols plasticized-starch reinforced with microcrystalline cellulose. Carbohydrate polymers, 149, 83-93.

Sanchez-Garcia, M. D., Gimenez, E., & Lagaron, J. M. (2007). Novel PET nanocomposites of interest in food packaging applications and comparative barrier performance with biopolyester nanocomposites. Journal of Plastic Film & Sheeting, 23(2), 133-148.

Shiku, Y., Hamaguchi, P. Y., Benjakul, S., Visessanguan, W., & Tanaka, M. (2004). Effect of surimi quality on properties of edible films based on Alaska pollack. Food Chemistry, 86(4), 493-499.

Swannack, C., Cox, C., Liakos, A., & Hirt, D. (2005). A three-dimensional simulation of barrier properties of nanocomposite films. Journal of membrane science, 263(1-2), 47-56.

Takahashi, S., Goldberg, H. A., Feeney, C. A., Karim, D. P., Farrell, M., O'leary, K., & Paul, D. R. (2006). Gas barrier properties of butyl rubber/vermiculite nanocomposite coatings. Polymer, 47(9), 3083-3093.

Tang, X. (2008). Use of extrusion for synthesis of starch-clay nanocomposites for biodegradable packaging films. Ph.D. Thesis, Kansas State University, Manhattan, USA.

Teixeira, E. D. M., Pasquini, D., Curvelo, A. A., Corradini, E., Belgacem, M. N. & Dufresne, A. (2009). Cassava bagasse cellulose nanofibrils reinforced thermo-plastic cassava starch. Carbohydrate Polymers, 78(3), 422–431.

Thellen, C., Orroth, C., Froio, D., Ziegler, D., Lucciarini, J., Farrell, R., & Ratto, J. A. (2005). Influence of montmorillonite layered silicate on plasticized poly (l-lactide) blown films. Polymer, 46(25), 11716-11727.

The New Plastics Economy: Rethinking the Future of Plastics. Retrieved from https://www.ellenmacarthurfoundation.org/publications/the-new-plastics-economy-rethinking-the-future-of-plastics (Ellen MacArthur Foundation, 2016).

Wacharawichanant, S., Ratchawong, S., Hoysang, P., & Phankokkruad, M. (2017). Morphology and Properties of Poly (Lactic Acid) and Ethylene-Methyl Acrylate Copolymer Blends with Organoclay. In MATEC Web of Conferences (Vol. 130, p. 07006). EDP Sciences.

Wang, L., Ma, W., Gross, R. A., & McCarthy, S. P. (1998). Reactive compatibilization of biodegradable blends of poly (lactic acid) and poly (ε-caprolactone). Polymer Degradation and Stability, 59(1-3), 161-168.

Wiedmann, W., & Strobel, E. (1991). Compounding of thermoplastic starch with twin-screw extruders. Starch - Stärke, 43(4), 138–145.

Yang, F., Ou, Y., & Yu, Z. (1998). Polyamide 6/silica nanocomposites prepared by in situ polymerization. Journal of Applied Polymer Science, 69(2), 355-361.

Yano, K., Usuki, A., Okada, A., Kurauchi, T., & Kamigaito, O. (1993). Synthesis and properties of polyimide–clay hybrid. Journal of Polymer Science Part A: Polymer Chemistry, 31(10), 2493-2498.

Zhao, P., Liu, W., Wu, Q., & Ren, J. (2010). Preparation, mechanical, and thermal properties of biodegradable polyesters/poly (lactic acid) blends. Journal of Nanomaterials, 2010, 4.

Zheng, Y. T., Cao, D. R., Wang, D. S., & Chen, J. J. (2007). Study on the interface modification of bagasse fibre and the mechanical properties of its composite with PVC. Composites part A: applied science and manufacturing, 38(1), 20-25.

Zhong, Y., Janes, D., Zheng, Y., Hetzer, M., & De Kee, D. (2007). Mechanical and oxygen barrier properties of organoclay-polyethylene nanocomposite films. Polymer Engineering & Science, 47(7), 1101-1107.

Chapter 2 - Bio-based poly(lactic acid)/ poly(butylene adipate-co-terephthalate) based nanocomposites for food packaging

Abstract

Poly(lactic acid) (PLA) is the most common bio-based & compostable polymer available commercially that is cost competitive and combines a range of desirable properties like melt processability, high strength and modulus. The films made from this aliphatic polyester tend to be brittle which can be overcome by blending PLA with another biodegradable polymer with high flexibility poly(butylene adipate-co-terephthalate) (PBAT) and nanofiller nanocrystalline cellulose (NCC). Glycidyl methacrylate (GMA) was used as a compatibilizer to improve the interfacial adhesion between PLA and PBAT. Up to 20% PBAT, 5% GMA and 4% NCC was blended with PLA using twin screw melt extrusion process before being pressed into 200 microns thick films. Mechanical, barrier, rheological, morphological and thermal properties of the films were characterized using instron, water vapor permeability (WVP), capillary rheometer, x-ray diffraction (XRD), fourier-transform infrared spectroscopy (FTIR), transmission electron microscope (TEM) and differential scanning calorimetry (DSC). Rheological study showed that PBAT and NCC addition increased the shear viscosity of PLA. DSC and XRD studies showed the increase in crystallinity with addition of NCC. Addition of PBAT along with GMA improved PLA film's elongation at break from 6.3 to 24.2% with a trade-off tensile strength reduction from 51.2 to 35.8 MPa, but NCC did not have any positive impact on the mechanical and barrier properties of the nanocomposites as NCC was aggregated in the polymer matrix due to the difference in polarity based on the hydrophilic nature of the nanofiller and hydrophobic nature of the polymer matrix.

2.1 Introduction

Food packaging prevents the spoilage of food through external influences – chemical (moisture, gases, light), biological (microorganisms), physical (mechanical damage) (Marsh & Bugusu, 2007). It is also essential to provide effective distribution, storage efficiency and preservation of food (Mihindukulasuriya & Lim, 2014), while satisfying the requirements of the industry and the consumers (product characteristics, marketing and environmental issues) in a cost-effective way. The use of petroleum-based plastics in food packaging is widely increasing due to the low cost and desirable mechanical and barrier properties of the material (Marsh & Bugusu, 2007).

However, petroleum-based plastic packaging also has some disadvantages as it contributes to environmental toxicity and waste disposal problems. These petroleum-based resources are also non-renewable. Renewable and bio-based plastics can be used to replace non-renewable petroleum-based resources. Among the bioplastics, poly(lactic acid) (PLA) is a promising material and one of the widely growing sector in the market of bioplastics in 2016 (Global bioplastics market, 2017). PLA is an aliphatic thermoplastic polyester with a range of desirable properties including biodegradability in composting conditions, high strength and high modulus (Wacharawichanant et al., 2017). The cost of PLA is also comparable to that of conventional polyolefin polymers. However, PLA based films are brittle i.e. low % elongation at break. To improve the elongation of PLA, it can be blended with other flexible polymers such as poly (caprolactone) (PCL), poly (butylene succinate) (PBS), poly (butylene adipate-co-terephthalate) (PBAT) (Kumar et al., 2010; Wang et al., 1998; Zhao et al., 2010). PBAT, a fully biodegradable aliphatic-aromatic copolyester is a good candidate to decrease the brittleness of PLA and is selected in our study. The properties of the PLA/PBAT blend depends on the

interfacial adhesion between the polymers. There have been many studies to improve the interfacial adhesion between PLA and PBAT (Kumar et al., 2010; Arruda et al., 2015; Jiang et al., 2006; Al-Itry et al., 2012). Kumar et al., 2010 used glycidyl methacrylate (GMA) as a reactive compatibilizer to improve the miscibility between PLA and PBAT. GMA is an epoxy compound which can react with carboxyl group of PLA and PBAT thereby increasing the interfacial adhesion between the polymers and enhance the properties of the blends. Figure 2.1 shows the predicted reaction between PLA, PBAT and GMA. The increase in elongation at break obtained in their study for PLA/PBAT/GMA blends is surprisingly very low (6.5%) compared to that of the virgin PLA (4.5%). They used melt blending technique in a batch mixer to prepare the blends. Reactive extrusion i.e. high heat and high shear conditions in extrusion can lead to better reaction of the epoxy groups with the polymers. Hence, twin-screw extrusion was used for melt blending of the polymers in our study.

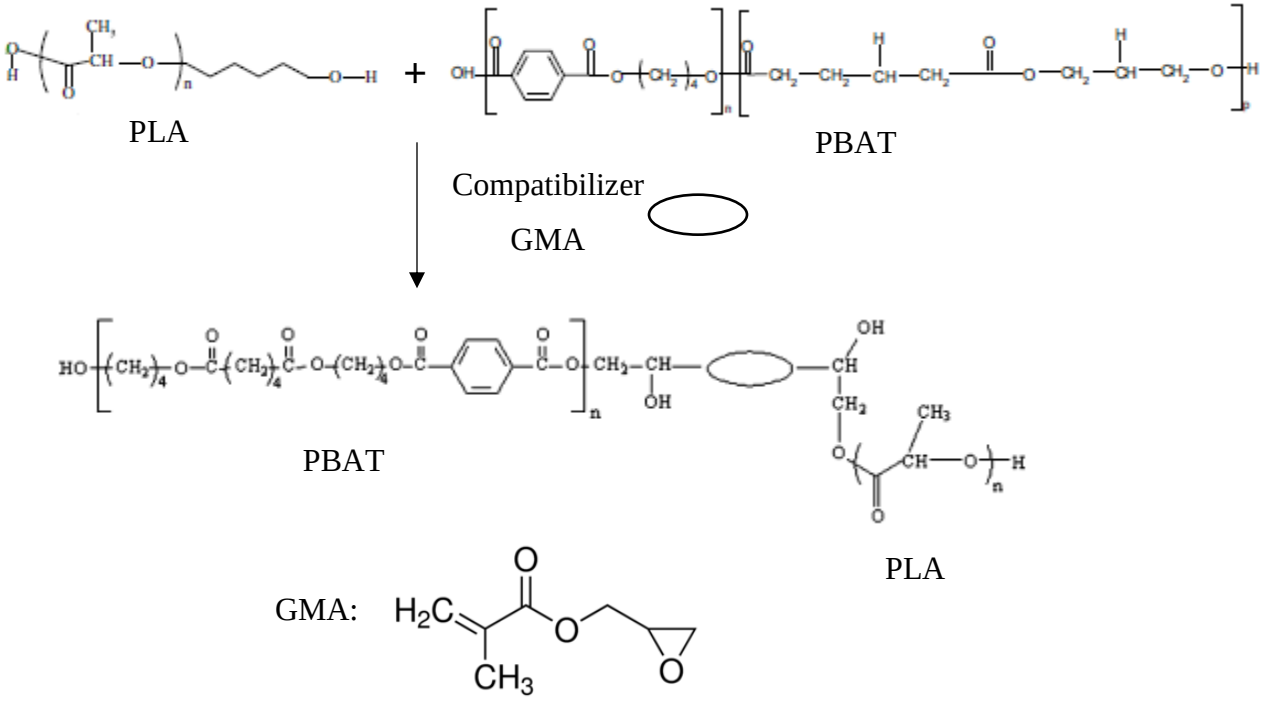

Figure 2.1 Predicted reaction between PLA, PBAT, GMA

The complete dispersion of the nanofillers in the polymer matrix helps in increasing the barrier properties of the nanocomposites as the diffusion pathway of the permeant (water vapor, gas etc.) through the nanocomposites is hindered and it must traverse a tortuous pathway thereby increasing the effective length of diffusion, which indirectly contributes to higher shelf life of the food. The incorporation of nanofillers into various natural and synthetic polymers such as polystyrene, polyamide, poly(ethylene terephthalate, poly(lactic acid), poly(vinyl chloride), thermoplastic starch etc. were widely reported over the past 30 years (Joon Choi et al., 2006; Nazarenko et al., 2007; Park et al., 2003; Pereira et al., 2009; Ray et al., 2003; Sanchez-Garcia et al., 2007; Thellen et al., 2005). The nanofiller used in this study was nanocrystalline cellulose (NCC). NCC offers various properties such as durability and high biodegradability (Brinchi et al., 2013). The structure of NCC is generally rod-shaped of about 5-10 nm in width and 100-200 nm in length (Fortunati et al., 2012a). They have a very high aspect ratio (length/diameter) and a large surface area (Matos Ruiz et al., 2000). NCC have a very high tendency to form strong hydrogen bonds within themselves due to high amount of hydroxyl groups on the surface (Favier et al., 1995).

In the present study, PLA/PBAT/GMA/NCC nanocomposites at various ratios have been melt blended using twin screw extrusion. Then, the mechanical, barrier, morphological, rheological and thermal properties of the nanocomposites were investigated.

2.2 Experimental

2.2.1 Materials

Poly (lactic acid), PLA4032D (Density: 1.25 g/cc, Average molecular weight: 100,000 g/mol), was purchased from Natureworks and poly(butylene adipate-co-terephthalate), Ecoflex®

F Blend C1200 (Density: 1.25 g/cc, Average molecular weight: 145,000 g/mol), was obtained from BASF. Glycidyl methacrylate (GMA) was purchased from Sigma Aldrich and nanocrystalline cellulose (NCC) was purchased from University of Maine.

Table 2.1 Sample designations and relevant sample components

Formulation	PLA(%)	PBAT(%)	GMA*(%)	NCC*(%)
PLA	100	0	0	0
PLA/2%NCC	100	0	0	2
PLA/4%NCC	100	0	0	4
PLA/10%PBAT	90	10	0	0
PLA/10%PBAT/5%GMA	90	10	5	0
PLA/10%PBAT/5%GMA/2%NCC	90	10	5	2
PLA/10%PBAT/5%GMA/4%NCC	90	10	5	4
PLA/20%PBAT	80	20	0	0
PLA/20%PBAT/5%GMA	80	20	5	0
PLA/20%PBAT/5%GMA/2%NCC	80	20	5	2
PLA/20%PBAT/5%GMA/4%NCC	80	20	5	4

*The weight of GMA and NCC was based on polymer basis

2.2.2 Melt blending

The materials were dried at 80^{o} C for 8 hours in an air oven to remove moisture. The nanocomposites were melt blended using a laboratory-scale co-rotating twin screw extruder (Micro-18, American Leistritz, Somerville, NJ). The extruder has a six head configuration, screw diameter of 18 mm and length-diameter ratio of 30:1. The barrel temperatures of the heads used for extrusion were 100-180-180-180-180-180 ^{o}C. The extrudates were ground using a Wiley mill

(Model 4, Thomas-Wiley Co., Philadelphia, PA) for further use. Sample designations and the relevant sample formulations are shown in Table 2.1.

2.2.3 Rheological analysis

Capillary rheometer (RH2000, Malvern Instruments Ltd, UK) was used to study the rheological properties of the blends. Test was conducted in the shear rate range from 20 to 5000 s^{-1} at 180^{o}C. The dimensions of the capillary die used was diameter of 1 mm and length of 16 mm.

2.2.4 Differential scanning calorimetry (DSC)

Differential scanning calorimeter (DSC Q100, TA Instruments, New Castle) was used to study the thermal properties of the blends. In this study, DSC measurements were carried out in the following steps; the samples were heated from 20^{o}C to 200^{o}C at 25^{o}C/min (first heating scan) and was kept at 200^{o}C for 2 minutes to erase the previous thermal history in the samples. They were subsequently cooled to 20^{o}C at 10^{o}C/min (cooling scan) to evaluate the crystallization ability of the component and then heated up to 200^{o}C at 10^{o}C/min (second heating scan). Crystallinity of PLA was calculated using the equation given below

$$X_c\,(\%) = \frac{Hm - Hcc}{Hm1} \times \frac{1}{Wpla} \times 100\%$$

where, H_m was the melting enthalpy and H_{cc} was the cold crystallization enthalpy, H_{m1} was the melting enthalpy of pure 100% crystalline PLA i.e.93 J/g (Arrieta et al., 2014, Fischer et al., 1993) and W_{PLA} represents the weight fraction of PLA. The analyses were conducted in duplicate.

2.2.5 X-ray diffraction (XRD)

X-ray diffraction analysis (XRD) was carried out using a wide-angle X-ray diffractometer (PANalytical, Almelo, Netherland) which has a Cu radiation source of wavelength 1.54 A^o operating at 45kV and 40mA. Scans were carried out at diffraction angle (2θ) of 5.0-40.0^o with step size of 0.007°.

2.2.6 Fourier-transform infrared spectroscopy (FTIR)

FTIR spectra of PLA/PBAT blends with and without compatibilizer GMA were recorded using FTIR spectrophotometer (Carey 630, Agilent Technology, Santa Clara, CA) with a diamond crystal collecting 32 scans. Each spectrum was obtained within the range of 4000–650 cm^{-1} with a resolution of 2 cm^{-1}.

2.2.7 Film preparation

Hot press (Model 3889, Carver Inc., Wabash, IN) with process parameter of force of 2100 lb and temperature of hot plates at 180^{o}C (top and bottom) was used to make the films of thickness of about 200 microns. The hot sample was preheated at 180°C for 5 min and then further pressed for 5 minutes using the hotpress.

2.2.8 Transmission electron microscopy (TEM)

FEI Tecnai F20XT transmission electron microscope (FEI North America, Hillsboro, OR) operated at 100 kV was used for TEM of the samples. The samples were obtained by using ultra-microtome to obtain slices of about 100nm thick. TEM images were used to study the morphological properties of the blends and visually characterize the interactions between the nanofiller and the base polymers.

2.2.9 Mechanical properties

Mechanical properties of the films were measured using Instron testing machine (Model 4465, Canton, MA, USA) based on standard ASTM D882 method. Films were cut into 1.3 cm wide and 10 cm long strips and conditioned at 23^{o} C and 50% RH for two days before testing for tensile strength and elongation ratio. The Tensile strength (TS) and elongation at break (EB) were calculated as given in the equations below:

$$TS=\frac{Lp}{a} \times 10^{-6}\ MPa$$

where Lp= peak load (N) and a= cross-sectional area (m^2)

$$EB= \delta L/L \times 100\ (\%)$$

where δL= increase in length at breaking point (mm) and L= original length (mm)

All the measurements were reported as the average of five samples.

2.2.10 Water vapor permeability (WVP)

Water vapor permeability (WVP) was determined gravimetrically according to the standard method E96-00 (ASTM 2000). The films were fixed on top of test cells containing a desiccant (silica gel). Test cells were placed in a relative humidity chamber with controlled temperature and relative humidity (25^{o} C and 85% RH). After steady-state conditions were reached, the weight of the test cells was measured every 24 hours over a five-day period. The slope of each line was calculated by linear regression (R^2>0.99), and the water vapor transmission rate (WVTR) was calculated from the slope of the straight line (W/t) divided by the transfer area (A):

$$WVTR = \frac{(\frac{W}{t})}{A}\ g/h.m^2$$

where W = change in weight (g), t = time (h) and A = area of transfer (m^2)

WVP was then calculated from WVP using the equation given below

$$\text{WVP} = \frac{WVTR*t}{\Delta P} \text{ g*mm/kPa.h.m}^2$$

where t = film thickness (mm) and ΔP = pressure difference across the films (kPa).

All the measurements were reported as the average of two samples.

2.2.11 Statistical analysis

Data was analyzed using SAS studio analysis software. Statistical significance of differences was calculated using Tukey's range test, $P < 0.05$.

2.3 Results and discussion

2.3.1 Rheological properties

The rheological properties of the PLA/PBAT nanocomposites are shown in Figure 2.2(a-c). The shear viscosity curves of the blends show their shear-thinning behavior. PBAT addition led to the increase in shear viscosity of the blends as reported previously (Jiang et al., 2006). Addition of GMA led to increase in viscosity of the PLA/PBAT blends as GMA improves the miscibility between the polymers PLA and PBAT (Figure 2.2a). This leads to the increase in molecular interactions which results in restriction of movement of molecular chains (Zhang et al., 2009). The shear thinning behavior of the blends also increases with addition of GMA due to the formation of long chain branches during the reactive extrusion. Addition of NCC led to increase in the shear viscosity of the blends (Figure 2.2b, 2.2c). This may be due to the hindrance of flow by the nanofiller particles in the polymer matrix, hence restricting the movement of polymer chains (Chow et al., 2005; Dangtungee et al., 2011).

a)

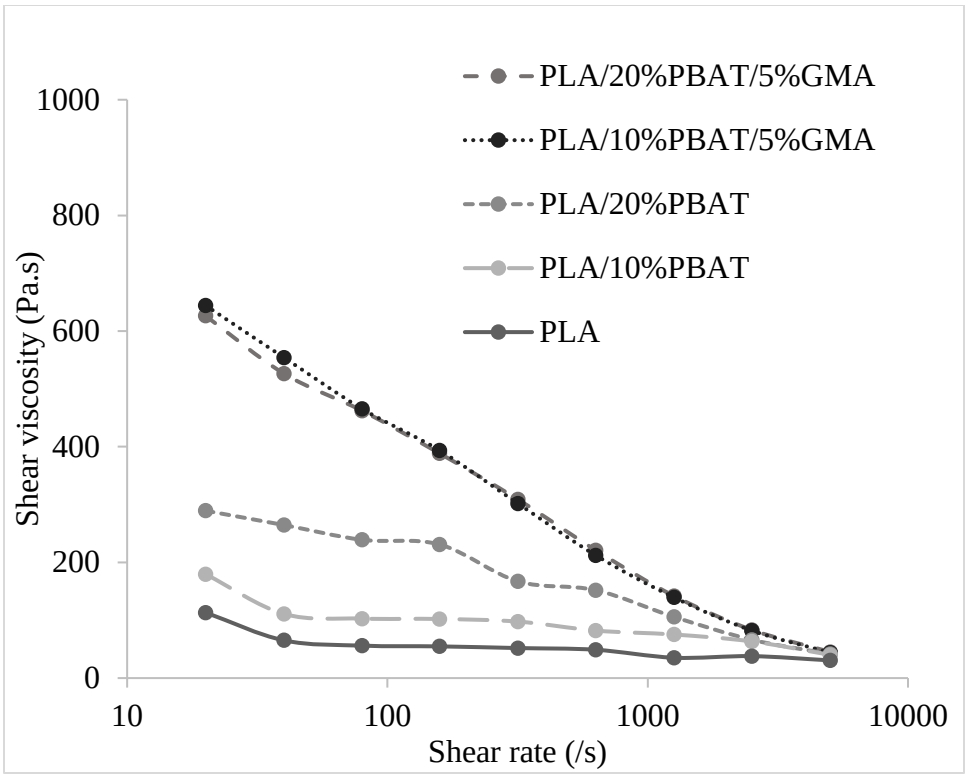
PLA/20%PBAT/5%GMA
PLA/10%PBAT/5%GMA
PLA/20%PBAT
PLA/10%PBAT
PLA
Shear viscosity (Pa.s)
1000
800
600
400
200
0
10
100
1000
10000
Shear rate (/s)

b)

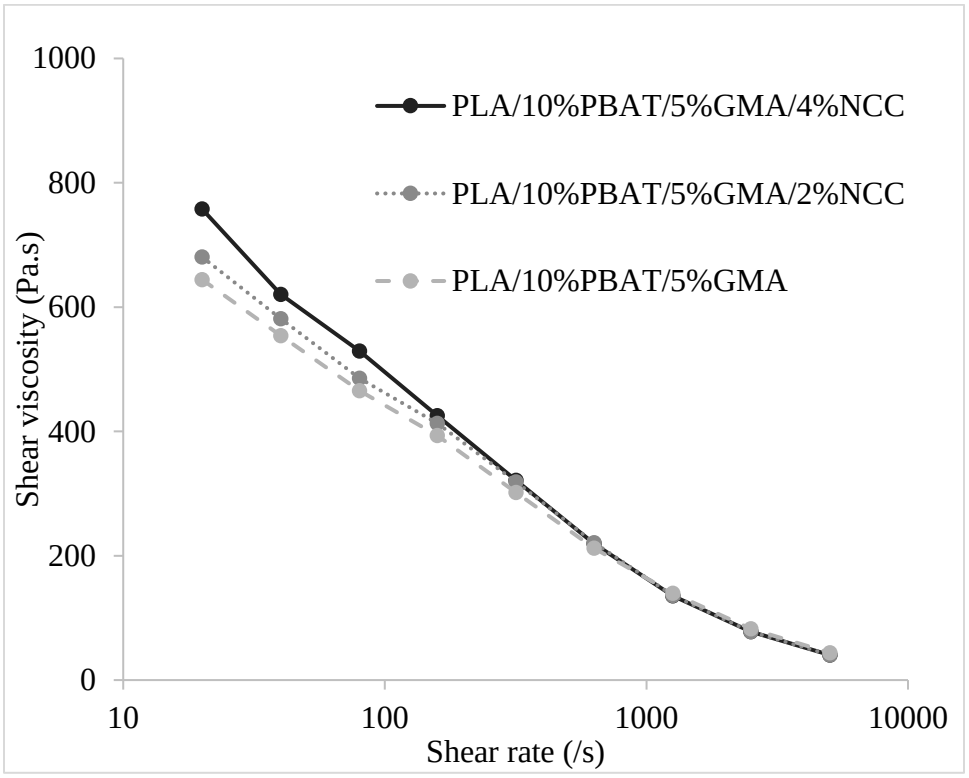
PLA/10%PBAT/5%GMA/4%NCC
PLA/10%PBAT/5%GMA/2%NCC
PLA/10%PBAT/5%GMA
Shear viscosity (Pa.s)
1000
800
600
400
200
0
10
100
1000
10000
Shear rate (/s)

c)

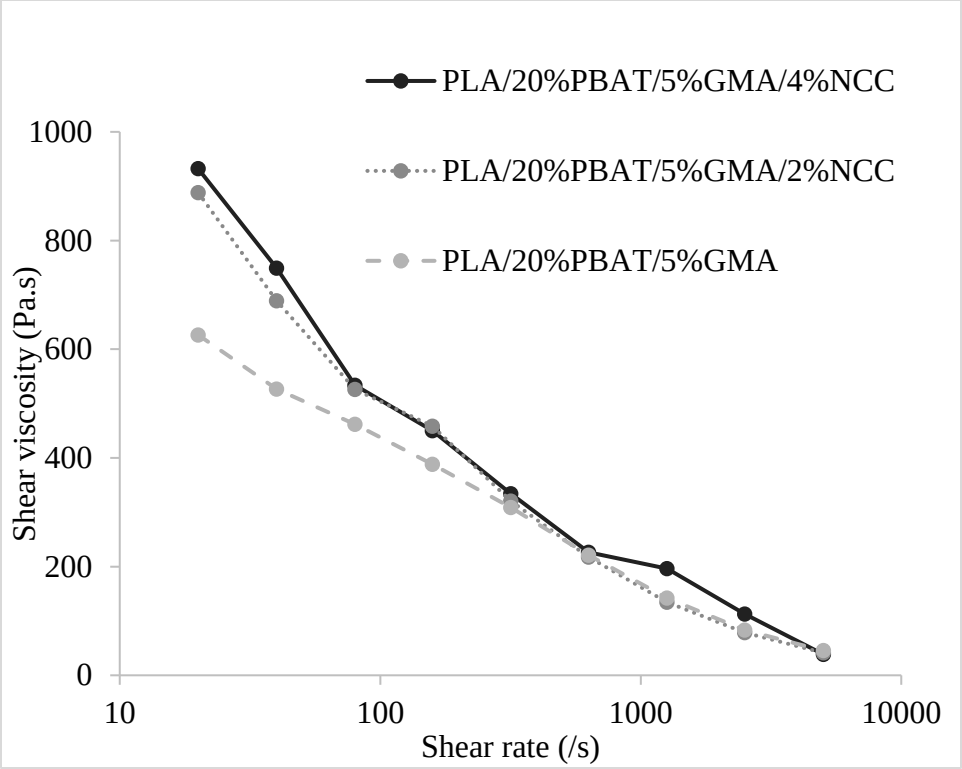

Figure 2.2 Rheological behavior of PLA/PBAT nanocomposites

2.3.2 Thermal properties

The DSC second heating scans of the PLA/PBAT blends are shown in Figure 2.3. Glass transition, crystallization and melting phenomena were observed for all the DSC thermograms. Additionally, the glass transition temperature (T_g), cold crystallization temperature (T_{cc}), melting temperature (T_m), cold crystallization enthalpy (H_{cc}), melting enthalpy (H_m) and percent of crystallinity (X_c) obtained from the second DSC heating thermograms are shown in Table 2.2. DSC thermogram of neat PLA exhibited a glass transition centered at 57^{o}C, an exothermic cold crystallization peak at 105^{o}C and an endothermic peak at 167^{o}C. These phenomena typically occur in PLA and the values are comparable to those reported in scientific literature (Battegazore et al., 2014; Frone et al., 2013; Petersson et al., 2007). Similarly, second heating scan of neat PBAT exhibited a glass transition temperature centered at -33^{o}C and an endothermic melting

phenomenon with onset at 91ºC and a broad peak at 120ºC. These phenomena typically occur in PLA and the values are comparable to those reported in scientific literature (Arruda et al., 2015; Kumar et al., 2010). Addition of PBAT decreased the T_c significantly and led to the decrease in

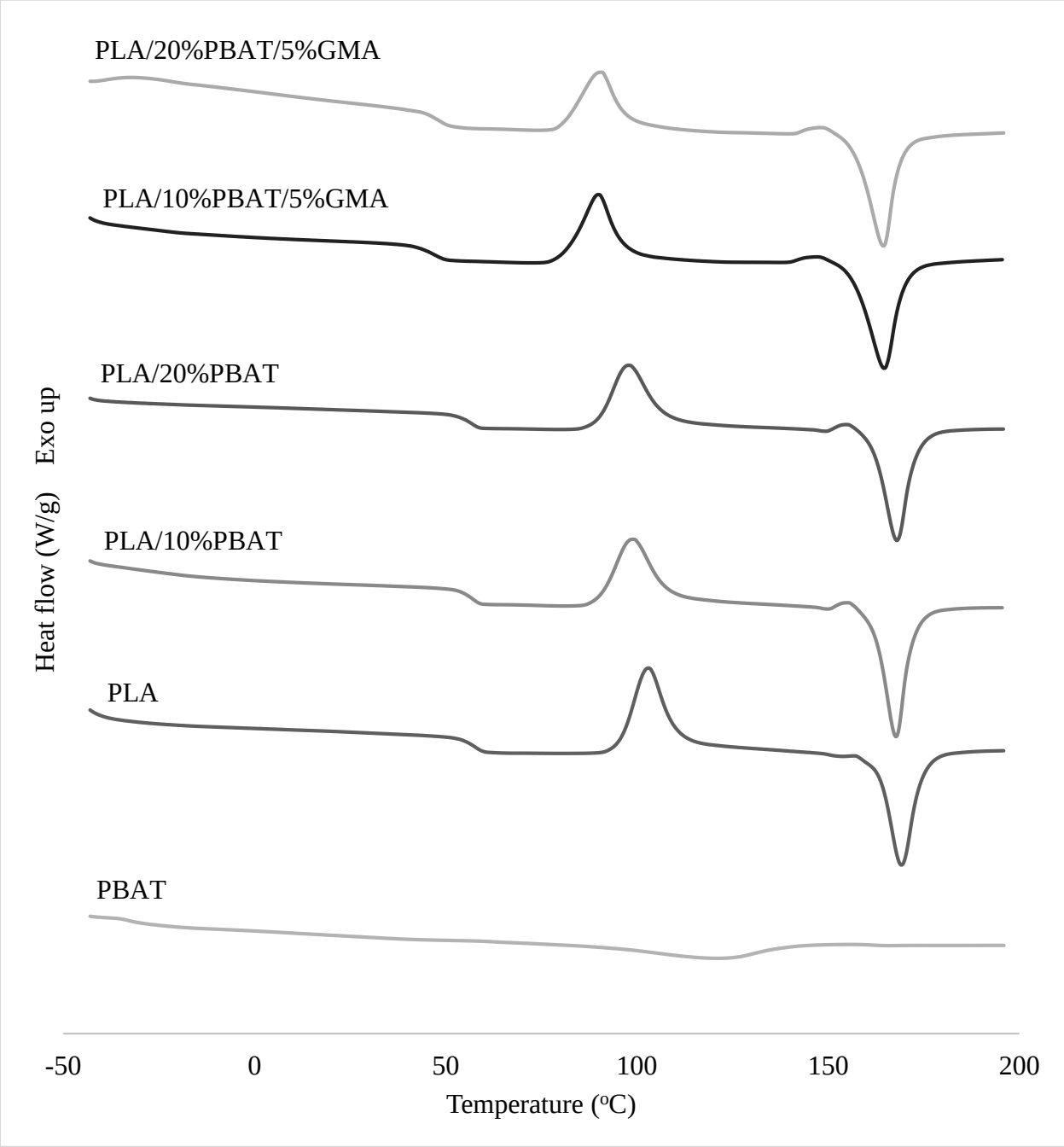

Figure 2.3 Second heating DSC thermograms of PLA/PBAT blends

Table 2.2 Data obtained from second DSC heating scans of PLA/PBAT nanocomposites

Formulation	T_g (°C)	T_c (°C)	T_m (°C)	H_{cc}(J/g)	H_m(J/g)	X_c(%)
PLA	57.45^{a}	105.3^{a}	168.91^{a}	28.45^{a}	30.76^{ab}	2.48^{a}
PLA/2%NCC	55.23^{bc}	99.33^{b}	167.43^{ab}	24.04^{b}	32.49^{ab}	9.28^{b}
PLA/4%NCC	54.72^{b}	101.69^{ab}	167.15^{b}	22.15^{bcd}	32.65^{ab}	11.75^{c}
PLA/10%PBAT	56.78^{c}	99.49^{b}	167.65^{ab}	23.46^{b}	31.01^{ab}	9.02^{b}
PLA/10%PBAT/5%GMA	45.81^{de}	89.61^{c}	163.92^{c}	22.42^{bc}	33.52^{a}	13.92^{d}
PLA/10%PBAT/5%GMA/2%NCC	45.03^{d}	90.38^{c}	164.35^{c}	19.61^{ef}	31.51^{ab}	15.22^{de}
PLA/10%PBAT/5%GMA/4%NCC	45.4^{d}	88.06^{c}	163.55^{c}	16.6^{g}	31^{ab}	18.74^{f}
PLA/20%PBAT	56.97^{ac}	98.93^{b}	167.84^{ab}	22.65^{bc}	30.05^{b}	9.95^{b}
PLA/20%PBAT/5%GMA	46.03^{de}	89.34^{c}	164.09^{c}	21.11^{cde}	31.74^{ab}	15^{de}
PLA/20%PBAT/5%GMA/2%NCC	47.48^{e}	91.3^{c}	164.45^{c}	20.08^{de}	31.17^{ab}	15.94^{e}
PLA/20%PBAT/5%GMA/4%NCC	46.02^{de}	89.24^{c}	163.61^{c}	17.64^{fg}	31.15^{ab}	19.79^{f}

Different superscripts within the same column indicate significant difference ($P<0.05$) between treatments.

H_{cc} thus indicating the increase in crystallization ability of PLA, as reported previously (Arruda et al., 2015; Jiang et al., 2006). The melting phenomenon of PBAT occurs at around the same temperature as the crystallization phenomenon of PLA. Hence, it was not possible to determine the melting temperature of PBAT in the blends. This may lead to slightly lower values of H_{cc} of PLA due to the melting enthalpy of PBAT. However, the content of PBAT in the PLA/PBAT blend used in this study is also low to affect the values of H_{cc} and X_c.

Addition of 5% GMA to the PLA/PBAT blends decreased the T_g of the blends significantly thus indicating the increase in the interfacial adhesion between the polymers PLA and PBAT. GMA acted a compatibilizer thereby contributing to the increase in chain mobility of

the polymers. GMA also decreased the T_c of the blends significantly. This may be an indication of the increased ability of crystallization of PLA due to increase in molecular interactions between PLA and PBAT. Addition of nanofiller NCC led to the significant decrease in H_{cc} of PLA/PBAT nanocomposites and increase in X_c as NCC promotes the recrystallization of PLA (Arrieta et al., 2014). The large surface area of the nanofiller causes them to act as nucleating agent during the crystallization of PLA thereby facilitating the crystallization process (Nam et al., 2003; Ray et al., 2002).

2.3.3 X-ray diffraction (XRD)

X-ray diffraction (XRD) was used to study to effect of nanofiller NCC and compatibilizer GMA on the crystallinity of the PLA matrix. Figure 2.4 (a, b) shows the XRD

a)

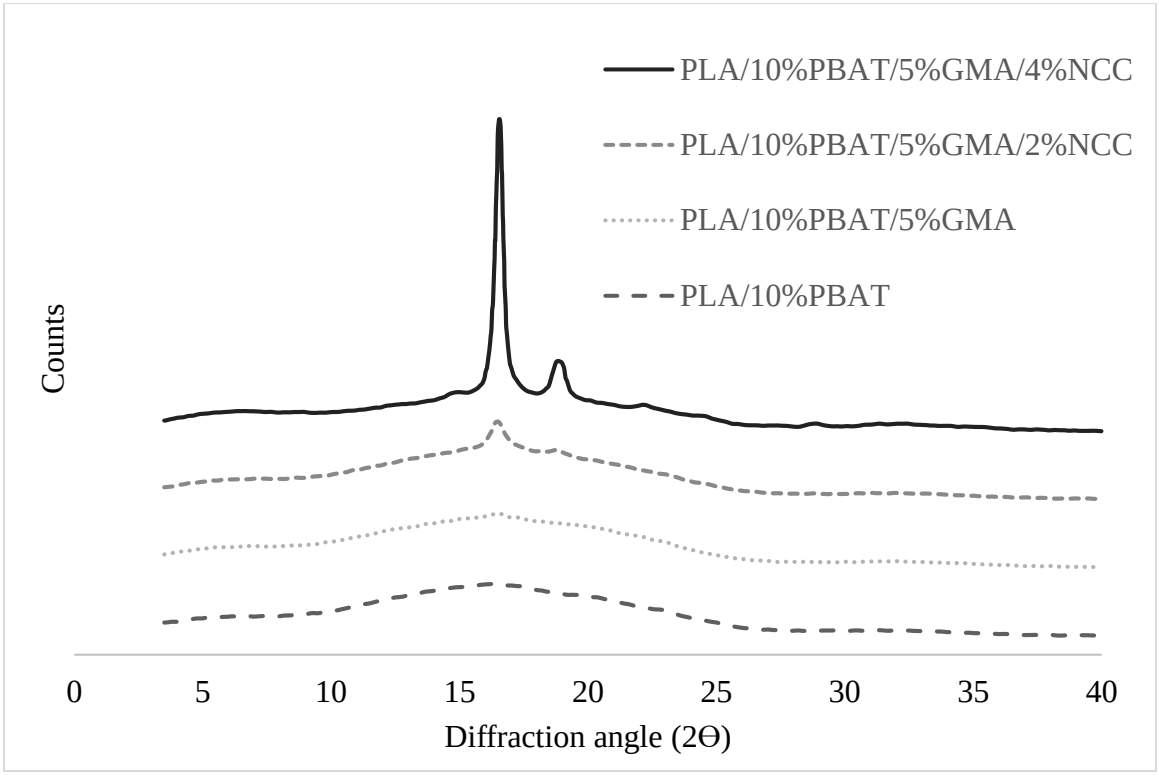

b)

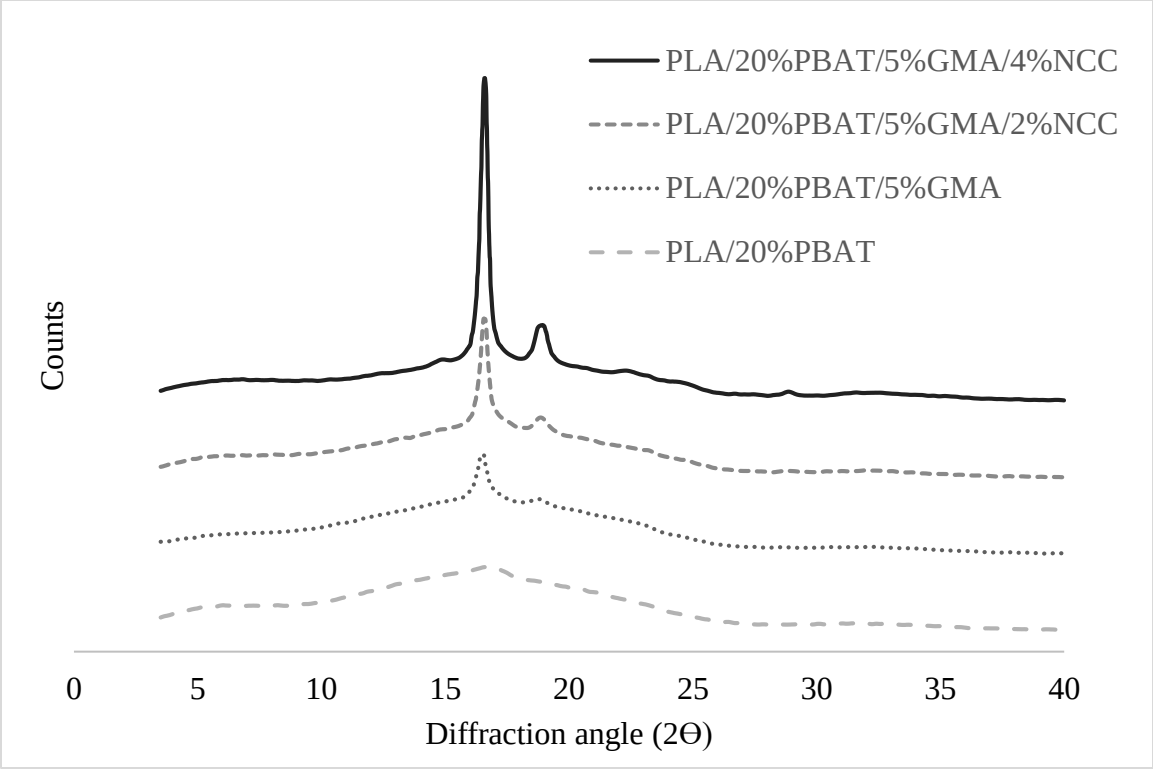

Figure 2.4 XRD of PLA/PBAT nanocomposites

curves of PLA/PBAT nanocomposites. PLA/10%PBAT and PLA/20%PBAT showed a broad diffraction peak at 2Θ = 16.5º which corresponds to (110/200) crystalline plane of PLA (Abdelwahab et al., 2012; Tabatabaei et al., 2012). Addition of GMA led to the presence of a shoulder at 2Θ = 19º. It corresponds to the (203) crystalline plane of PLA (Tabatabaei et al., 2012) which is also an indication of increased ability of crystallization of PLA as confirmed by DSC data. Addition of NCC led to an increase in intensity of the peaks as NCC acts as a nucleating agent which promotes the recrystallization of PLA (Arrieta et al., 2014). There was a steady increase in the intensity of peak at 2Θ = 22.5º with addition of NCC which is indicative of cellulose crystallinity (Fortunati et al., 2012b).

2.3.4 Fourier-transform infrared spectroscopy (FTIR)

The FTIR spectra of PLA/PBAT blends with and without compatibilizer GMA is shown in Figure 2.5. The two peaks in the region of 2900-3000 cm^{-1} correspond to the antisymmetric and symmetric stretching vibrations of the axial C-H groups in PLA and PBAT.

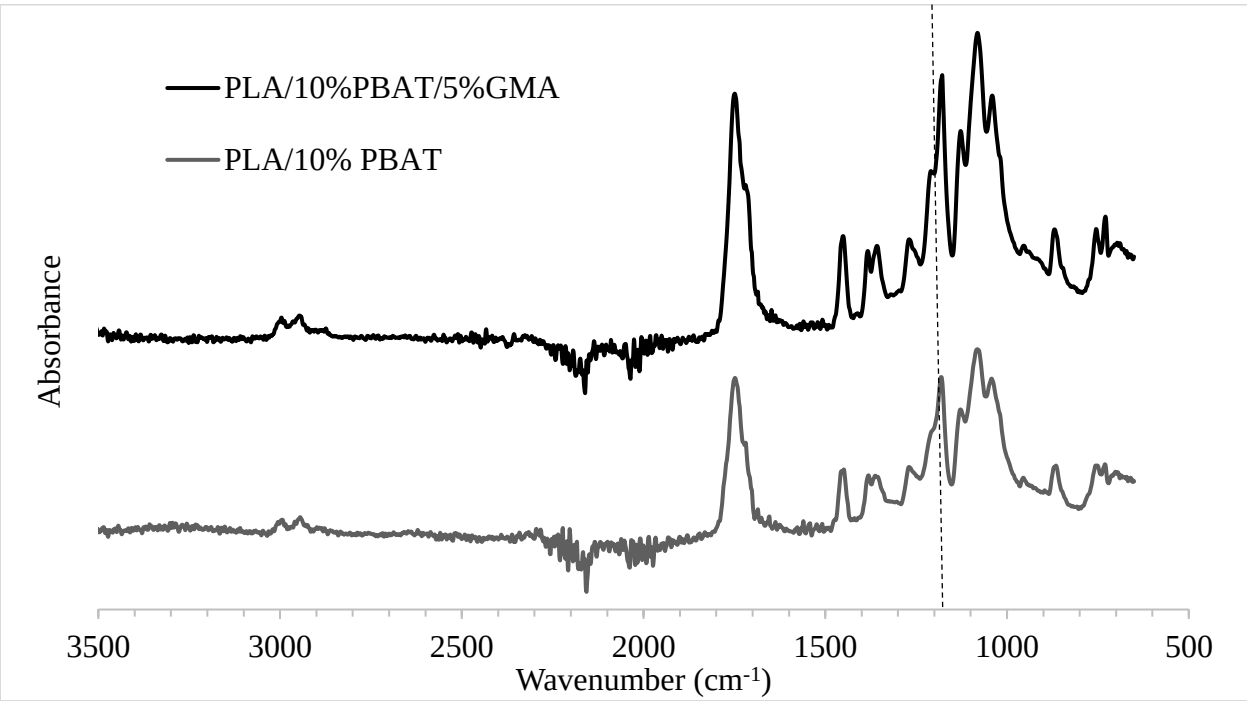

Figure 2.5 FTIR spectra of PLA/PBAT blends with and without compatibilizer GMA

The sharp peak at 1748 cm^{-1} in the FTIR spectra is associated with the stretching of C=O in the ester linkages. There was a shift in the peak towards lower wavenumber 1182 cm^{-1} to 1178 cm^{-1} with the addition of GMA to the PLA/PBAT blend which is indicative of an increase in C-O stretching in carboxylic group due to the reaction of epoxy group of GMA with the carboxylic group of PLA and PBAT. Similar stretching peaks of carboxylic groups in PLA/PBAT blends are observed in Kumar et al., 2010.

2.3.5 Transmission electron microscopy (TEM)

TEM images of the nanocomposites are depicted in Figure 2.6 (a-c) and aggregation of NCC was observed in all the matrices. Dispersion of hydrophilic NCC is difficult to obtain in hydrophobic polymers such as PLA, PBAT due to the difference in polarity based on the hydrophilic nature of the nanofiller and intermolecular hydrogen bonding between the nanofillers (Espino-Perez et al., 2013; Martinez-Sanz et al., 2013). The aggregation of NCC in polymer matrix was also observed in previous studies (Arrieta et al., 2014; Xu et al., 2015).

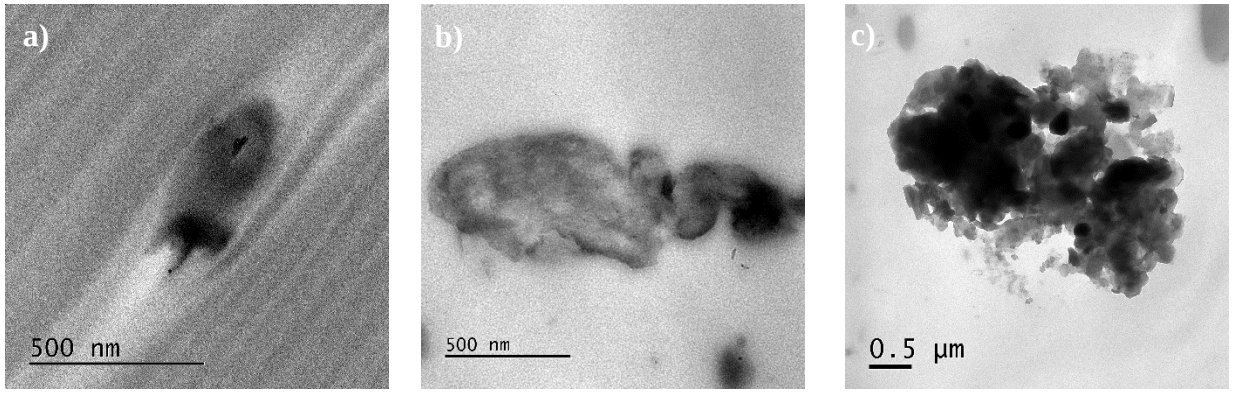

Figure 2.6 TEM image of a) PLA/2%NCC b) PLA/10%PBAT/5%GMA/2%NCC c) PLA/10%PBAT/5%GMA/4%NCC

2.3.6 Mechanical properties

The mechanical properties of the PLA/PBAT nanocomposites are shown in Table 2.3. It is evident that addition of PBAT (up to 10%) led to about 200% increase in the elongation at break of PLA. However, addition of 20% PBAT did not increase the elongation at break significantly compared to addition of 10% PBAT. Tensile strength decreased by 20% from 51 (neat PLA) to 40 MPa (PLA/20%PBAT) which was expected due to lower strength of PBAT compared to PLA. Addition of 5% GMA compatibilizer to the PLA/PBAT blends increased the elongation at break by 100% from 12% (PLA/10%PBAT) to 24% (PLA/10%PBAT/5%GMA) due to the increase in interfacial adhesion between PLA and PBAT. GMA was effective as a

Table 2.3 Mechanical properties of PLA/PBAT nanocomposites

Formulation	Tensile Strength (MPa)	Elongation at break (%)
PLA	51.18 ± 2.21^{a}	6.3 ± 0.57^{a}
PLA/2%NCC	50.26 ± 1.67^{a}	5.9 ± 0.19^{a}
PLA/4%NCC	50.56 ± 3.11^{a}	6.38 ± 0.7^{a}
PLA/10%PBAT	43.05 ± 2.56^{b}	12.63 ± 0.79^{b}
PLA/10%PBAT/5%GMA	35.83 ± 2.49^{cde}	24.17 ± 2.59^{c}
PLA/10%PBAT/5%GMA/2%NCC	37.55 ± 1.76^{cd}	7.11 ± 0.4^{a}
PLA/10%PBAT/5%GMA/4%NCC	33.98 ± 2.56^{def}	7.98 ± 0.94^{a}
PLA/20%PBAT	40.59 ± 3.03^{bc}	15.24 ± 2.11^{b}
PLA/20%PBAT/5%GMA	30.83 ± 2.77^{ef}	22.64 ± 3.12^{c}
PLA/20%PBAT/5%GMA/2%NCC	33.15 ± 3.01^{def}	7.91 ± 0.49^{a}
PLA/20%PBAT/5%GMA/4%NCC	29.55 ± 1.84^{f}	7.59 ± 0.93^{a}

Different superscripts within the same column indicate significant difference ($P < 0.05$) between treatments.

reactive compatibilizer due to the presence of carboxylic groups in PLA and PBAT which reacted with epoxy groups in GMA under high shear and heat during extrusion. This was also in confirmation with the FTIR results. However, addition of NCC did not have any effect on the tensile strength of the PLA/PBAT blends. Theoretically, the complete dispersion of nanofiller in the polymer matrix facilitates the increase in available reinforcing elements for carrying an applied stress. The coupling between the polymer matrix and the large surface area of the nanofiller optimizes the load transfer to the reinforcement elements, thereby leading to increase in tensile strength. However, TEM images showed the aggregation of NCC in all the matrices (Figure 2.6) which caused NCC to act as a microcomposite rather than as a nanocomposite

thereby negating the reinforcement effect of the nanofillers. Addition of nanofiller also led to decrease in elongation at break as the nanofiller reduces the mobility of the polymer chain i.e. confinement of polymer chains and contributes to the higher breaking tendency of the nanocomposite films. Several other studies also showed the decrease in elongation at break with increase in nanofiller content (Ali et al., 2011; Tang et al., 2008; Khalil et al., 2017).

2.3.7 Barrier properties

Table 2.4 Barrier properties of PLA/PBAT nanocomposites

Formulation	WVP ($g.mm/m^2.day.kPa$)
PLA	1.63 ± 0.03^{a}
PLA/2%NCC	1.59 ± 0.03^{a}
PLA/4%NCC	1.56 ± 0.04^{a}
PLA/10%PBAT	1.84 ± 0.01
PLA/10%PBAT/5%GMA	1.65 ± 0.08^{a}
PLA/10%PBAT/5%GMA/2%NCC	1.68 ± 0.1^{ab}
PLA/10%PBAT/5%GMA/4%NCC	1.7 ± 0.1^{ab}
PLA/20%PBAT	1.95 ± 0.1^{b}
PLA/20%PBAT/5%GMA	1.73 ± 0.09^{ab}
PLA/20%PBAT/5%GMA/2%NCC	1.66 ± 0.02^{a}
PLA/20%PBAT/5%GMA/4%NCC	1.69 ± 0.09^{ab}

Different superscripts within the same column indicate significant difference ($P<0.05$) between treatments.

Water vapor permeability (WVP) of the films was measured to evaluate the barrier performance of the PLA/PBAT nanocomposites and is shown in Table 2.4. Addition of PBAT led to a slight increase in WVP because PLA is more hydrophobic in nature compared to PBAT

(Shirai et al., 2013; Wang et al., 2016). Addition of GMA decreased the WVP of the PLA/PBAT blends. This may be due to the increase in molecular interactions between the polymers PLA and PBAT which leads to the decrease in free volume fraction thereby restricting the diffusion of water vapor molecules through the polymer matrix (Yampolskii et al., 2001). Addition of nanofiller NCC did not have any effect on WVP of the PLA/PBAT binary blends. Theoretically, the complete dispersion of nanofiller in the polymer matrix increases the tortuosity leading to slower diffusion of water vapor through the polymer matrix i.e. reduction of WVP (Azeredo et al., 2010). However, TEM images showed the aggregation of NCC in the PLA/PBAT matrix (Figure 2.6) which led to no change in WVP for the binary blends.

2.3.8 Comparison with commercial plastics

Table 2.5 shows the comparison of the films developed in the current study with those of the commercial plastics currently used in the industry. The mechanical and barrier properties of the films developed show that the barrier properties and elongation at break are in the moderate range while the tensile strength is in a good range. The additional benefit that the films developed in this current study is that they are biodegradable in composting conditions and are cost competitive to that of conventional polyolefin polymers. Hence, the films developed have a good scope to be used in the food packaging industry.

Table 2.5 Comparison with commercial plastics

Material	Cost[a]	WVP[b]	Tensile strength[c]	Elongation at break[d]	Reference
PET	Moderate	Good	Good	Good	Auras et al., 2005
PP	Moderate	Good	Moderate	Good	Ismail, 2002
PE	Moderate	Moderate	Moderate	Good	Zhong et al., 2007
PS	High	Moderate	Moderate	Poor	Nair et al., 1996
PVC	Moderate	Good	Good	Good	Zheng et al., 2007
PA	High	Moderate	Good	Good	Yang et al., 1998
PVDC	Moderate	Good	Good	Moderate	Shiku et al., 2004
PLA	Moderate	Moderate	Good	Poor	Oksman et al., 2003
PLA/PBAT films	**Moderate**	**Moderate**	**Good**	**Moderate**	**Current study**

[a]Cost	[b]Test conditions:23°C, 85% RH	[c]Tensile strength	[d]Elongation at break
Low: <5$/kg	Poor: 10-100 g*mm/m^2*day*kPa	Poor: <10 MPa	Poor: <10%
Moderate: 5-10$/kg	Moderate: 1-10 g*mm/m^2*day*kPa	Moderate: 10-50 MPa	Moderate: 10-50%
High: >10$/kg	Good: 0.1-1 g*mm/m^2*day*kPa	Good: >50 MPa	Good: >50%

PET=Poly(ethylene terephthalate), PP=Polypropylene, PE= Polyethylene, PS=Polystyrene, PVC=Poly(vinyl chloride), PA=polyamide, PVDC=Poly(vinylidene chloride)

2.4 Conclusions

Melt extrusion was used to prepare PLA/PBAT nanocomposites with NCC as the nanofiller. The effect of compatibilizer GMA on the interfacial adhesion between the polymers PLA and PBAT was studied. Rheological study showed the increase in shear viscosity of the PLA/PBAT blends with addition of GMA and NCC. DSC study showed the decrease in H_{cc} of PLA/PBAT nanocomposites with addition of NCC signifying the nucleating action of the nanofiller during the crystallization of PLA. Addition of GMA led to decrease in T_g of the PLA/PBAT blends confirming the improvement in miscibility between the polymers. It also led

to decrease in T_c which showed the increased ability of crystallization of PLA. XRD analysis also confirmed the same due to the presence of a shoulder at $2\Theta = 19^o$. TEM showed the aggregation of NCC in all the matrices due to difference in polarity based on the hydrophilic nature of nanofiller and hydrophobic polymers PLA and PBAT and intermolecular hydrogen bonding between the nanofillers. Mechanical studies showed a significant increase in elongation at break of PLA with addition of PBAT. Addition of GMA further resulted in increase in elongation at break of PLA/PBAT blends due to the increase in interfacial adhesion between the polymers PLA and PBAT. Addition of NCC did not have any effect of the tensile strength of the PLA/PBAT blends as aggregation of NCC caused it to act as a microcomposite rather than as a nanocomposite thereby negating the reinforcement effect of the nanofillers. Addition of PBAT led to a slight increase in WVP. Addition of GMA decreased the WVP of the PLA/PBAT blends due to the increase in molecular interactions between the polymers PLA and PBAT. Addition of NCC did not have any effect on the WVP of PLA/PBAT nanocomposites due to the aggregation of the nanofiller.

2.5 References

Abdelwahab, M. A., Flynn, A., Chiou, B. S., Imam, S., Orts, W., & Chiellini, E. (2012). Thermal, mechanical and morphological characterization of plasticized PLA–PHB blends. Polymer Degradation and Stability, 97(9), 1822-1828.

Ali, S. S., Tang, X., Alavi, S., & Faubion, J. (2011). Structure and physical properties of starch/poly vinyl alcohol/sodium montmorillonite nanocomposite films. Journal of agricultural and food chemistry, 59(23), 12384-12395.

Al-Itry, R., Lamnawar, K., & Maazouz, A. (2012). Improvement of thermal stability, rheological and mechanical properties of PLA, PBAT and their blends by reactive extrusion with functionalized epoxy. Polymer Degradation and Stability, 97(10), 1898-1914.

Arrieta, M. P., Fortunati, E., Dominici, F., Rayón, E., López, J., & Kenny, J. M. (2014). Multifunctional PLA–PHB/cellulose nanocrystal films: Processing, structural and thermal properties. Carbohydrate polymers, 107, 16-24.

Arruda, L. C., Magaton, M., Bretas, R. E. S., & Ueki, M. M. (2015). Influence of chain extender on mechanical, thermal and morphological properties of blown films of PLA/PBAT blends. Polymer Testing, 43, 27-37.

Auras, R. A., Singh, S. P., & Singh, J. J. (2005). Evaluation of oriented poly (lactide) polymers vs. existing PET and oriented PS for fresh food service containers. Packaging technology and science, 18(4), 207-216.

Azeredo, H. M., Mattoso, L. H. C., Avena-Bustillos, R. J., Filho, G. C., Munford, M. L., Wood, D., & McHugh, T. H. (2010). Nanocellulose reinforced chitosan composite films as affected by nanofiller loading and plasticizer content. Journal of Food Science, 75(1), N1-N7.

Battegazzore, D., Alongi, J., & Frache, A. (2014). Poly (lactic acid)-based composites containing natural fillers: thermal, mechanical and barrier properties. Journal of Polymers and the Environment, 22(1), 88-98.

Brinchi, L., Cotana, F., Fortunati, E., & Kenny, J. M. (2013). Production of nanocrystalline cellulose from lignocellulosic biomass: Technology and applications. Carbohydrate Polymers, 94(1), 154–169.

Chow, W. S., Mohd Ishak, Z. A., & Karger-Kocsis, J. (2005). Morphological and rheological properties of polyamide 6/poly (propylene)/organoclay nanocomposites. Macromolecular Materials and Engineering, 290(2), 122-127.

Dangtungee, R., Petcharoen, K., Pinijsattawong, K., & Siengchin, S. (2012). Investigation of the rheological properties and die swell of polylactic acid/nanoclay composites in a capillary rheometer. Mechanics of Composite Materials, 47(6), 663-670.

Espino-Pérez, E., Bras, J., Ducruet, V., Guinault, A., Dufresne, A., & Domenek, S. (2013). Influence of chemical surface modification of cellulose nanowhiskers on thermal, mechanical, and barrier properties of poly (lactide) based bionanocomposites. European Polymer Journal, 49(10), 3144-3154.

Favier V., Chanzy H., & Cavaille J.Y. (1995). Polymer nanocomposites reinforced by cellulose whiskers. Macromolecules, 28(18), 6365–6367.

Fischer, E. W., Sterzel, H. J., & Wegner, G. K. Z. Z. (1973). Investigation of the structure of solution grown crystals of lactide copolymers by means of chemical reactions. Kolloid-Zeitschrift und Zeitschrift für Polymere, 251(11), 980-990.

Fortunati, E., Armentano, I., Zhou, Q., Iannoni, A., Saino, E., Visai, L., Berglund, L. A., & Kenny, J. M. (2012a). Multifunctional bionanocomposite films of poly(lactic acid),cellulose nanocrystals and silver nanoparticles. Carbohydrate Polymers, 87(2), 1596–1605.

Fortunati, E., Peltzer, M., Armentano, I., Torre, L., Jiménez, A., & Kenny, J. M. (2012b). Effects of modified cellulose nanocrystals on the barrier and migration properties of PLA nano-biocomposites. Carbohydrate polymers, 90(2), 948-956.

Frone, A. N., Berlioz, S., Chailan, J. F., & Panaitescu, D. M. (2013). Morphology and thermal properties of PLA–cellulose nanofibers composites. Carbohydrate Polymers, 91(1), 377-384.

Global bio plastics market to be driven by demand from packaging in North America, 2017. Retrieved from: http://www.plastemart.com/plastic-technical-articles/global-bio-plastics-market-to-be-driven-by-demand-from-packaging-in-north-america/2350.

Ismail, H. (2002). Thermoplastic elastomers based on polypropylene/natural rubber and polypropylene/recycle rubber blends. Polymer Testing, 21(4), 389-395.

Jiang, L., Wolcott, M. P., & Zhang, J. (2006). Study of biodegradable polylactide/poly (butylene adipate-co-terephthalate) blends. Biomacromolecules, 7(1), 199-207.

Joon Choi, W., Kim, H. J., Han Yoon, K., Hyeong Kwon, O., & Ik Hwang, C. (2006). Preparation and barrier property of poly (ethylene terephthalate)/clay nanocomposite using clay-supported catalyst. Journal of Applied Polymer Science, 100(6), 4875-4879.

Khalil, H. A., Tye, Y. Y., Ismail, Z., Leong, J. Y., Saurabh, C. K., Lai, T. K., Chong, E. W., Aditiawati, P., Tahir, P. M. & Dungani, R. (2017). Oil palm shell nanofiller in seaweed-based composite film: Mechanical, physical, and morphological properties. BioResources, 12(3), 5996-6010.

Kumar, M., Mohanty, S., Nayak, S. K., & Parvaiz, M. R. (2010). Effect of glycidyl methacrylate (GMA) on the thermal, mechanical and morphological property of biodegradable PLA/PBAT blend and its nanocomposites. Bioresource technology, 101(21), 8406-8415.

Marsh, K., & Bugusu, B. (2007). Food packaging - Roles, materials, and environmental issues. Journal of Food Science, 72(3), R39-R55.

Martínez-Sanz, M., Lopez-Rubio, A., & Lagaron, J. M. (2013). High-barrier coated bacterial cellulose nanowhiskers films with reduced moisture sensitivity. Carbohydrate polymers, 98(1), 1072-1082.

Matos Ruiz, M., Cavaille, J. Y., Dufresne, A., Gerard, J. F., & Graillat, C. (2000). Processing and characterization of new thermoset nanocomposites based on cellulose whiskers. Composite Interfaces, 7(2), 117-131.

Mihindukulasuriya, S.D.F., & Lim, L.T. (2014). Nanotechnology development in food packaging: A review. Trends in Food Science & Technology, 40(2), 149-167.

Nair, K. C., Diwan, S. M., & Thomas, S. (1996). Tensile properties of short sisal fiber reinforced polystyrene composites. Journal of applied polymer science, 60(9), 1483-1497.

Nam, J. Y., Sinha Ray, S., & Okamoto, M. (2003). Crystallization behavior and morphology of biodegradable polylactide/layered silicate nanocomposite. Macromolecules, 36(19), 7126-7131.

Nazarenko, S., Meneghetti, P., Julmon, P., Olson, B. G., & Qutubuddin, S. (2007). Gas barrier of polystyrene montmorillonite clay nanocomposites: effect of mineral layer aggregation. Journal of Polymer Science Part B: Polymer Physics, 45(13), 1733-1753.

Oksman, K., Skrifvars, M., & Selin, J. F. (2003). Natural fibres as reinforcement in polylactic acid (PLA) composites. Composites science and technology, 63(9), 1317-1324.

Park, H. M., Lee, W. K., Park, C. Y., Cho, W. J., & Ha, C. S. (2003). Environmentally friendly polymer hybrids Part I Mechanical, thermal, and barrier properties of thermoplastic starch/clay nanocomposites. Journal of Materials Science, 38(5), 909-915.

Pereira, D., Losada, P. P., Angulo, I., Greaves, W., & Cruz, J. M. (2009). Development of a polyamide nanocomposite for food industry: morphological structure, processing, and properties. Polymer Composites, 30(4), 436-444.

Petersson, L., Kvien, I., & Oksman, K. (2007). Structure and thermal properties of poly (lactic acid)/cellulose whiskers nanocomposite materials. Composites Science and Technology, 67(11-12), 2535-2544.

Ray, S. S., Yamada, K., Ogami, A., Okamoto, M., & Ueda, K. (2002). New polylactide/layered silicate nanocomposite: nanoscale control over multiple properties. Macromolecular Rapid Communications, 23(16), 943-947.

Ray, S. S., Yamada, K., Okamoto, M., Fujimoto, Y., Ogami, A., & Ueda, K. (2003). New polylactide/layered silicate nanocomposites. 5. Designing of materials with desired properties. Polymer, 44(21), 6633-6646.

Sanchez-Garcia, M. D., Gimenez, E., & Lagaron, J. M. (2007). Novel PET nanocomposites of interest in food packaging applications and comparative barrier performance with biopolyester nanocomposites. Journal of Plastic Film & Sheeting, 23(2), 133-148.

Shiku, Y., Hamaguchi, P. Y., Benjakul, S., Visessanguan, W., & Tanaka, M. (2004). Effect of surimi quality on properties of edible films based on Alaska pollack. Food Chemistry, 86(4), 493-499.

Shirai, M. A., Olivato, J. B., Garcia, P. S., Müller, C. M. O., Grossmann, M. V. E., & Yamashita, F. (2013). Thermoplastic starch/polyester films: effects of extrusion process and poly (lactic acid) addition. Materials Science and Engineering: C, 33(7), 4112-4117.

Tabatabaei, S. H., & Ajji, A. (2012). Crystal structure and orientation of uniaxially and biaxially oriented PLA and PP nanoclay composite films. Journal of Applied Polymer Science, 124(6), 4854-4863.

Tang, X., Alavi, S., & Herald, T. J. (2008). Barrier and mechanical properties of starch-clay nanocomposite films. Cereal Chemistry, 85(3), 433-439.

Thellen, C., Orroth, C., Froio, D., Ziegler, D., Lucciarini, J., Farrell, R., & Ratto, J. A. (2005). Influence of montmorillonite layered silicate on plasticized poly (l-lactide) blown films. Polymer, 46(25), 11716-11727.

Wacharawichanant, S., Ratchawong, S., Hoysang, P., & Phankokkruad, M. (2017). Morphology and Properties of Poly (Lactic Acid) and Ethylene-Methyl Acrylate Copolymer Blends with Organoclay. In MATEC Web of Conferences (Vol. 130, p. 07006). EDP Sciences.

Wang, L., Ma, W., Gross, R. A., & McCarthy, S. P. (1998). Reactive compatibilization of biodegradable blends of poly (lactic acid) and poly (ε-caprolactone). Polymer Degradation and Stability, 59(1-3), 161-168.

Wang, L. F., Rhim, J. W., & Hong, S. I. (2016). Preparation of poly (lactide)/poly (butylene adipate-co-terephthalate) blend films using a solvent casting method and their food packaging application. LWT-Food Science and Technology, 68, 454-461.

Xu, J. (2015). Biobased nanocomposites for packaging applications—synthesis using melt extrusion of poly (lactic acid), poly (butylene succinate) and/or starch blended with natural nanofillers (Masters dissertation, Kansas State University).

Yampolskii, Y. P., Korikov, A. P., Shantarovich, V. P., Nagai, K., Freeman, B. D., Masuda, T., Teraguchi, M. & Kwak, G. (2001). Gas permeability and free volume of highly branched substituted acetylene polymers. Macromolecules, 34(6), 1788-1796.

Yang, F., Ou, Y., & Yu, Z. (1998). Polyamide 6/silica nanocomposites prepared by in situ polymerization. Journal of Applied Polymer Science, 69(2), 355-361.

Zhang, N., Wang, Q., Ren, J., & Wang, L. (2009). Preparation and properties of biodegradable poly (lactic acid)/poly (butylene adipate-co-terephthalate) blend with glycidyl methacrylate as reactive processing agent. Journal of Materials Science, 44(1), 250-256.

Zhao, P., Liu, W., Wu, Q., & Ren, J. (2010). Preparation, mechanical, and thermal properties of biodegradable polyesters/poly (lactic acid) blends. Journal of Nanomaterials, 2010, 4.

Zheng, Y. T., Cao, D. R., Wang, D. S., & Chen, J. J. (2007). Study on the interface modification of bagasse fibre and the mechanical properties of its composite with PVC. Composites part A: applied science and manufacturing, 38(1), 20-25.

Zhong, Y., Janes, D., Zheng, Y., Hetzer, M., & De Kee, D. (2007). Mechanical and oxygen barrier properties of organoclay-polyethylene nanocomposite films. Polymer Engineering & Science, 47(7), 1101-1107.

Chapter 3 - Use of thermoplastic starch in poly(lactic acid)/poly(butylene adipate-co-terephthalate) based nanocomposites for bio-based food packaging

Abstract

The primary focus of this study was incorporation of thermoplastic starch (TPS) in poly(lactic acid) (PLA)/poly(butylene adipate-co-terephthalate) (PBAT) blends to reduce the cost. Joncryl was used as a compatibilizer. Up to 40% TPS, 10% PBAT, 0.5% Joncryl and 2% NCC was blended with PLA using twin screw melt extrusion process before being pressed into 200 microns thick films. Mechanical, barrier, rheological, morphological and thermal properties of the films were characterized using instron, water vapor permeability (WVP), oxygen permeability (OP), capillary rheometer, x-ray diffraction (XRD), fourier-transform infrared spectroscopy (FTIR), transmission electron microscope (TEM) and differential scanning calorimetry (DSC). Rheological study showed that PBAT, TPS and NCC addition increased the shear viscosity of PLA. DSC study showed that crystallinity of the films decreased with the addition of Joncryl. Addition of PBAT along with Joncryl improved PLA film's elongation at break from 6.3 to 30.5% with a trade-off tensile strength reduction from 51.2 to 47.8 MPa. TPS addition decreased the mechanical properties, OP and increased the WVP; but addition of NCC increased the tensile strength of the PLA/PBAT/TPS blends and decreased the WVP and OP. TEM study showed that the dispersion of NCC improved with the addition of hydrophilic TPS.

3.1 Introduction

The primary role of food packaging is to protect the food from external factors such as biological (microorganisms), chemical (gases, moisture, light) and physical (mechanical damage) (Marsh & Bugusu, 2007). It is also essential to provide effective distribution, storage efficiency and preservation of food (Mihindukulasuriya & Lim, 2014), while satisfying the requirements of the industry and the consumers (product characteristics, marketing and environmental issues) in a cost-effective way. The desirable barrier and mechanical properties of the material and low cost is widely increasing the use of petroleum-based plastics in food packaging (Marsh & Bugusu, 2007).

However, petroleum-based plastic packaging also has some disadvantages as it contributes to waste disposal problems and environmental toxicity. These petroleum-based resources are also non-renewable. Renewable and bio-based plastics can be used to replace non-renewable petroleum-based resources. Among the bioplastics, poly(lactic acid) (PLA) is a promising material and one of the widely growing sector in the market of bioplastics in 2016 (Global bioplastics market, 2017). PLA is an aliphatic thermoplastic polyester with a range of desirable properties including biodegradability in composting conditions, high strength and high modulus (Wacharawichanant et al., 2017). The cost of PLA is also comparable to that of conventional polyolefin polymers. However, PLA based films are brittle i.e. low % elongation at break. To improve the elongation of PLA, it can be blended with other flexible polymers such as poly (caprolactone) (PCL), poly (butylene succinate) (PBS), poly (butylene adipate-co-terephthalate) (PBAT) (Kumar et al., 2010; Wang et al., 1998; Zhao et al., 2010). PBAT, a fully biodegradable aliphatic-aromatic copolyester is a good candidate to decrease the brittleness of PLA and is selected in our study. Due to high cost of polymers PLA and PBAT, it can be

blended with starch to make it cost-effective. Starch is a widely available and naturally occurring biodegradable polymer and hence can be considered as an economically viable alternative (Ayana et al., 2014).

The melting temperature of native starch (T_m = 220–250^o C) is high and is close to its degradation temperature (~220^o C) (Ayana et al., 2014). Plasticizers can be used to decrease the melting temperature of starch as they form a hydrogen bond with the starch (i.e. amylose) molecules and decrease the inter-molecular hydrogen bonding sites in the crystalline parts of starch. Hence, native starch can be converted into thermoplastic starch (TPS) using thermo-mechanical treatment in the presence of plasticizers such as water, glycerol, sorbitol etc. (Wiedmann & Strobel, 1991). Addition of TPS also increases the rate of biodegradation of PLA in all conditions (Akrami et al., 2016; Iovino et al., 2008) as the various microorganisms can easily use starch as an energy source. Previous studies on PLA/TPS blends and PBAT/TPS blends have shown poor mechanical properties due to poor interfacial adhesion between hydrophilic TPS and hydrophobic PLA, PBAT (Brandelero et al., 2011; Garcia et al., 2014; Ke & Sun, 2000; Olivato et al., 2013; Ren et al., 2007; Stagner & Narayan, 2011; Wang et al., 2008). A compatibilizer can be used to increase the miscibility between these polymers. The typical compatibilizers used in PBAT/TPS blends are maleated TPS (Hablot et al., 2013; Stagner et al., 2012), maleated PBAT (Mohanty & Nayak, 2010; Nabar et al., 2005), maleic anhydride, citric acid (Olivato et al., 2011; Olivato et al., 2012), adipic acid (Silva et al., 2013) and the typical compatibilizers used in PLA/TPS blends are maleated TPS (Huneault & Li, 2007), acrylic acid (Wu, 2005). Joncryl ADR 4368C is a compatibilizer that contains GMA/epoxide functions. It is a multi-functional oligomeric chain extender that reacts with both the hydroxyl groups of TPS and carboxyl groups of PLA and PBAT thereby improving the interfacial

adhesion between various polymers (Al-Itry et al., 2012; Walha et al., 2016; Wei et al., 2015). Figure 3.1 shows the predicted reaction of Joncryl with PLA, PBAT and TPS.

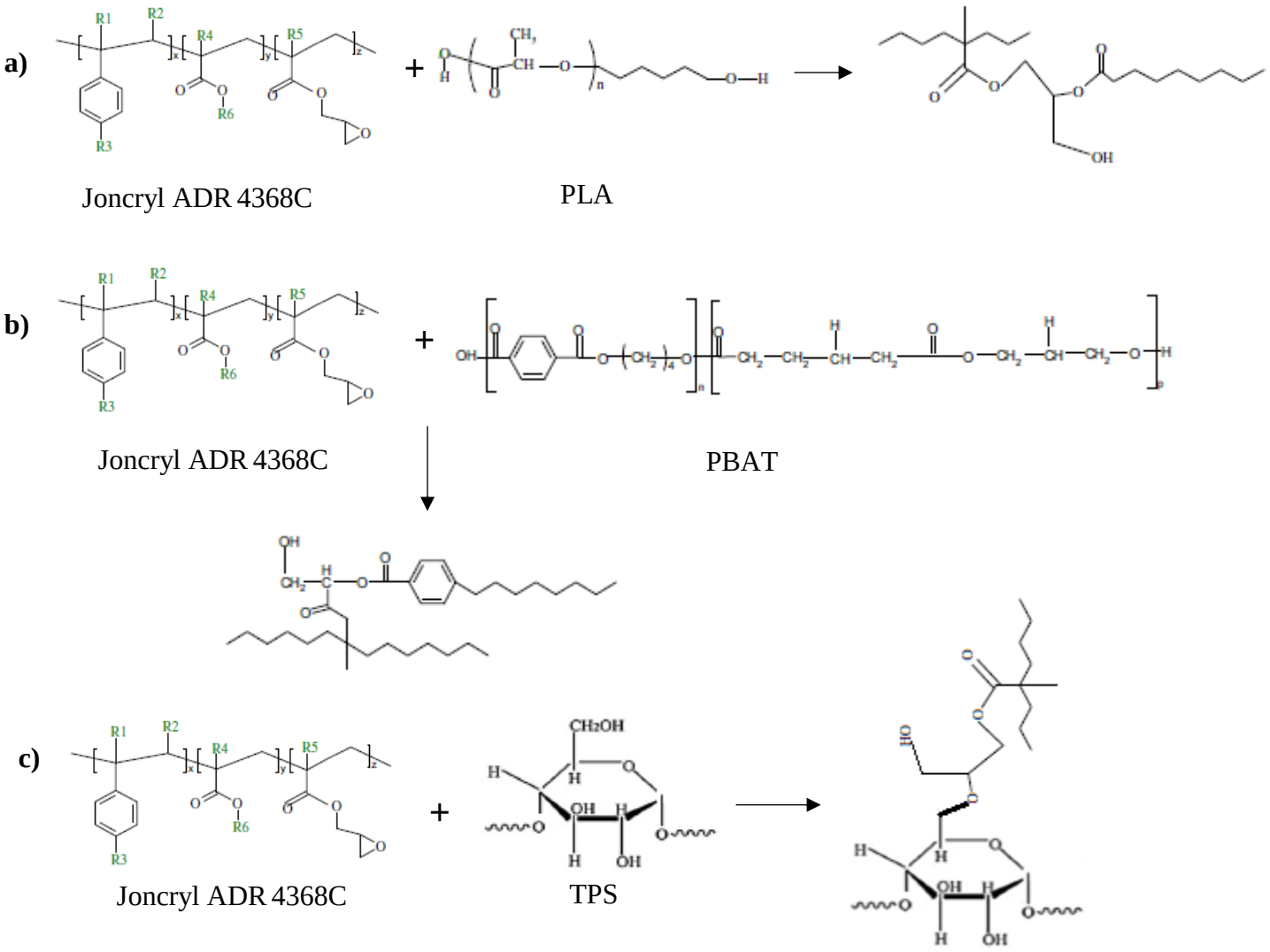

Figure 3.1 Reaction of compatibilizer Joncryl ADR 4368C with a) PLA b) PBAT c) TPS where R1–R5 are H, CH3, a higher alkyl group or combinations of them and R6 is an alkyl group; x, y, z are between 1 and 20.

However, TPS based packaging have some limitations due to its high hydrophilic nature and weak mechanical properties (Babaee et al., 2015; Rico et al., 2016; Teixeira et al., 2009). One of the promising methods to address this limitation is the use of nanofiller to improve the

mechanical and barrier properties of bioplastics (Fortunati et al., 2012b). The incorporation of nanofillers into various natural and synthetic polymers such as polystyrene, polyamide, poly(ethylene terephthalate, poly(lactic acid), poly(vinyl chloride), thermoplastic starch etc. were widely reported over the past 30 years (Joon Choi et al., 2006; Nazarenko et al., 2007; Park et al., 2003; Pereira et al., 2009; Ray et al., 2003; Sanchez-Garcia et al., 2007; Thellen et al., 2005). The nanofiller used in this study was nanocrystalline cellulose (NCC). NCC has various properties such as durability and high biodegradability (Brinchi et al., 2013). The structure of NCC is generally rod-shaped of about 5-10 nm in width and 100-200 nm in length (Fortunati et al., 2012a). They have a very high aspect ratio (length/diameter) and a large surface area (Matos Ruiz et al., 2000).

In the present study, PLA/PBAT/TPS/NCC nanocomposites at various ratios have been melt blended using twin screw extrusion. Then, the mechanical, barrier, morphological, rheological and thermal properties of the nanocomposites were investigated.

3.2 Experimental

3.2.1 Materials

High amylose corn starch Hylon V (~55% amylose content) was supplied by Ingredion. Poly (lactic acid), PLA4032D (Density: 1.25 g/cc, Average molecular weight: 100,000 g/mol), was purchased from Natureworks and Poly (butylene adipate-co-terephthalate), Ecoflex® F Blend C1200 (Density: 1.25 g/cc, Average molecular weight: 145,000 g/mol) and Joncryl ADR 4368C were obtained from BASF. Plasticizer sorbitol was purchased from Sigma-aldrich and nanocrystalline cellulose (NCC) was purchased from University of Maine.

3.2.2 Synthesis of thermoplastic starch (TPS)

Thermoplastic starch (TPS) was prepared by mixing dry starch (64%) with sorbitol (36%) using a corotating lab-scale twin screw extruder (Micro-18, American Leistritz, Somerville, NJ, USA). The extruder has a six head configuration, screw diameter of 18 mm and length-diameter ratio of 30:1. The barrel temperatures of the heads used for extrusion were 100-140-140-140-140-140 ^{o}C. The extrudate was then ground using a Wiley mill (Model 4, Thomas-Wiley Co., Philadelphia, PA) for further use.

3.2.3 Melt blending

All the materials were dried at 80^{o} C for 8 hours in an air oven to remove moisture. The nanocomposites were melt blended using a laboratory-scale co-rotating twin screw extruder (Micro-18, American Leistritz, Somerville, NJ). The barrel temperatures of the heads used for extrusion were 100-180-180-180-180-180 ^{o}C. The extrudates were ground using a Wiley mill (Model 4, Thomas-Wiley Co., Philadelphia, PA) for further use. Sample designations and the relevant sample formulations are shown in Table 3.1. PLA to PBAT ratio of 9:1 was used based on the previous study (Chapter 2) which showed an increase in elongation of PLA with addition of 10% PBAT.

3.2.4 Rheological analysis

Capillary rheometer (RH2000, Malvern Instruments Ltd, UK) was used to study the rheological properties of the blends. Test was conducted in the shear rate range from 20 to 5000 s^{-1} at 180^{o}C. The dimensions of the capillary die used was diameter of 1 mm and length of 16 mm.

3.2.5 Differential scanning calorimetry (DSC)

Differential scanning calorimeter (DSC Q100, TA Instruments, New Castle) was used to study the thermal properties of the blends. In this study, DSC measurements were carried out in the following steps; the samples were heated from 20°C to 200°C at 25°C/min (first heating scan) and was kept at 200°C for 2 minutes to erase the previous thermal history in the samples. They were subsequently cooled to 20°C at 10°C/min (cooling scan) to evaluate the crystallization ability of the component and then heated up to 200°C at 10°C/min (second heating scan).

Table 3.1 Sample designations and relevant sample components

Formulation	(PLA-PBAT)* (%)	TPS (%)	Joncryl** (%)	NCC** (%)
100%(PLA-PBAT)	100	0	0	0
100%(PLA-PBAT)/JC	100	0	0.5	0
100%(PLA-PBAT)/JC /1%NCC	100	0	0.5	1
100%(PLA-PBAT)/JC /2%NCC	100	0	0.5	2
80%(PLA-PBAT)/20%TPS/JC	80	20	0.5	0
80%(PLA-PBAT)/20%TPS/JC/1%NCC	80	20	0.5	1
80%(PLA-PBAT)/20%TPS/JC/2%NCC	80	20	0.5	2
60%(PLA-PBAT)/40%TPS/JC	60	40	0.5	0
60%(PLA-PBAT)/40%TPS/JC/1%NCC	60	40	0.5	1
60%(PLA-PBAT)/40%TPS/JC/2%NCC	60	40	0.5	2

*(PLA-PBAT) contains 9:1 ratio of PLA:PBAT
**The weight of Joncryl and NCC was based on polymer basis

Crystallinity of PLA was calculated using the equation given below

$$X_c\,(\%) = \frac{Hm - Hcc}{Hm1} \times \frac{1}{Wpla} \times 100\%$$

where, H_m was the melting enthalpy and H_{cc} was the cold crystallization enthalpy, H_{m1} was the melting enthalpy of pure 100% crystalline PLA i.e.93 J/g (Arrieta et al., 2014, Fischer et al., 1993) and W_{PLA} represents the weight fraction of PLA. The analyses were conducted in duplicate.

3.2.6 X-ray diffraction (XRD)

X-ray diffraction analysis (XRD) was carried out using a wide-angle X-ray diffractometer (PANalytical, Almelo, Netherland) which has a Cu radiation source of wavelength 1.54 A^o operating at 45kV and 40mA. Scans were carried out at diffraction angle (2θ) of 5.0-40.0^o with step size of 0.007°.

3.2.7 Fourier-transform infrared spectroscopy (FTIR)

FTIR spectra of PLA/PBAT blends with and without compatibilizer Joncryl were recorded using FTIR spectrophotometer (Carey 630, Agilent Technology, Santa Clara, CA) with a diamond crystal collecting 32 scans. Each spectrum was obtained within the range of 4000–650 cm^{-1} with a resolution of 2 cm^{-1}.

3.2.8 Film preparation

Hot press (Model 3889, Carver Inc., Wabash, IN) with process parameter of force of 2100 lb and temperature of hot plates at 180^{o}C (top and bottom) was used to make the films of thickness of about 200 microns. The hot sample was preheated at 180°C for 5 min and then further pressed for 5 minutes using the hotpress.

3.2.9 Transmission electron microscopy (TEM)

FEI Tecnai F20XT transmission electron microscope (FEI North America, Hillsboro, OR) operated at 100 kV was used for TEM of the samples. The samples were obtained by using ultra-microtome to obtain slices of about 100nm thick. TEM images were used to study the morphological properties of the blends and visually characterize the interactions between the nanofiller and the base polymers.

3.2.10 Mechanical properties

Mechanical properties of the films were measured using Instron testing machine (Model 4465, Canton, MA, USA) based on standard ASTM D882 method. Films were cut into 1.3 cm wide and 10 cm long strips and conditioned at 23^{o} C and 50% RH for two days before testing for tensile strength and elongation ratio. The Tensile strength (TS) and elongation at break (EB) were calculated as given in the equations below:

$$TS=\frac{Lp}{a} \times 10^{-6}\ MPa$$

where Lp= peak load (N) and a= cross-sectional area (m^2)

$$EB= \delta L/L \times 100\ (\%)$$

where δL= increase in length at breaking point (mm) and L= original length (mm)

All the measurements were reported as the average of five samples.

3.2.11 Water vapor permeability (WVP)

Water vapor permeability (WVP) was determined gravimetrically according to the standard method E96-00 (ASTM 2000). The films were fixed on top of test cells containing a desiccant (silica gel). Test cells were placed in a relative humidity chamber with controlled temperature and relative humidity (25^{o} C and 85% RH). After steady-state conditions were

reached, the weight of the test cells was measured every 24 hours over a five-day period. The slope of each line was calculated by linear regression (R^2>0.99), and the water vapor transmission rate (WVTR) was calculated from the slope of the straight line (W/t) divided by the transfer area (A):

$$\text{WVTR} = \frac{(\frac{W}{t})}{A} \text{ g/h.m}^2$$

where W = change in weight (g), t = time (h) and A = area of transfer (m^2)

WVP was then calculated from WVP using the equation given below

$$\text{WVP} = \frac{WVTR * t}{\Delta P} \text{ g*mm/kPa.h.m}^2$$

where t = film thickness (mm) and ΔP = pressure difference across the films (kPa).

All the measurements were reported as the average of two samples.

3.2.12 Oxygen permeability (OP)

Oxygen permeability of the film was determined by Mocon Ox-Tran® 2/21 model (MOCON Inc., Minneapolis, MN) using a standard ASTM D-3985 method. Exposed film area of 50 cm^2 and film thickness of 200 micron was used for analysis. 100% Oxygen was used on one side of the film and a mixture of 98% nitrogen (N_2) and 2% Oxygen (O_2) was used on the other side. Measurements were carried out at 22.8^o C. Oxygen transmission rate (OTR) obtained from the instrument is converted to oxygen permeability (OP) by dividing it by the pressure difference of oxygen across the film (100 kPa) and multiplying it with thickness of the film (200 microns).

3.2.13 Statistical analysis

Data was analyzed using SAS studio analysis software. Statistical significance of differences was calculated using Tukey's range test, $P < 0.05$.

3.3 Results and discussion

3.3.1 Rheological properties

The rheological properties of the PLA/PBAT/TPS nanocomposites are shown in Figure 3.2(a-c). The shear viscosity curves of the blends show their shear-thinning behavior. Addition of Joncryl led to increase in viscosity of the PLA/PBAT blends as Joncryl improves the miscibility between the polymers PLA and PBAT (Figure 3.2a). This leads to the increase in molecular interactions which results in restriction of movement of molecular chains (Zhang et al., 2009). It leads to formation of long chain branching structure which indirectly increases the average molecular weight. The shear thinning behavior of the blends also increases with addition of Joncryl due to the formation of long chain branches during the reactive extrusion. TPS addition led to increase in shear viscosity (Figure 3.2a) due to high average molecular weight of starch. Other rheological studies have reported the increase in viscosity with addition of starch in

a)

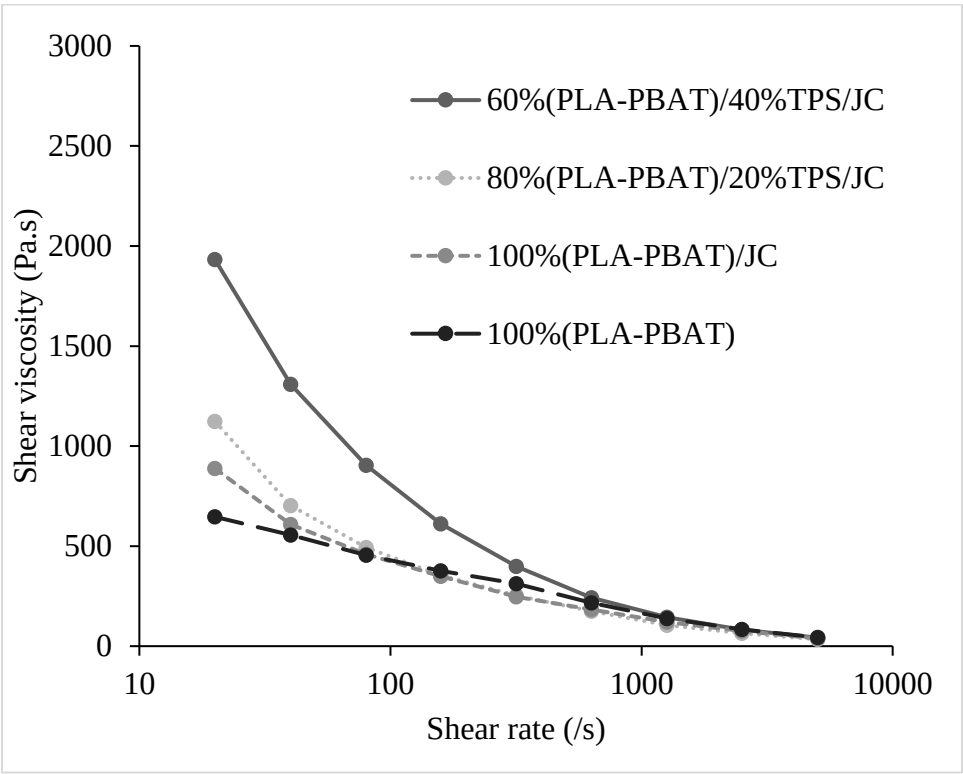

b)

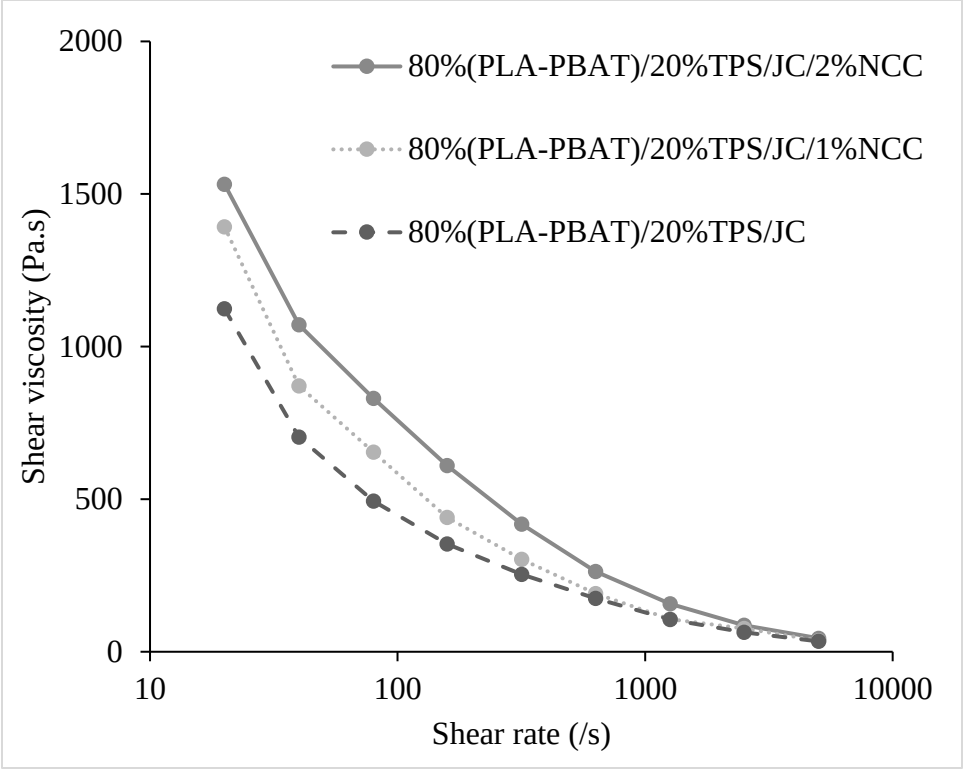

c)

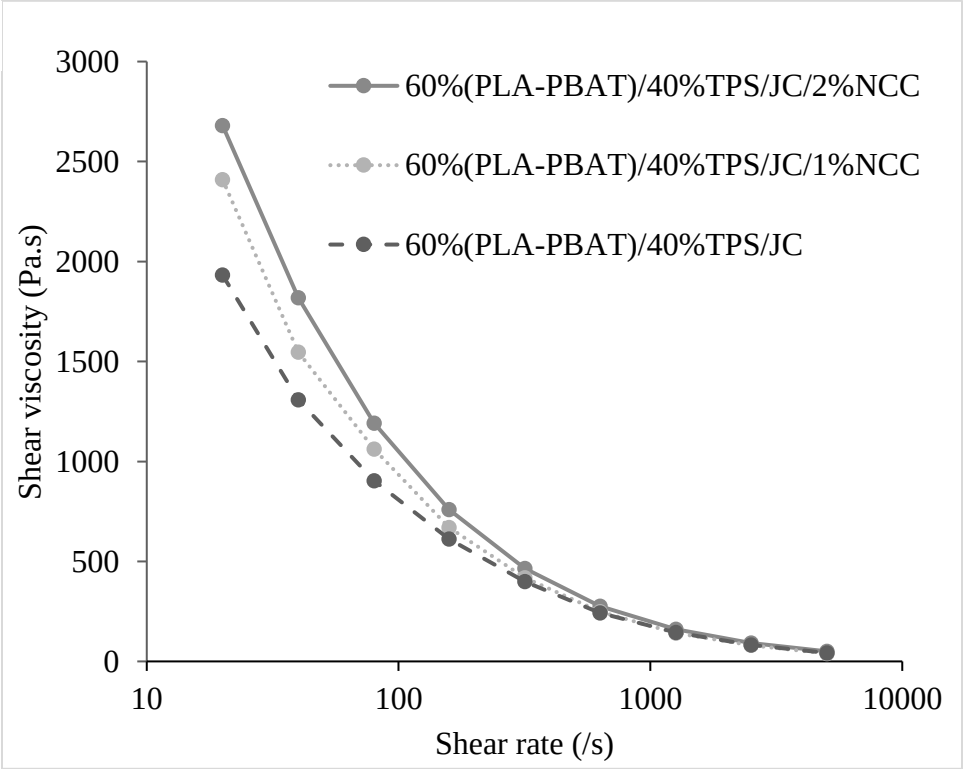

Figure 3.2 Rheological behavior of PLA/PBAT/TPS nanocomposites

starch-polyvinyl alcohol blends (Villar et al., 1995), starch-polyethylene blends (Nield et al., 2000, Peres et al., 2016), starch-polycaprolactone blends (Kalambur & Rizvi, 2006). Addition of NCC led to increase in the shear viscosity of the blends (Figure 3.2b, 3.2c). This may be due to the hindrance of flow by the nanofiller particles in the polymer matrix, hence restricting the movement of polymer chains (Chow et al., 2005; Dangtungee et al., 2011).

3.3.2 Thermal properties

The mechanical and barrier properties of the polymers can also be related to the thermal properties of the nanocomposites i.e. crystallinity. Hence, DSC was used to evaluate the thermal properties of the nanocomposites. The DSC thermogram of 60%(PLA-PBAT)/40%TPS/JC with all the heating and cooling scans is shown in Figure 3.3. Glass transition, crystallization and melting phenomena were observed for all the DSC thermograms. The glass transition

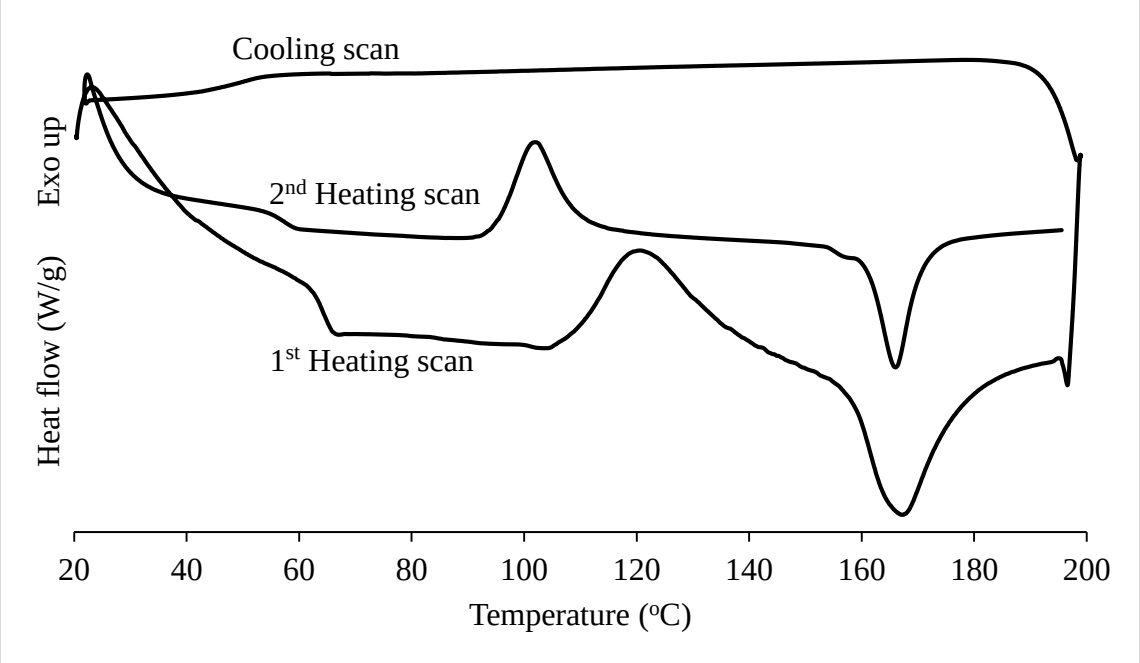

Figure 3.3 DSC thermogram of 60%(PLA-PBAT)/40%TPS/JC with all the heating and cooling scans

temperature during cooling scan (T_g^c) and second heating scan (T_g^h) is shown in Table 3.2. The range of glass transition temperature during cooling scan was slightly broader (~11^{o}C) than the range of glass transition temperature during second heating scan (~4^{o}C) and T_g^c were lower compared to T_g^h. Assymetry and hysteresis, the inherent characteristics of the glass transition phenomena contributes to the difference in glass transition temperatures between the cooling and the second heating scan. A monotonic decrease in heat capacity occurs during the cooling scan while a nonmonotonic and overshoot of small endothermic peak occurs during the second heating scan (Ruiz-Cabrera & Schmidt, 2015). The exhibition of different glass transition temperatures during cooling and second heating scan is common and depends on the ratio of cooling rate to heating rate (Badrinarayan et al., 2007; Hutchinson, 2009; Keys et al., 2013).

Table 3.2 Glass transition temperatures during cooling scan and second heating scan of DSC thermograms

Formulation	T_g^c (^{o}C)	T_g^h (^{o}C)
100%(PLA-PBAT)	56.57 ± 0.49	51.43 ± 0.35
100%(PLA-PBAT)/JC	57.02 ± 0.16	51.88 ± 1.22
100%(PLA-PBAT)/JC/1%NCC	57.05 ± 0.4	51.54 ± 0.05
100%(PLA-PBAT)/JC/2%NCC	57.22 ± 0.06	51.72 ± 0.39
80%(PLA-PBAT)/20%TPS/JC	55.87 ± 0.11	51.01 ± 0.03
80%(PLA-PBAT)/20%TPS/JC/1%NCC	56.37 ± 0.67	50.22 ± 0.5
80%(PLA-PBAT)/20%TPS/JC/2%NCC	56.12 ± 0.11	50.53 ± 0.46
60%(PLA-PBAT)/40%TPS/JC	57.42 ± 0.11	50.74 ± 0.4
60%(PLA-PBAT)/40%TPS/JC/1%NCC	57.78 ± 0.09	50.31 ± 0.57
60%(PLA-PBAT)/40%TPS/JC/2%NCC	57.33 ± 0.3	50.99 ± 0.15

T_g^c – Glass transition temperature during cooling scan, T_g^h – during second heating scan

The DSC second heating scans of the PLA/PBAT/TPS blends are shown in Figure 3.4. Additionally, cold crystallization temperature (T_{cc}), melting temperature (T_m), cold crystallization enthalpy (H_{cc}), melting enthalpy (H_m) and percent of crystallinity (X_c) obtained from the second DSC heating thermograms are shown in Table 3.3. DSC thermogram of neat PLA exhibited a glass transition centered at 57ºC, an exothermic cold crystallization peak at 105ºC and an endothermic peak at 167ºC. These phenomena typically occur in PLA and the values are comparable to those reported in scientific literature (Battegazore et al., 2014; Frone et

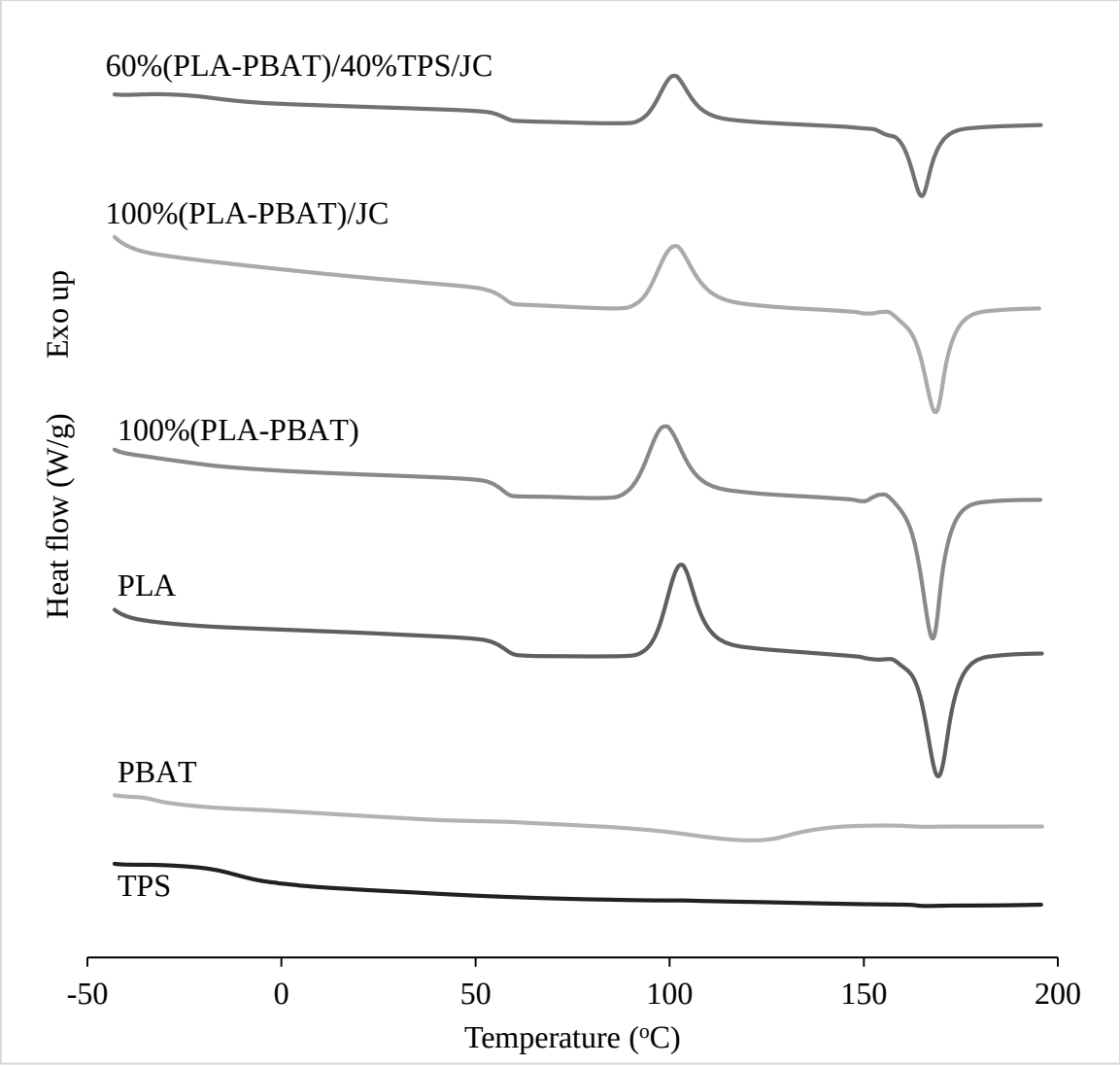

Figure 3.4 Second heating DSC thermograms of PLA/PBAT/TPS blends

al., 2013; Petersson et al., 2007). Similarly, second heating scan of neat PBAT exhibited a glass transition temperature centered at -33^{o}C and an endothermic melting phenomenon with onset at 91^{o}C and a broad peak at 120^{o}C. These phenomena typically occur in PBAT and the values are comparable to those reported in scientific literature (Arruda et al., 2015; Kumar et al., 2010). Addition of PBAT decreased the T_c significantly from 105^{o}C to 99^{o}C and led to the decrease in H_{cc} from 28.45 to 21.6 J/g thus indicating the increase in crystallization ability of PLA, as reported previously (Arruda et al., 2015; Jiang et al., 2006). The melting phenomena of PBAT occurs at around the same temperature as the crystallization phenomena of PLA. Hence, it was not possible to determine the melting temperature of PBAT in the blends. This may lead to slightly lower values of H_{cc} of PLA due to the melting enthalpy of PBAT. However, the content of PBAT in the PLA/PBAT/TPS nanocomposites used in this study is also low to affect the values of H_{cc} and X_c. The second heating scan of pure TPS displayed a glass transition peak centered at -18^{o}C. This value is in good agreement with the glass transition reported in literature (Averous et al., 2000; Lourdin et al., 1997). DSC thermogram of 60%(PLA-PBAT)/40%TPS/JC showed the glass transitions of TPS and the three transformations of PLA – glass transition, crystallization and melting phenomena. Addition of Joncryl increased the crystallization temperature T_c and decreased the crystallinity of the blends (X_c) as it leads to formation of a long chain branching structure which is not easily incorporated in the crystal lattice instead of forming a long chain linear structure like other chain extenders (Najafi et al., 2012; Jaszkiewicz et al., 2014). Hence, Joncryl interrupts the packing of molecular chains thereby hindering the crystallization of PLA. The formation of long chain branching structure was also in confirmation with the rheological results.

Table 3.3 Data obtained from second DSC heating scans of PLA/PBAT/TPS nanocomposites

Formulation	T_c (°C)	T_m (°C)	H_{cc}(J/g)	H_m(J/g)	X_c(%)
100%(PLA-PBAT)	98.87^{a}	167.7^{a}	21.6^{ab}	29.27^{a}	9.16^{a}
100%(PLA-PBAT)/JC	101.86^{bc}	167.67^{a}	22.67^{b}	24.61^{b}	2.36^{b}
100%(PLA-PBAT)/JC/1%NCC	104.41^{d}	165.86^{a}	22.03^{ab}	23.92^{bc}	2.28^{b}
100%(PLA-PBAT)/JC/2%NCC	103.31^{bd}	167.45^{a}	21.35^{ab}	23.51^{bc}	2.64^{b}
80%(PLA-PBAT)/20%TPS/JC	100.51^{ace}	164.9^{a}	19.97^{ab}	21.3^{cd}	1.99^{b}
80%(PLA-PBAT)/20%TPS/JC/1%NCC	101.08^{ce}	166.19^{a}	18.73^{bc}	20.12^{d}	2.1^{b}
80%(PLA-PBAT)/20%TPS/JC/2%NCC	99.98^{ae}	165.35^{a}	19.73^{ab}	21.27^{cd}	2.35^{b}
60%(PLA-PBAT)/40%TPS/JC	101.81^{bc}	166^{a}	15.77^{cd}	17.04^{e}	2.52^{b}
60%(PLA-PBAT)/40%TPS/JC/1%NCC	102.17^{bc}	165.67^{a}	14^{d}	14.49^{e}	2.05^{b}
60%(PLA-PBAT)/40%TPS/JC/2%NCC	101.37^{ce}	165.45^{a}	13.48^{d}	15.19^{e}	2.41^{b}

Different superscripts within the same column indicate significant difference ($P<0.05$) between treatments.

3.3.3 X-ray diffraction (XRD)

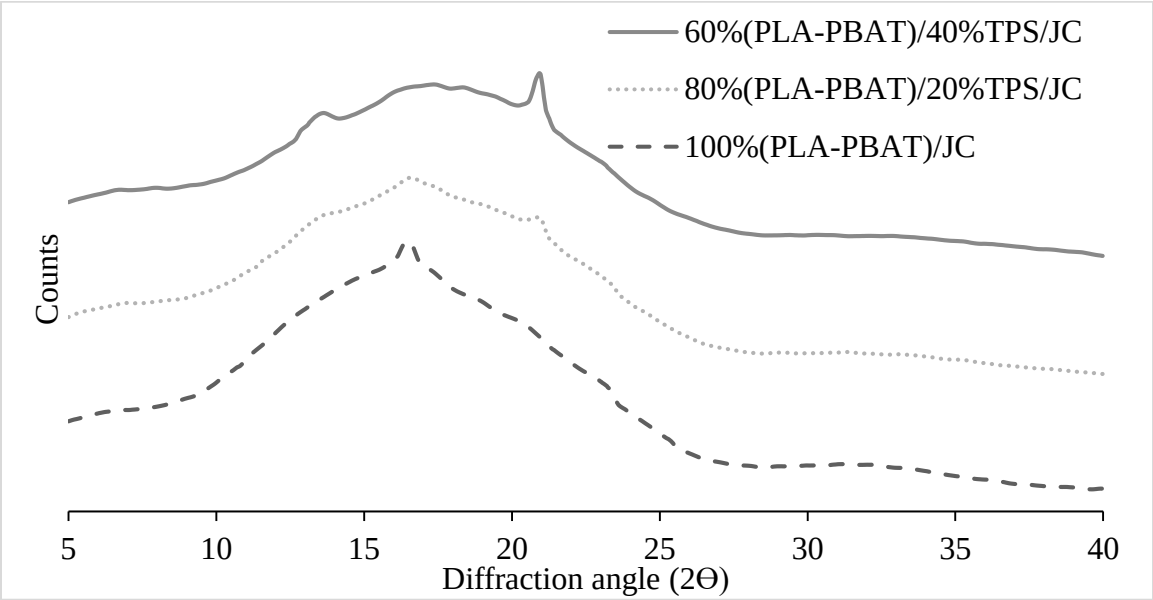

Figure 3.5 XRD of PLA/PBAT/TPS blends

X-ray diffraction (XRD) was used to study the changes in the crystalline structure of the blends. Figure 3.5 shows the XRD curves of PLA/PBAT/TPS blends. 100%(PLA-PBAT)/JC showed a diffraction peak at $2\Theta = 16.5^{o}$ which is attributed to (110/200) crystalline plane of PLA (Abdelwahab et al., 2012; Tabatabaei et al., 2012). Addition of TPS led to the appearance of new peaks at 13.5^{o} and 21^{o}. Native corn starch generally displays a A-type crystallinity with peaks at around 15^{o}, 18^{o} and 23^{o} (Castano et al., 2012; Rico et al., 2016). These crystalline peaks may be related to the recrystallization of sorbitol. However, pure sorbitol shows very significant crystalline peak at $2\Theta = 18.5^{o}$ (Mathew & Dufresne, 2002) which did not appear on the XRD of the blends. Previous studies have shown that these peaks may also correspond to the V- type crystal structure which is formed by the complexing of plasticizers with starch (Angles & Dufresne, 2000; Li & Huneault, 2011; Liu et al., 2009; Rico et al., 2016). Further experiments are needed to verify the formation of the V-type structure. One way to verify the formation would be melt blending the waxy starch with sorbitol and evaluating the XRD peaks of this

blend. V-type structure consists of six-fold single helices of amylose forming complexes with the plasticizer (sorbitol). Hence, absence of these peaks in the blend of sorbitol and waxy starch can lead to confirmation of the formation of V-type crystals.

3.3.4 Fourier-transform infrared spectroscopy (FTIR)

The FTIR spectra of PLA/PBAT/TPS blends is shown in Figure 3.6. The two peaks in the region of 2900-3000 cm^{-1} correspond to the antisymmetric and symmetric stretching vibrations of the axial C-H groups in PLA and PBAT. The sharp peak at 1748 cm^{-1} in the FTIR spectra is associated with the stretching of C=O in the ester linkages. There was a shift in the peak towards lower wavenumber 1182 cm^{-1} to 1176 cm^{-1} with the addition of Joncryl to the PLA/PBAT blend which is an indicative of an increase in C-O stretching in carboxylic group. This indicates a strong chemical interaction between the polymers. Addition of TPS led to the presence of a broad peak in 3000-3400 cm^{-1} which corresponds to the O-H stretch in hydroxyl groups and additional peak at 1010 cm^{-1} which correspond to the C-O stretch in hydroxyl groups. The reaction of epoxy group of Joncryl with carboxyl groups of PLA, PBAT and hydroxyl group of TPS led to the presence of a new C-O-C peak at 1735 cm^{-1}. Hence, Joncryl addition can lead to increase in interfacial adhesion between the polymers.

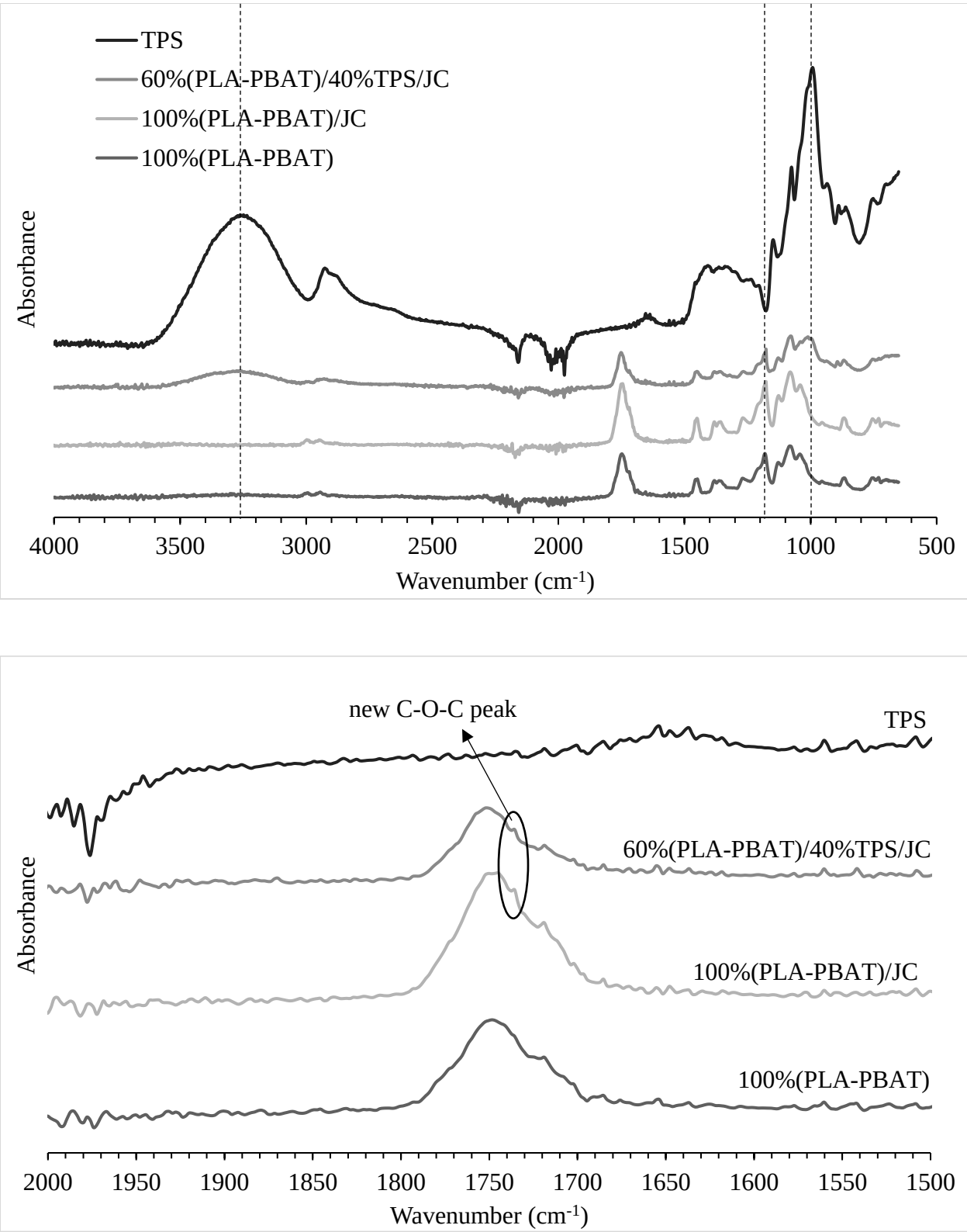

Figure 3.6 FTIR spectra of PLA/PBAT/TPS blends

3.3.5 Transmission electron microscopy (TEM)

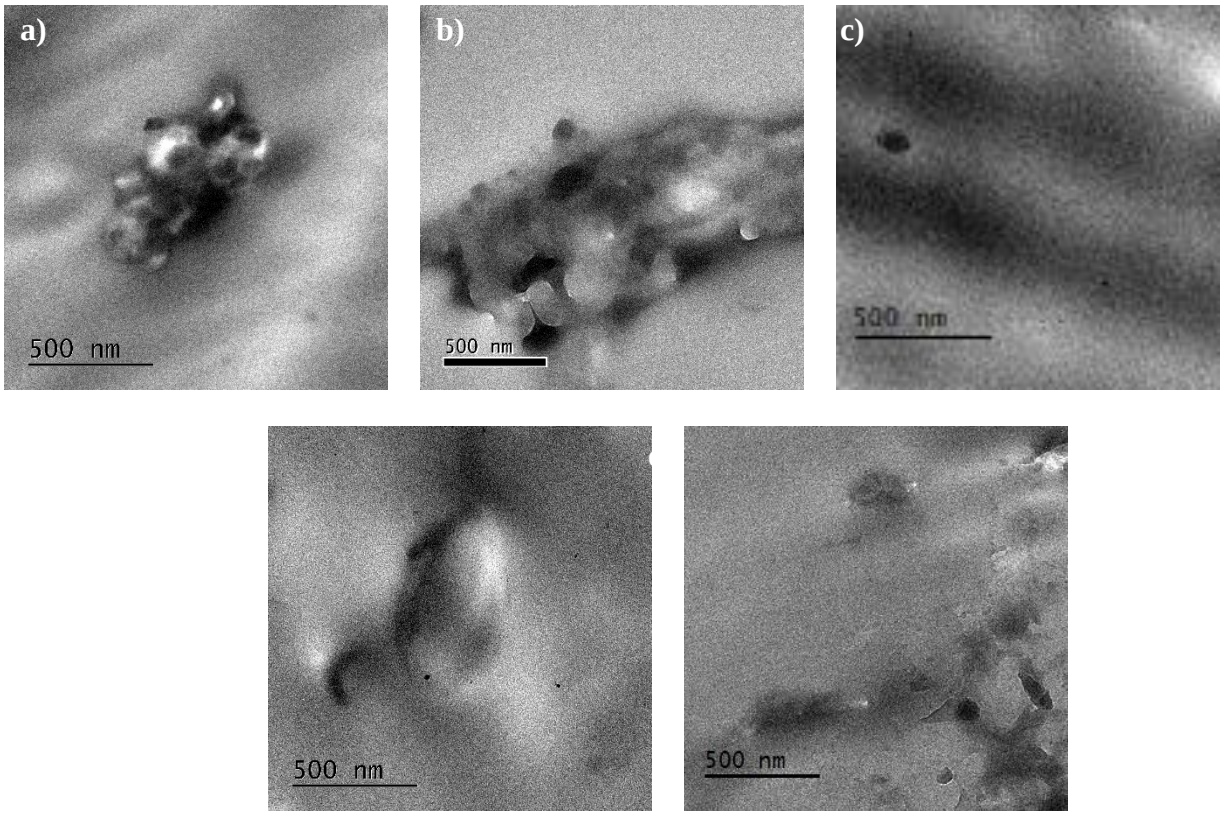

Figure 3.7 TEM image of a)100%(PLA-PBAT)/JC/1%NCC b)100%(PLA-PBAT)/JC/2%NCC c)80%(PLA-PBAT)/20%TPS/JC/2%NCC d)60%(PLA-PBAT)/40%TPS/JC/1%NCC e)60%(PLA-PBAT)/40%TPS/JC/2%NCC

Figure 3.7(a-e) shows the nanostructure dispersion in the PLA/PBAT/TPS nanocomposites analyzed by TEM. For the PLA/PBAT binary blend (Figure 3.6a, b), it was observed that the nanofiller NCC was aggregated in the PLA/PBAT matrices. Dispersion of hydrophilic NCC is difficult to obtain in hydrophobic polymers such as PLA, PBAT due to the difference in polarity based on the hydrophilic nature of the nanofiller and intermolecular hydrogen bonding between the nanofillers (Espino-Perez et al., 2013; Martinez-Sanz et al., 2013). The aggregation of NCC in polymer matrix was also observed in previous studies (Arrieta et al., 2014; Xu et al., 2015). Dispersion of NCC was more uniform in the ternary blends PLA/PBAT/TPS (Figure 3.7c-e).

This may be due to the addition of hydrophilic TPS which led to better dispersion of the nanofiller in the polymer matrix.

3.3.6 Mechanical properties

Table 3.4 shows the mechanical properties of the PLA/PBAT/TPS nanocomposites. Regarding the elongation at break of PLA, addition of 10% PBAT led to about 100% increase from 6.3% to 12.6% (Chapter 2). Addition of Joncryl to the PLA/PBAT binary blend further increased the elongation at break from 12.6% (100%(PLA-PBAT)) to 30.5% (100%(PLA-PBAT)/JC). This may be due to the increase in interfacial adhesion between PLA and PBAT due to epoxy reaction of Joncryl with carboxyl groups of PLA and PBAT. However, addition of NCC did not have any effect on the tensile strength of the PLA/PBAT binary blends. Theoretically, the complete dispersion of nanofiller in the polymer matrix facilitates the increase in available reinforcing elements for carrying an applied stress. The coupling between the polymer matrix and the large surface area of the nanofiller optimizes the load transfer to the reinforcement elements, thereby leading to increase in tensile strength. However, TEM images showed the aggregation of NCC in the PLA/PBAT matrix (Figure 3.7a, b) which caused NCC to act as a microcomposite rather than as a nanocomposite thereby negating the reinforcement effect of the nanofillers. Addition of nanofiller also led to decrease in elongation at break as the nanofiller reduces the mobility of the polymer chain i.e. confinement of polymer chains and contributes to the higher breaking tendency of the nanocomposite films. Several other studies also showed the decrease in elongation at break with increase in nanofiller content (Ali et al., 2011; Khalil et al., 2017; Tang et al., 2008).

Table 3.4 Mechanical properties of PLA/PBAT/TPS nanocomposites

Formulation	Tensile Strength (MPa)	Elongation at break (%)
100%(PLA-PBAT)	45.37 ± 3.86^{a}	15.07 ± 2.7^{a}
100%(PLA-PBAT)/JC	47.84 ± 2.13^{a}	30.52 ± 1.81^{b}
100%(PLA-PBAT)/JC /1%NCC	47.45 ± 1.59^{a}	10 ± 1.55^{c}
100%(PLA-PBAT)/JC /2%NCC	47.82 ± 1.9^{a}	11.33 ± 2.15^{c}
80%(PLA-PBAT)/20%TPS/JC	25.46 ± 2.05^{b}	10.09 ± 0.49^{c}
80%(PLA-PBAT)/20%TPS/JC/1%NCC	28.85 ± 1.69^{bc}	10.15 ± 0.69^{c}
80%(PLA-PBAT)/20%TPS/JC/2%NCC	30.98 ± 1.32^{c}	10.13 ± 1.5^{c}
60%(PLA-PBAT)/40%TPS/JC	15.88 ± 0.97^{d}	10.19 ± 1.11^{c}
60%(PLA-PBAT)/40%TPS/JC/1%NCC	17.53 ± 0.74^{de}	10.52 ± 0.89^{c}
60%(PLA-PBAT)/40%TPS/JC/2%NCC	20.54 ± 0.95^{e}	10.02 ± 1.45^{c}

Different superscripts within the same column indicate significant difference ($P<0.05$) between treatments.

Addition of TPS decreased the tensile strength of the films which was expected due to lower strength of TPS compared to the polymers. In case of ternary PLA/PBAT/TPS blends, addition of nanofiller NCC led to the increase in tensile strength. This may be due to uniform dispersion of NCC in the polymer matrix due to the addition of hydrophilic TPS. This is in confirmation with the TEM results which showed better dispersion of nanofiller with addition of TPS (Figure 3.7c-e).

3.3.7 Barrier properties

Table 3.5 Water vapor permeability (WVP) of PLA/PBAT/TPS nanocomposites

Formulation	WVP (g.mm/m^2.day.kPa)
100%(PLA-PBAT)	1.81 ± 0.03^a
100%(PLA-PBAT)/JC	1.62 ± 0.05^a
100%(PLA-PBAT)/JC /1%NCC	1.63 ± 0.02^a
100%(PLA-PBAT)/JC /2%NCC	1.64 ± 0.06^a
80%(PLA-PBAT)/20%TPS/JC	2.44 ± 0.1^b
80%(PLA-PBAT)/20%TPS/JC/1%NCC	2.31 ± 0.04^b
80%(PLA-PBAT)/20%TPS/JC/2%NCC	2.21 ± 0.06^b
60%(PLA-PBAT)/40%TPS/JC	8.32 ± 0.05^c
60%(PLA-PBAT)/40%TPS/JC/1%NCC	7.03 ± 0.03^d
60%(PLA-PBAT)/40%TPS/JC/2%NCC	5.63 ± 0.13^e

Different superscripts within the same column indicate significant difference ($P<0.05$) between treatments.

Water vapor permeability (WVP) of the films was measured to evaluate the barrier performance of the PLA/PBAT/TPS nanocomposites and is shown in Table 3.5. Addition of Joncryl decreased the WVP by 11% from 1.81 (100%(PLA-PBAT)) to 1.62 (100%(PLA-PBAT)/JC) g.mm/m^2.day.kPa. This may be due to the formation of long chain branching structure among the polymer chains which leads to the decrease in free volume fraction thereby restricting the diffusion of water vapor molecules through the polymer matrix (Yampolskii et al., 2001). Rheological and thermal studies also confirmed the formation of long chain branching structure. Similar reduction of WVP due to formation of long chain branching structure among

the polymer chains is observed in PLA/Poly(propylene carbonate) blends (Sun et al., 2016). Addition of nanofiller NCC did not have any effect on WVP of the PLA/PBAT binary blends. Theoretically, the complete dispersion of nanofiller in the polymer matrix increases the tortuosity leading to slower diffusion of water vapor through the polymer matrix i.e. reduction of WVP (Azeredo et al., 2010). However, TEM images showed the aggregation of NCC in the PLA/PBAT matrix (Figure 3.7a, b) which led to no change in WVP for the binary blends. Addition of TPS increased the WVP of the films. This was expected due to the hydrophilic nature of TPS whereas the polymers PLA and PBAT are hydrophobic. The dispersion of NCC improved with the addition of hydrophilic TPS. Hence, addition of NCC decreased the WVP in PLA/PBAT/TPS ternary blends. At 20% TPS level, WVP reduced by 9% from 2.44 to 2.21 g.mm/m^2.day.kPa with addition of 2% NCC. The reduction of WVP with addition of NCC was more prominent in case of 40% TPS level. It decreased by 32% from 8.32 to 5.63 g.mm/m^2.day.kPa with addition of 2%NCC. Similar reduction of WVP with addition of NCC is observed in chitosan-based films (Khan et al., 2012), mango puree films (Azeredo et al., 2009) and poly(vinyl alcohol) based films (Paralikar et al., 2008).

Oxygen permeability (OP) of the films is shown in Figure 3.8. Addition of TPS decreased the oxygen permeability of the films as PLA have poor gas barrier properties while TPS display good barrier properties to oxygen (Dole et al., 2004; Li & Huneault, 2011). Hence, addition of TPS improved the barrier properties of the PLA based films. Similar to the WVP results, addition of NCC did not have any influence on the OP of the PLA/PBAT binary blends. Addition of TPS improved the dispersion of the nanofiller which led to slight reduction of OP in 60%(PLA-PBAT)/40%TPS/JC with addition of NCC.

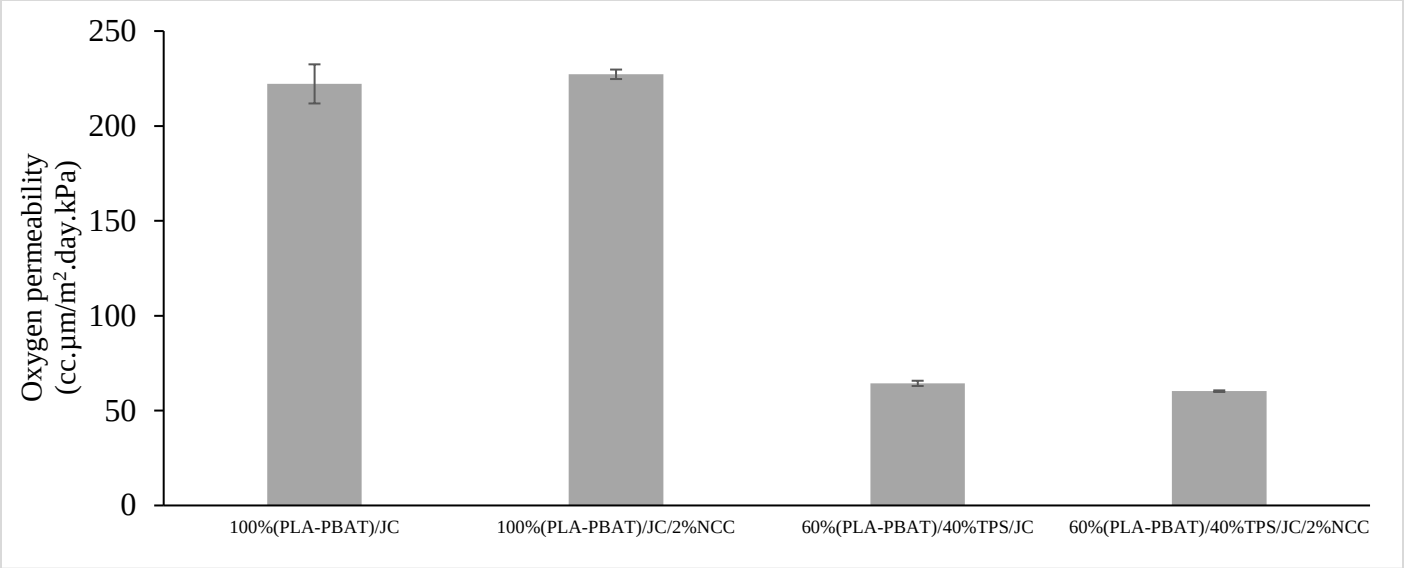

Figure 3.8 Oxygen permeability of PLA/PBAT/TPS/NCC nanocomposites

3.3.8 Comparison with commercial plastics

Table 3.6 shows the comparison of the films developed in the current study with those of the commercial plastics currently used in the industry. The mechanical and barrier properties of the films developed show that they are in the moderate range. The other advantages of the films developed in this study is the cost and the biodegradability in normal soil conditions. The cost is less compared to the films used commercially due to addition of starch. Components such as TPS and NCC are completely biodegradable in normal soil conditions. Also, these films are completely biodegradable in composting conditions. Hence, the films developed have a good scope to be used in the food packaging industry.

Table 3.6 Comparison with commercial plastics

Material	Biodegradability in normal conditions	Cost[a]	WVP[b]	Tensile strength[c]	Elongation at break[d]	Reference
PET	None	Moderate	Good	Good	Good	Auras et al., 2005
PP	None	Moderate	Good	Moderate	Good	Ismail, 2002
PE	None	High	Moderate	Moderate	Good	Zhong et al., 2007
PS	None	High	Moderate	Moderate	Poor	Nair et al., 1996
PVC	None	Moderate	Good	Good	Good	Zheng et al., 2007
PA	None	High	Moderate	Good	Good	Yang et al., 1998
PVDC	None	Moderate	Good	Good	Moderate	Shiku et al., 2004
PLA	None	Moderate	Moderate	Good	Poor	Oksman et al., 2003
PLA/PBAT/TPS/NCC	**Moderate**	**Low**	**Moderate**	**Moderate**	**Moderate**	**Current study**

[a]Cost: Low: <5$/kg; Moderate: 5-10$/kg; High: >10$/kg

[b]Test conditions:23°C, 85% RH: Poor: 10-100 g*mm/m^2*day*kPa; Moderate: 1-10 g*mm/m^2*day*kPa; Good: 0.1-1 g*mm/m^2*day*kPa

[c]Tensile strength: Poor: <10 MPa; Moderate: 10-50 MPa; Good: >50 MPa

[d]Elongation at break: Poor: <10%; Moderate: 10-50%; Good: >50%

PET=Poly(ethylene terephthalate), PP=Polypropylene, PE= Polyethylene, PS=Polystyrene, PVC=Poly(vinyl chloride), PA=polyamide, PVDC=Poly(vinylidene chloride)

3.4 Conclusions

Melt extrusion was used to prepare PLA/PBAT/TPS nanocomposites with NCC as the nanofiller. The effect of compatibilizer Joncryl on the interfacial adhesion between the polymers PLA, PBAT, TPS was studied. Rheological study showed the increase in shear viscosity of the PLA/PBAT blends with addition of Joncryl, TPS and NCC. DSC study showed that addition of Joncryl increased the crystallization temperature T_c and decreased the crystallinity of the blends (X_c). TEM showed the aggregation of NCC in the PLA/PBAT matrix due to difference in polarity based on the hydrophilic nature of nanofiller and hydrophobic polymers PLA and PBAT

and intermolecular hydrogen bonding between the nanofillers. Addition of hydrophilic TPS led to better dispersion of NCC in the polymer matrix. Mechanical studies showed a significant increase in elongation at break of PLA with addition of PBAT. Addition of Joncryl further resulted in increase in elongation at break of PLA/PBAT blends due to the increase in interfacial adhesion between the polymers PLA and PBAT. Addition of NCC did not have any effect of the tensile strength of the PLA/PBAT blends as aggregation of NCC caused it to act as a microcomposite rather than as a nanocomposite thereby negating the reinforcement effect of the nanofillers. TPS addition decreased the mechanical properties of PLA/PBAT blends. Due to better dispersion of NCC with addition of TPS, NCC addition increased the tensile strength of PLA/PBAT/TPS nanocomposites. Addition of Joncryl decreased the WVP of the PLA/PBAT blends due to the increase in molecular interactions between the polymers PLA and PBAT Addition of hydrophilic TPS led to the increase in WVP and decrease in OP of the PLA/PBAT binary blends. Barrier properties improved i.e. WVP and OP decreased with the addition of NCC to PLA/PBAT/TPS nanocomposites.

3.5 References

Ali, S. S., Tang, X., Alavi, S., & Faubion, J. (2011). Structure and physical properties of starch/poly vinyl alcohol/sodium montmorillonite nanocomposite films. Journal of agricultural and food chemistry, 59(23), 12384-12395.

Al-Itry, R., Lamnawar, K., & Maazouz, A. (2012). Improvement of thermal stability, rheological and mechanical properties of PLA, PBAT and their blends by reactive extrusion with functionalized epoxy. Polymer Degradation and Stability, 97(10), 1898-1914.

Angles, M. N., & Dufresne, A. (2000). Plasticized starch/tunicin whiskers nanocomposites. 1. Structural analysis. Macromolecules, 33(22), 8344-8353.

Arrieta, M. P., Fortunati, E., Dominici, F., Rayón, E., López, J., & Kenny, J. M. (2014). Multifunctional PLA–PHB/cellulose nanocrystal films: Processing, structural and thermal properties. Carbohydrate polymers, 107, 16-24.

Arruda, L. C., Magaton, M., Bretas, R. E. S., & Ueki, M. M. (2015). Influence of chain extender on mechanical, thermal and morphological properties of blown films of PLA/PBAT blends. Polymer Testing, 43, 27-37.

Auras, R. A., Singh, S. P., & Singh, J. J. (2005). Evaluation of oriented poly (lactide) polymers vs. existing PET and oriented PS for fresh food service containers. Packaging technology and science, 18(4), 207-216.

Averous, L., Moro, L., Dole, P., & Fringant, C. (2000). Properties of thermoplastic blends: starch–polycaprolactone. Polymer, 41(11), 4157-4167.

Ayana, B., Suin, S., & Khatua, B. B. (2014). Highly exfoliated eco-friendly thermoplastic starch (TPS)/poly (lactic acid)(PLA)/clay nanocomposites using unmodified nanoclay. Carbohydrate polymers, 110, 430-439.

Azeredo, H. M., Mattoso, L. H. C., Wood, D., Williams, T. G., Avena-Bustillos, R. J., & McHugh, T. H. (2009). Nanocomposite edible films from mango puree reinforced with cellulose nanofibers. Journal of food science, 74(5), N31-N35.

Azeredo, H. M., Mattoso, L. H. C., Avena-Bustillos, R. J., Filho, G. C., Munford, M. L., Wood, D., & McHugh, T. H. (2010). Nanocellulose reinforced chitosan composite films as affected by nanofiller loading and plasticizer content. Journal of Food Science, 75(1), N1-N7.

Babaee, M., Jonoobi, M., Hamzeh, Y., & Ashori, A. (2015). Biodegradability and mechanical properties of reinforced starch nanocomposites using cellulose nanofibers. Carbohydrate polymers, 132, 1-8.

Badrinarayanan, P., Zheng, W., Li, Q., & Simon, S. L. (2007). The glass transition temperature versus the fictive temperature. Journal of Non-crystalline solids, 353(26), 2603-2612.

Battegazzore, D., Alongi, J., & Frache, A. (2014). Poly (lactic acid)-based composites containing natural fillers: thermal, mechanical and barrier properties. Journal of Polymers and the Environment, 22(1), 88-98.

Brandelero, R. P. H., Grossmann, M. V. E., & Yamashita, F. (2011). Effect of the method of production of the blends on mechanical and structural properties of biodegradable starch films produced by blown extrusion. Carbohydrate Polymers, 86(3), 1344-1350.

Brinchi, L., Cotana, F., Fortunati, E., & Kenny, J. M. (2013). Production of nanocrystalline cellulose from lignocellulosic biomass: Technology and applications. Carbohydrate Polymers, 94(1), 154–169.

Castaño, J., Bouza, R., Rodríguez-Llamazares, S., Carrasco, C., & Vinicius, R. V. B. (2012). Processing and characterization of starch-based materials from pehuen seeds (Araucaria araucana (Mol) K. Koch). Carbohydrate polymers, 88(1), 299-307.

Chow, W. S., Mohd Ishak, Z. A., & Karger-Kocsis, J. (2005). Morphological and rheological properties of polyamide 6/poly (propylene)/organoclay nanocomposites. Macromolecular Materials and Engineering, 290(2), 122-127.

Dangtungee, R., Petcharoen, K., Pinijsattawong, K., & Siengchin, S. (2012). Investigation of the rheological properties and die swell of polylactic acid/nanoclay composites in a capillary rheometer. Mechanics of Composite Materials, 47(6), 663-670.

Dole, P., Joly, C., Espuche, E., Alric, I., & Gontard, N. (2004). Gas transport properties of starch based films. Carbohydrate Polymers, 58(3), 335-343.

Espino-Pérez, E., Bras, J., Ducruet, V., Guinault, A., Dufresne, A., & Domenek, S. (2013). Influence of chemical surface modification of cellulose nanowhiskers on thermal, mechanical, and barrier properties of poly (lactide) based bionanocomposites. European Polymer Journal, 49(10), 3144-3154.

Fischer, E. W., Sterzel, H. J., & Wegner, G. K. Z. Z. (1973). Investigation of the structure of solution grown crystals of lactide copolymers by means of chemical reactions. Kolloid-Zeitschrift und Zeitschrift für Polymere, 251(11), 980-990.

Fortunati, E., Armentano, I., Zhou, Q., Iannoni, A., Saino, E., Visai, L., Berglund, L. A., & Kenny, J. M. (2012a). Multifunctional bionanocomposite films of poly(lactic acid),cellulose nanocrystals and silver nanoparticles. Carbohydrate Polymers, 87(2), 1596–1605.

Fortunati, E., Peltzer, M., Armentano, I., Torre, L., Jiménez, A., & Kenny, J. M. (2012b). Effects of modified cellulose nanocrystals on the barrier and migration properties of PLA nano-biocomposites. Carbohydrate Polymers, 90(2), 948–956.

Frone, A. N., Berlioz, S., Chailan, J. F., & Panaitescu, D. M. (2013). Morphology and thermal properties of PLA–cellulose nanofibers composites. Carbohydrate Polymers, 91(1), 377-384.

Garcia, P. S., Grossmann, M. V. E., Shirai, M. A., Lazaretti, M. M., Yamashita, F., Muller, C. M. O., & Mali, S. (2014). Improving action of citric acid as compatibiliser in starch/polyester blown films. Industrial Crops and Products, 52, 305-312.

Global bio plastics market to be driven by demand from packaging in North America, 2017. Retrieved from: http://www.plastemart.com/plastic-technical-articles/global-bio-plastics-market-to-be-driven-by-demand-from-packaging-in-north-america/2350.

Hablot, E., Dewasthale, S., Zhao, Y., Zhiguan, Y., Shi, X., Graiver, D., & Narayan, R. (2013). Reactive extrusion of glycerylated starch and starch–polyester graft copolymers. European Polymer Journal, 49(4), 873-881.

Ho, K. L. G., Pometto, A. L., & Hinz, P. N. (1999). Effects of temperature and relative humidity on polylactic acid plastic degradation. Journal of environmental polymer degradation, 7(2), 83-92.

Huneault, M. A., & Li, H. (2007). Morphology and properties of compatibilized polylactide/thermoplastic starch blends. Polymer, 48(1), 270-280.

Hutchinson, J. (2009). Determination of the glass transition temperature: methods correlation and structural heterogeneity. Journal of thermal analysis and calorimetry, 98(3), 579-589.

Iovino, R., Zullo, R., Rao, M. A., Cassar, L., & Gianfreda, L. (2008). Biodegradation of poly (lactic acid)/starch/coir biocomposites under controlled composting conditions. Polymer Degradation and Stability, 93(1), 147-157.

Ismail, H. (2002). Thermoplastic elastomers based on polypropylene/natural rubber and polypropylene/recycle rubber blends. Polymer Testing, 21(4), 389-395.

Jaszkiewicz, A., Bledzki, A. K., van der Meer, R., Franciszczak, P., & Meljon, A. (2014). How does a chain-extended polylactide behave?: a comprehensive analysis of the material, structural and mechanical properties. Polymer Bulletin, 71(7), 1675-1690.

Jiang, L., Wolcott, M. P., & Zhang, J. (2006). Study of biodegradable polylactide/poly (butylene adipate-co-terephthalate) blends. Biomacromolecules, 7(1), 199-207.

Joon Choi, W., Kim, H. J., Han Yoon, K., Hyeong Kwon, O., & Ik Hwang, C. (2006). Preparation and barrier property of poly (ethylene terephthalate)/clay nanocomposite using clay-supported catalyst. Journal of Applied Polymer Science, 100(6), 4875-4879.

Kalambur, S., & Rizvi, S. S. (2006). Rheological behavior of starch–polycaprolactone (PCL) nanocomposite melts synthesized by reactive extrusion. Polymer Engineering & Science, 46(5), 650-658.

Ke, T., & Sun, X. (2000). Physical properties of poly (lactic acid) and starch composites with various blending ratios. Cereal chemistry, 77(6), 761-768.

Keys, A. S., Garrahan, J. P., & Chandler, D. (2013). Calorimetric glass transition explained by hierarchical dynamic facilitation. Proceedings of the National Academy of Sciences, 201302665.

Khalil, H. A., Tye, Y. Y., Ismail, Z., Leong, J. Y., Saurabh, C. K., Lai, T. K., Chong, E. W., Aditiawati, P., Tahir, P. M. & Dungani, R. (2017). Oil palm shell nanofiller in seaweed-based composite film: Mechanical, physical, and morphological properties. BioResources, 12(3), 5996-6010.

Khan, A., Khan, R. A., Salmieri, S., Le Tien, C., Riedl, B., Bouchard, J., Chauve, G., Tan, V., Kamal, M. R & Lacroix, M. (2012). Mechanical and barrier properties of nanocrystalline cellulose reinforced chitosan based nanocomposite films. Carbohydrate polymers, 90(4), 1601-1608.

Krishnan, S., Mohanty, S., & Nayak, S. K. (2017). Renewable Resource based blends of Polylactic acid (PLA) and Thermoplastic starch (TPS) using Novel Reactive Compatibilization. Journal of Polymer Materials, 34(3), 525-538.

Kumar, M., Mohanty, S., Nayak, S. K., & Parvaiz, M. R. (2010). Effect of glycidyl methacrylate (GMA) on the thermal, mechanical and morphological property of biodegradable PLA/PBAT blend and its nanocomposites. Bioresource technology, 101(21), 8406-8415.

Le Bail, P., Bizot, H., Ollivon, M., Keller, G., Bourgaux, C., & Buléon, A. (1999). Monitoring the crystallization of amylose–lipid complexes during maize starch melting by synchrotron x-ray diffraction. Biopolymers: Original Research on Biomolecules, 50(1), 99-110.

Li, H., & Huneault, M. A. (2011). Comparison of sorbitol and glycerol as plasticizers for thermoplastic starch in TPS/PLA blends. Journal of Applied Polymer Science, 119(4), 2439-2448.

Liu, H., Chaudhary, D., Yusa, S. I., & Tadé, M. O. (2011). Preparation and characterization of sorbitol modified nanoclay with high amylose bionanocomposites. Carbohydrate polymers, 85(1), 97-104.

Lourdin, D., Bizot, H., & Colonna, P. (1997). “Antiplasticization” in starch-glycerol films? Journal of Applied Polymer Science, 63(8), 1047-1053.

Marsh, K., & Bugusu, B. (2007). Food packaging - Roles, materials, and environmental issues. Journal of Food Science, 72(3), R39-R55.

Martínez-Sanz, M., Lopez-Rubio, A., & Lagaron, J. M. (2013). High-barrier coated bacterial cellulose nanowhiskers films with reduced moisture sensitivity. Carbohydrate polymers, 98(1), 1072-1082.

Mathew, A. P., & Dufresne, A. (2002). Morphological investigation of nanocomposites from sorbitol plasticized starch and tunicin whiskers. Biomacromolecules, 3(3), 609-617.

Matos Ruiz, M., Cavaille, J. Y., Dufresne, A., Gerard, J. F. & Graillat, C. (2000). Processing and characterization of new thermoset nanocomposites based on cellulose whiskers. Composite Interfaces, 7(2), 117-131.

Mihindukulasuriya, S.D.F., & Lim, L.T. (2014). Nanotechnology development in food packaging: A review. Trends in Food Science & Technology, 40(2), 149-167.

Mohanty, S., & Nayak, S. K. (2009). Starch based biodegradable PBAT nanocomposites: Effect of starch modification on mechanical, thermal, morphological and biodegradability behavior. International Journal of Plastics Technology, 13(2), 163-185.

Nabar, Y., Raquez, J. M., Dubois, P., & Narayan, R. (2005). Production of starch foams by twin-screw extrusion: Effect of maleated poly (butylene adipate-co-terephthalate) as a compatibilizer. Biomacromolecules, 6(2), 807-817.

Nair, K. C., Diwan, S. M., & Thomas, S. (1996). Tensile properties of short sisal fiber reinforced polystyrene composites. Journal of applied polymer science, 60(9), 1483-1497.

Najafi, N., Heuzey, M. C., & Carreau, P. J. (2012). Polylactide (PLA)-clay nanocomposites prepared by melt compounding in the presence of a chain extender. Composites Science and Technology, 72(5), 608-615.

Nayak, S. K. (2010). Biodegradable PBAT/starch nanocomposites. Polymer-Plastics Technology and Engineering, 49(14), 1406-1418.

Nazarenko, S., Meneghetti, P., Julmon, P., Olson, B. G., & Qutubuddin, S. (2007). Gas barrier of polystyrene montmorillonite clay nanocomposites: effect of mineral layer aggregation. Journal of Polymer Science Part B: Polymer Physics, 45(13), 1733-1753.

Nield, S. A., Budman, H. M., & Tzoganakis, C. (2000). Control of a LDPE reactive extrusion process. Control Engineering Practice, 8(8), 911-920.

Oksman, K., Skrifvars, M., & Selin, J. F. (2003). Natural fibres as reinforcement in polylactic acid (PLA) composites. Composites science and technology, 63(9), 1317-1324.

Olivato, J. B., Grossmann, M. V., Yamashita, F., Nobrega, M. M., Scapin, M. R., Eiras, D., & Pessan, L. A. (2011). Compatibilisation of starch/poly (butylene adipate co-terephthalate) blends in blown films. International journal of food science & technology, 46(9), 1934-1939.

Olivato, J. B., Grossmann, M. V. E., Yamashita, F., Eiras, D., & Pessan, L. A. (2012). Citric acid and maleic anhydride as compatibilizers in starch/poly (butylene adipate-co-terephthalate) blends by one-step reactive extrusion. Carbohydrate Polymers, 87(4), 2614-2618.

Olivato, J. B., Nobrega, M. M., Müller, C. M. O., Shirai, M. A., Yamashita, F., & Grossmann, M. V. E. (2013). Mixture design applied for the study of the tartaric acid effect on starch/polyester films. Carbohydrate polymers, 92(2), 1705-1710.

Paralikar, S. A., Simonsen, J., & Lombardi, J. (2008). Poly (vinyl alcohol)/cellulose nanocrystal barrier membranes. Journal of Membrane Science, 320(1-2), 248-258.

Park, H. M., Lee, W. K., Park, C. Y., Cho, W. J., & Ha, C. S. (2003). Environmentally friendly polymer hybrids Part I Mechanical, thermal, and barrier properties of thermoplastic starch/clay nanocomposites. Journal of Materials Science, 38(5), 909-915.

Pereira, D., Losada, P. P., Angulo, I., Greaves, W., & Cruz, J. M. (2009). Development of a polyamide nanocomposite for food industry: morphological structure, processing, and properties. Polymer Composites, 30(4), 436-444.

Peres, A. M., Pires, R. R., & Oréfice, R. L. (2016). Evaluation of the effect of reprocessing on the structure and properties of low density polyethylene/thermoplastic starch blends. Carbohydrate polymers, 136, 210-215.

Petersson, L., Kvien, I., & Oksman, K. (2007). Structure and thermal properties of poly (lactic acid)/cellulose whiskers nanocomposite materials. Composites Science and Technology, 67(11-12), 2535-2544.

Ray, S. S., Yamada, K., Okamoto, M., Fujimoto, Y., Ogami, A., & Ueda, K. (2003). New polylactide/layered silicate nanocomposites. 5. Designing of materials with desired properties. Polymer, 44(21), 6633-6646.

Ren, J., Liu, Z., & Ren, T. (2007). Mechanical and thermal properties of poly (lactic acid)/starch/montmorillonite biodegradable blends. Polymers and Polymer Composites, 15(8), 633-638.

Rico, M., Rodríguez-Llamazares, S., Barral, L., Bouza, R., & Montero, B. (2016). Processing and characterization of polyols plasticized-starch reinforced with microcrystalline cellulose. Carbohydrate polymers, 149, 83-93.

Ruiz-Cabrera, M. A., & Schmidt, S. J. (2015). Determination of glass transition temperatures during cooling and heating of low-moisture amorphous sugar mixtures. Journal of food engineering, 146, 36-43.

Sanchez-Garcia, M. D., Gimenez, E., & Lagaron, J. M. (2007). Novel PET nanocomposites of interest in food packaging applications and comparative barrier performance with biopolyester nanocomposites. Journal of Plastic Film & Sheeting, 23(2), 133-148.

Shi, R., Zhang, Z., Liu, Q., Han, Y., Zhang, L., Chen, D., & Tian, W. (2007). Characterization of citric acid/glycerol co-plasticized thermoplastic starch prepared by melt blending. Carbohydrate Polymers, 69(4), 748-755.

Shiku, Y., Hamaguchi, P. Y., Benjakul, S., Visessanguan, W., & Tanaka, M. (2004). Effect of surimi quality on properties of edible films based on Alaska pollack. Food Chemistry, 86(4), 493-499.

Shogren, R. L., Doane, W. M., Garlotta, D., Lawton, J. W., & Willett, J. L. (2003). Biodegradation of starch/polylactic acid/poly (hydroxyester-ether) composite bars in soil. Polymer Degradation and Stability, 79(3), 405-411.

Silva, I. F., Yamashita, F., Müller, C. M., Mali, S., Olivato, J. B., Bilck, A. P., & Grossmann, M. V. (2013). How reactive extrusion with adipic acid improves the mechanical and barrier properties of starch/poly (butylene adipate-co-terephthalate) films. International Journal of Food Science & Technology, 48(8), 1762-1769.

Stagner, J., & Narayan, R. (2011). Preparation and properties of biodegradable foams. Journal of Polymers and the Environment, 19(3), 598-606.

Stagner, J. A., Alves, V. D., & Narayan, R. (2012). Application and performance of maleated thermoplastic starch–poly (butylene adipate-co-terephthalate) blends for films. Journal of Applied Polymer Science, 126(S1), E135-E142.

Sun, Q., Mekonnen, T., Misra, M., & Mohanty, A. K. (2016). Novel biodegradable cast film from carbon dioxide based copolymer and poly (lactic acid). Journal of Polymers and the Environment, 24(1), 23-36.

Tang, X., Alavi, S., & Herald, T. J. (2008). Barrier and mechanical properties of starch-clay nanocomposite films. Cereal Chemistry, 85(3), 433-439.

Teixeira, E. D. M., Pasquini, D., Curvelo, A. A., Corradini, E., Belgacem, M. N. & Dufresne, A. (2009). Cassava bagasse cellulose nanofibrils reinforced thermo-plastic cassava starch. Carbohydrate Polymers, 78(3), 422–431.

Thellen, C., Orroth, C., Froio, D., Ziegler, D., Lucciarini, J., Farrell, R., & Ratto, J. A. (2005). Influence of montmorillonite layered silicate on plasticized poly (l-lactide) blown films. Polymer, 46(25), 11716-11727.

Villar, M. A., Thomas, E. L., & Armstrong, R. C. (1995). Rheological properties of thermoplastic starch and starch/poly (ethylene-co-vinyl alcohol) blends. Polymer, 36(9), 1869-1876.

Wacharawichanant, S., Ratchawong, S., Hoysang, P., & Phankokkruad, M. (2017). Morphology and Properties of Poly (Lactic Acid) and Ethylene-Methyl Acrylate Copolymer Blends with Organoclay. In MATEC Web of Conferences (Vol. 130, p. 07006). EDP Sciences.

Walha, F., Lamnawar, K., Maazouz, A., & Jaziri, M. (2016). Rheological, morphological and mechanical studies of sustainably sourced polymer blends based on poly (Lactic acid) and polyamide 11. Polymers, 8(3), 61.

Wang, L., Ma, W., Gross, R. A., & McCarthy, S. P. (1998). Reactive compatibilization of biodegradable blends of poly (lactic acid) and poly (ε-caprolactone). Polymer Degradation and Stability, 59(1-3), 161-168.

Wang, N., Yu, J., Chang, P. R., & Ma, X. (2008). Influence of formamide and water on the properties of thermoplastic starch/poly (lactic acid) blends. Carbohydrate Polymers, 71(1), 109-118.

Wang, H., Wei, D., Zheng, A., & Xiao, H. (2015). Soil burial biodegradation of antimicrobial biodegradable PBAT films. Polymer Degradation and Stability, 116, 14-22.

Wei, D., Wang, H., Xiao, H., Zheng, A., & Yang, Y. (2015). Morphology and mechanical properties of poly (butylene adipate-co-terephthalate)/potato starch blends in the presence of synthesized reactive compatibilizer or modified poly (butylene adipate-co-terephthalate). Carbohydrate polymers, 123, 275-282.

Wiedmann, W., & Strobel, E. (1991). Compounding of thermoplastic starch with twin-screw extruders. Starch - Stärke, 43(4), 138–145.

Wu, C. S. (2005). Improving polylactide/starch biocomposites by grafting polylactide with acrylic acid–characterization and biodegradability assessment. Macromolecular bioscience, 5(4), 352-361.

Xu, J. (2015). Biobased nanocomposites for packaging applications—synthesis using melt extrusion of poly (lactic acid), poly (butylene succinate) and/or starch blended with natural nanofillers (Masters dissertation, Kansas State University).

Yampolskii, Y. P., Korikov, A. P., Shantarovich, V. P., Nagai, K., Freeman, B. D., Masuda, T., Teraguchi, M. & Kwak, G. (2001). Gas permeability and free volume of highly branched substituted acetylene polymers. Macromolecules, 34(6), 1788-1796.

Yang, F., Ou, Y., & Yu, Z. (1998). Polyamide 6/silica nanocomposites prepared by in situ polymerization. Journal of Applied Polymer Science, 69(2), 355-361.

Zhang, N., Wang, Q., Ren, J., & Wang, L. (2009). Preparation and properties of biodegradable poly (lactic acid)/poly (butylene adipate-co-terephthalate) blend with glycidyl methacrylate as reactive processing agent. Journal of Materials Science, 44(1), 250-256.

Zhao, P., Liu, W., Wu, Q., & Ren, J. (2010). Preparation, mechanical, and thermal properties of biodegradable polyesters/poly (lactic acid) blends. Journal of Nanomaterials, 2010, 4.

Zheng, Y. T., Cao, D. R., Wang, D. S., & Chen, J. J. (2007). Study on the interface modification of bagasse fibre and the mechanical properties of its composite with PVC. Composites part A: applied science and manufacturing, 38(1), 20-25.

Zhong, Y., Janes, D., Zheng, Y., Hetzer, M., & De Kee, D. (2007). Mechanical and oxygen barrier properties of organoclay-polyethylene nanocomposite films. Polymer Engineering & Science, 47(7), 1101-1107.

Chapter 4 - Optimization of poly(lactic acid)/poly(butylene co-adipate-terephthalate)/thermoplastic starch nanocomposite films for barrier and mechanical properties

Abstract

Mixture response surface methods were used to investigate the effect of poly(lactic acid) (PLA), poly(butylene co-adipate-terephthalate) (PBAT), thermoplastic starch (TPS) and nanofiller nanocrystalline cellulose (NCC) on the responses water vapor permeability (WVP), tensile strength (TS), elongation at break (EB). All factors including levels of PLA, PBAT, TPS, NCC influenced the mechanical and barrier properties of the films. Quadratic models with good predicted R^2 (between 84.3% and 97.59%) were developed for all the responses. Addition of PBAT improved the EB of the films while NCC and TPS addition decreased the EB. TPS addition decreased the mechanical properties and increased the WVP; but addition of NCC increased the tensile strength of the PLA/PBAT/TPS blends and decreased the WVP. Optimization study was done that could yield films with optimum properties comparable to commercial plastics and maximizing the level of TPS. Films with optimum properties (TS = 29.5 MPa, EB = 12%, WVP = 1.99 g.mm/kPa.h.m^2) were predicted at levels of 64.3% PLA, 14.5% PBAT, 18% TPS and 2.6% NCC along with 0.5% Joncryl.

4.1 Introduction

Petroleum-based plastic packaging has some disadvantages as it contributes to waste disposal problems and environmental toxicity These petroleum-based resources are also non-renewable. Renewable and bio-based plastics can be used to replace non-renewable petroleum-based resources. Among the bioplastics, poly(lactic acid) (PLA) is a promising material and one of the widely growing sector in the market of bioplastics in 2016 (Global bioplastics market, 2017). PLA is an aliphatic thermoplastic polyester with a range of desirable properties including biodegradability in composting conditions, high strength and high modulus (Wacharawichanant et al., 2017). The cost of PLA is also comparable to that of conventional polyolefin polymers. However, PLA based films are brittle i.e. low % elongation at break.

PLA can be blended with other polymers such as poly (caprolactone) (PCL), poly (butylene succinate) (PBS), poly (butylene adipate-co-terephthalate) (PBAT) (Kumar et al., 2010; Wang et al., 1998; Zhao et al., 2010) to improve the elongation. PBAT, a fully biodegradable aliphatic-aromatic copolyester is a good candidate to decrease the brittleness of PLA and is selected in our study. Due to high cost of polymers of PLA and PBAT, it can be blended with starch to make it cost-effective. Starch is a widely available and naturally occurring biodegradable polymer and hence can be considered as an economically viable alternative (Ayana et al., 2014).

The melting temperature of native starch (T_m = 220–250^o C) is high and is close to its degradation temperature (~220^o C) (Ayana et al., 2014). Plasticizers can be used to decrease the melting temperature of starch as they form a hydrogen bond with the starch (i.e. amylose) molecules and decrease the inter-molecular hydrogen bonding sites in the crystalline parts of

starch. Hence, native starch can be converted into thermoplastic starch (TPS) using thermo-mechanical treatment in the presence of plasticizers such as water, glycerol, sorbitol etc. (Wiedmann & Strobel, 1991). Addition of TPS also increases the rate of biodegradation of PLA in all conditions (Akrami et al., 2016; Iovino et al., 2008) as the various microorganisms can easily use starch as an energy source. However, TPS based packaging have some limitations due to its high hydrophilic nature and weak mechanical properties (Babaee et al., 2015; Rico et al., 2016; Teixeira et al., 2009). One of the promising methods to address this limitation is the use of nanofiller to improve the mechanical and barrier properties of bioplastics (Fortunati et al., 2012b). The incorporation of nanofillers into various natural and synthetic polymers such as polystyrene, polyamide, poly(ethylene terephthalate, poly(lactic acid), poly(vinyl chloride), thermoplastic starch etc. were widely reported over the past 30 years (Joon Choi et al., 2006; Nazarenko et al., 2007; Park et al., 2003; Pereira et al., 2009; Ray et al., 2003; Sanchez-Garcia et al., 2007; Thellen et al., 2005). The nanofiller used in this study was nanocrystalline cellulose (NCC). NCC has various properties such as durability and high biodegradability (Brinchi et al., 2013). The structure of NCC is generally rod-shaped of about 5-10 nm in width and 100-200 nm in length (Fortunati et al., 2012a). They have a very high aspect ratio (length/diameter) and a large surface area (Matos Ruiz et al., 2000).

D-Optimal mixture design is an effective technique in optimizing a complex mixture process. This design is very useful when there are high number of variables or components (Campos-Requena et al., 2015). In this design, the proportions of the mixture components change while the sum of the mixture components is kept constant. This design has been used for optimization in several areas like UV cured epoxy acrylate resins (Kardar et al., 2009), epoxy-based hybrid nanocomposite (Rostamiyan et al., 2014), natural fermentative medium for

selenium-enriched yeast (Yin et al., 2009), short glass fiber and polytetrafluoroethylene reinforced polycarbonate composites (Lin et al., 2010), edible whey protein films (Ozdemir & Floros, 2008) etc. Response surface methodology (RSM) utilizes experimental data to find a mathematical equation to predict the responses of the system by statistical means. It is very useful in determining the optimal combination in the mixture that can yield desired responses of the system.

The objective of this study was to investigate the effect of PLA, PBAT, TPS, NCC on the mechanical and barrier properties of the films and utilize response surface methodology to determine the optimum levels of these components in the mixture that can yield the desired water vapor permeability (WVP), tensile strength (TS) and elongation at break (EB).

4.2 Experimental

4.2.1 Materials

High amylose corn starch Hylon V (~55% amylose content) was supplied by Ingredion. Poly (lactic acid), PLA4032D (Density: 1.25 g/cc, Average molecular weight: 100,000 g/mol), was purchased from Natureworks and Poly (butylene adipate-co-terephthalate), Ecoflex® F Blend C1200 (Density: 1.25 g/cc, Average molecular weight: 145,000 g/mol) and Joncryl ADR 4368C were obtained from BASF. Plasticizer sorbitol was purchased from Sigma-aldrich and nanocrystalline cellulose (NCC) was purchased from University of Maine.

4.2.2 Synthesis of thermoplastic starch (TPS)

Thermoplastic starch (TPS) was prepared by mixing dry starch (64%) with sorbitol (36%) using a corotating lab-scale twin screw extruder (Micro-18, American Leistritz, Somerville, NJ, USA). The extruder has a six head configuration, screw diameter of 18 mm and length-diameter

ratio of 30:1. The barrel temperatures of the heads used for extrusion were 100-140-140-140-140-140 ^{o}C. The extrudate was then ground using a Wiley mill (Model 4, Thomas-Wiley Co., Philadelphia, PA) for further use.

4.2.3 Experimental design

D-optimal mixture design was used in this study. This design was used to find the optimum level of PLA, PBAT, TPS, NCC that provides good barrier and mechanical properties. The sum of the fractions of components should be equal to one. The factors are the fractions of components and their levels are not independent. 0.5% Joncryl was added in all the treatments based on previous studies (Chapter 3) which showed the compatibilizer action of Joncryl in increasing the interfacial adhesion between PLA, PBAT, TPS. Hence, the sum of the rest of the fractions i.e. amount of PLA, PBAT, TPS and NCC should amount to 0.995 (i.e. 99.5%).

$$X_1 + X_2 + X_3 + X_4 = 0.995$$

where X_1, X_2, X_3 and X_4 refer to fractions of PLA, PBAT, TPS and NCC respectively. The type of mixture design used was extreme vertices mixture design. This design covers only a small region within the simplex mixture design as there are upper bound constraints on some of the components like level of PBAT, NCC and TPS. The upper bound constraint of these components was considered based on the results from previous studies (Chapters 2 and 3).

Table 4.1 Low and high levels of proportions of factors

Factor	Low	High
X_1	0	0.995
X_2	0	0.2
X_3	0	0.5
X_4	0	0.04

Table 4.2 Experimental design

Formulation[a]	X_1	X_2	X_3	X_4
1	0.995	0	0	0
2	0.495	0	0.5	0
3	0.955	0	0	0.04
4	0.455	0	0.5	0.04
5	0.795	0.2	0	0
6	0.755	0.2	0	0.04
7	0.295	0.2	0.5	0
8	0.255	0.2	0.5	0.04
9	0.81	0.05	0.125	0.01
10	0.79	0.05	0.125	0.03
11	0.56	0.05	0.375	0.01
12	0.54	0.05	0.375	0.03
13	0.71	0.15	0.125	0.01
14	0.69	0.15	0.125	0.03
15	0.46	0.15	0.375	0.01
16	0.44	0.15	0.375	0.03
17	0.625	0.1	0.25	0.02

[a]Experimental runs were performed in random order

Table 4.1 shows the low and high levels of proportions of PLA, PBAT, TPS and NCC. Minitab software version 18.1.0 was used to generate the mixture design based on all the constraints provided. Table 4.2 shows the experimental design and levels of these four

components. These formulations consist of one single-ingredient treatment, three two-ingredient treatments, three three-ingredient treatments and ten four-ingredient treatments. Total of 17 treatments were run randomly based on extreme vertices mixture design with no replicate.

4.2.4 Melt blending

All the materials were dried at 80^{o} C for 8 hours in an air oven to remove moisture. The nanocomposites were melt blended using a laboratory-scale co-rotating twin screw extruder (Micro-18, American Leistritz, Somerville, NJ). The barrel temperatures of the heads used for extrusion were 100-180-180-180-180-180 ^{o}C. The extrudates were ground using a Wiley mill (Model 4, Thomas-Wiley Co., Philadelphia, PA) for further use.

4.2.5 Film preparation

Hot press (Model 3889, Carver Inc., Wabash, IN) with process parameter of force of 2100 lb and temperature of hot plates at 180^{o}C (top and bottom) was used to make the films of thickness of about 200 microns. The hot sample was preheated at 180°C for 5 min and then further pressed for 5 minutes using the hotpress.

4.2.6 Mechanical properties

Mechanical properties of the films were measured using Instron testing machine (Model 4465, Canton, MA, USA) based on standard ASTM D882 method. Films were cut into 1.3 cm wide and 10 cm long strips and conditioned at 23^{o} C and 50% RH for two days before testing for tensile strength and elongation ratio. The Tensile strength (TS) and elongation at break (EB) were calculated as given in the equations below:

$$TS=\frac{Lp}{a} \times 10^{-6}\ MPa$$

where Lp= peak load (N) and a= cross-sectional area (m^2)

$$EB = \delta L/L \times 100\ (\%)$$

where δL= increase in length at breaking point (mm) and L= original length (mm)

All the measurements were reported as the average of five samples.

4.2.7 Water vapor permeability (WVP)

Water vapor permeability (WVP) was determined gravimetrically according to the standard method E96-00 (ASTM 2000). The films were fixed on top of test cells containing a desiccant (silica gel). Test cells were placed in a relative humidity chamber with controlled temperature and relative humidity (25° C and 85% RH). After steady-state conditions were reached, the weight of the test cells was measured every 24 hours over a five-day period. The slope of each line was calculated by linear regression (R^2>0.99), and the water vapor transmission rate (WVTR) was calculated from the slope of the straight line (W/t) divided by the transfer area (A):

$$WVTR = \frac{(\frac{W}{t})}{A}\ g/h.m^2$$

where W = change in weight (g), t = time (h) and A = area of transfer (m^2)

WVP was then calculated from WVP using the equation given below

$$WVP = \frac{WVTR * t}{\Delta P}\ g*mm/kPa.h.m^2$$

where t = film thickness (mm) and ΔP = pressure difference across the films (kPa).

All the measurements were reported as the average of two samples.

4.2.8 Statistical analysis

Responses WVP, TS and EB were analyzed using Minitab software version 18.1.0. Linear, quadratic and special cubic models were used to fit the experimental data.

Linear: $Y = \beta_1X_1 + \beta_2X_2 + \beta_3X_3 + \beta_4X_4$

Quadratic: $Y = \beta_1X_1 + \beta_2X_2 + \beta_3X_3 + \beta_4X_4 + \beta_{12}X_1X_2 + \beta_{13}X_1X_3 + \beta_{14}X_1X_4 + \beta_{23}X_2X_3 + \beta_{24}X_2X_4 + \beta_{34}X_3X_4$

Special Cubic: $Y = \beta_1X_1 + \beta_2X_2 + \beta_3X_3 + \beta_4X_4 + \beta_{12}X_1X_2 + \beta_{13}X_1X_3 + \beta_{14}X_1X_4 + \beta_{23}X_2X_3 + \beta_{24}X_2X_4 + \beta_{34}X_3X_4 + \beta_{123}X_1X_2X_3 + \beta_{124}X_1X_2X_4 + \beta_{134}X_1X_3X_4 + \beta_{234}X_2X_3X_4$

where Y is the response and β_i's are the equation coefficients of the respective terms.

Of these models, the model chosen should have low standard deviation, high R^2 and predicted sum of squares. Also, with the addition of interaction terms, the goodness of the model fit needs to be tested using likelihood ratio test to avoid the overfitting of the model. In this study, the best fitted model was found to be quadratic model for all the responses. Some of the terms in the model were removed based on backward elimination of terms that are not significant i.e. p-value > 0.05. Contour and trace plots of the responses (WVP, TS, EB) were generated based using the Minitab software. Contour plots show the changes in response with respect to the components graphically and trace plots were used to show the effect of changes in each component from the reference blend on the response.

4.2.9 Optimization of the parameters

A multi-response method called desirability was used to optimize the levels of PLA, PBAT, TPS and NCC (Derringer & Suich, 1980). In this method, all the responses Y_i's were transformed into the individual desirability d_i's calculated using the equation below.

$$d_i = \frac{Y_i - Y_{min}}{Y_{max} - Y_{min}}$$

where Y_{min} and Y_{max} are the minimum and maximum range for response respectively.

d_i is set to zero if the response is outside the acceptable range and it is set to one if the response is equal to the target value. In case of WVP, the equation for d_i is redesigned to obtain the minimum value for WVP.

$$d_i = \frac{Y_{max} - Y_i}{Y_{max} - Y_{min}}$$

Overall desirability of the films (D) is the geometric average of the desirability of all the individual responses and was maximized using the Minitab software to obtain the optimum levels of the components. High D value shows that the all the responses Y_i's are close to the target responses. Optimization was also done with maximizing the level of TPS as one factor to reduce the cost of the nanocomposite films.

4.3 Results and discussion

4.3.1 Model development

The tensile strength (TS), elongation at break (EB), water vapor permeability (WVP) of the films obtained are shown in Table 4.3. The ranges of the response obtained were TS (8.05-50.72 MPa), EB (6.47-33.64%) and WVP (1.59-16.8 g*mm/kPa.h.m^2). Formulation 5 was removed from the model development as it was leading to very low predictability of EB and large residual. This formulation does not have any TPS and NCC which led to very high elongation at break. Some of the terms in the model were removed based on backward elimination of terms that are not significant i.e. p-value > 0.05. Table 4.4 shows the analysis of variance obtained for these responses. Analysis of variance showed that the linear terms and only PLA*PBAT in quadratic terms were significant for TS and EB i.e. p-value < 0.05. In case of WVP, all the linear terms and PLA*TPS, PLA*NCC, PBAT*TPS quadratic terms were significant for WVP.

Table 4.3 Mechanical and barrier properties of the films

Formulation	TS (MPa)	EB (%)	WVP (g*mm/kPa.h.m^2)
1	50.66 ± 1.8^{a}	6.59 ± 0.4^{a}	1.62 ± 0.02^{a}
2	8.24 ± 0.59^{b}	9.12 ± 0.65^{bc}	16.2 ± 0.36^{b}
3	50.72 ± 2.15^{a}	6.47 ± 0.28^{a}	1.59 ± 0.03^{a}
4	11.94 ± 0.58^{cd}	8.35 ± 0.61^{ab}	13.64 ± 0.3^{c}
5	40.21 ± 1.31^{e}	33.64 ± 2.03^{d}	1.72 ± 0.04^{a}
6	40.74 ± 0.82^{e}	12.92 ± 0.72^{ef}	1.68 ± 0.04^{a}
7	8.05 ± 0.55^{b}	13.88 ± 0.66^{f}	16.8 ± 0.3^{b}
8	10.96 ± 0.49^{d}	12.47 ± 0.67^{efg}	14.15 ± 0.43^{c}
9	39.28 ± 1.5^{e}	10.13 ± 0.9^{bch}	1.87 ± 0.08^{a}
10	40.25 ± 1.76^{e}	9.77 ± 0.82^{bch}	1.76 ± 0.05^{a}
11	16.27 ± 1.07^{fg}	9.37 ± 0.69^{bch}	7.25 ± 0.02^{d}
12	20.37 ± 0.85^{h}	9.17 ± 0.64^{bch}	6.9 ± 0.12^{d}
13	29.3 ± 1.42^{i}	13.28 ± 1.67^{ef}	1.91 ± 0.04^{a}
14	30.72 ± 1.21^{i}	12.71 ± 1.63^{ef}	1.93 ± 0.04^{a}
15	13.89 ± 0.54^{cg}	11.39 ± 1.26^{egh}	7.48 ± 0.04^{d}
16	18.5 ± 0.95^{fh}	11.03 ± 0.52^{cegh}	7.1 ± 0.13^{d}
17	26.44 ± 0.97^{j}	10.39 ± 0.7^{bcgh}	4.59 ± 0.23^{e}

Different superscripts within the same column indicate significant difference ($P<0.05$) between treatments.

Table 4.4 Analysis of variance for all the responses

	Source	DF	Seq SS	Adj SS	Adj MS	F-Value	P-Value
TS	Regression	4	3204.88	3204.88	801.22	252.58	< 0.001
	Linear	3	3121.25	3192.33	1064.11	335.46	< 0.001
	Quadratic	1	83.63	83.63	83.63	26.36	< 0.001
	$X_1 * X_2$	1	83.63	83.63	83.63	26.36	< 0.001
	Residual Error	11	34.89	34.89	3.17	-	-
	Total	15	3239.77	-	-	-	-
EB	Regression	4	71.157	71.157	17.7893	35.68	< 0.001
	Linear	3	67.035	18.902	6.3005	12.64	0.001
	Quadratic	1	4.123	4.123	4.1228	8.27	0.015
	$X_1 * X_2$	1	4.123	4.123	4.1228	8.27	0.015
	Residual Error	11	5.485	5.485	0.4986	-	-
	Total	15	76.642	-	-	-	-
WVP	Regression	6	466.621	466.621	77.7701	128.75	< 0.001
	Linear	3	402.610	157.033	52.3442	86.66	< 0.001
	Quadratic	3	64.011	64.011	21.3368	35.32	< 0.001
	$X_1 *X_3$	1	39.562	59.294	59.2939	98.16	< 0.001
	$X_1 * X_4$	1	6.879	5.849	5.8489	9.68	0.012
	$X_2 * X_3$	1	17.570	17.570	17.5701	29.09	< 0.001
	Residual Error	9	5.436	5.436	0.6041	-	-
	Total	15	472.057	-	-	-	-

4.3.2 Regression coefficients in quadratic models

The regression coefficients of all the terms of quadratic model for the responses were obtained using Minitab software. The fitted quadratic equations for all the responses are shown below.

$TS = 50.34\ X_1 + 81.3\ X_2 - 32.25\ X_3 + 125.59\ X_4 - 132.11\ X_1X_2$

$EB = 7.36\ X_1 + 20.27\ X_2 + 10.62\ X_3 - 13.21\ X_4 + 29.33\ X_1X_2$

$WVP = 1.88\ X_1 + 9.01\ X_2 + 70.12\ X_3 - 152.33\ X_4 - 83.05\ X_1X_3 + 160.59\ X_1X_4 - 85.92\ X_2X_3$

The summaries of the models developed for the three responses is shown in Table 4.5. Predicted R^2 gives the indication of how well a regression model can provide a valid prediction of the responses for new observations. Hence, high predicted R^2 is a good indication of the predictive ability of the developed model. The models developed for the responses TS, EB and EVP had a good predicted R^2 value (between 84.3% and 97.59%). Therefore, these models were sufficiently satisfactory to predict the responses for new observations.

Table 4.5 Summaries of the quadratic models developed for the three responses

Response	S*	R^2	R^2 (adjusted)	PRESS*	R^2 (predicted)
TS	1.78	98.92%	98.53%	78	97.59%
EB	0.71	92.84%	90.24%	12.03	84.3%
WVP	0.78	98.85%	98.08%	20.11	95.74%

*S represents the standard error of the regression and PRESS represents the predicted residual error sum of squares

4.3.3 Trace plot for all responses

Cox's direction (Cox, 1971) was used to generate the trace plot based on the quadratic models developed for TS, EB and WVP to investigate the effect of each component on the

a)

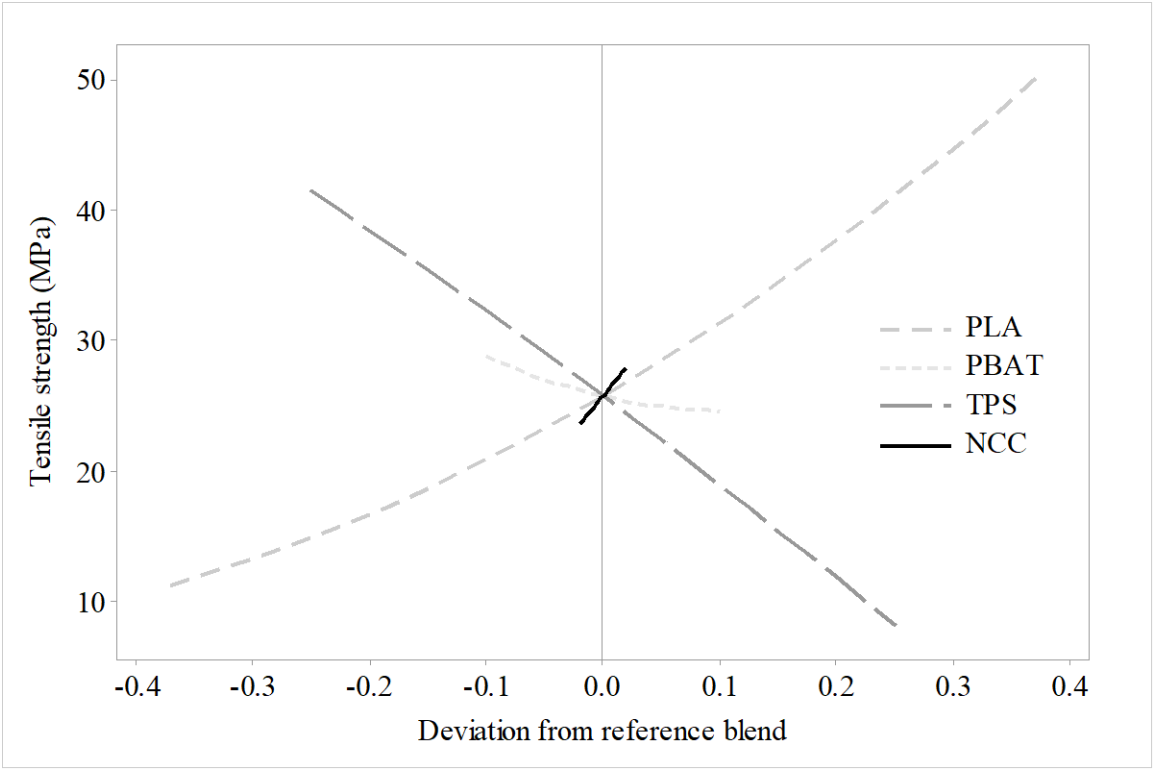
Tensile strength (MPa)
50
40
30
20
10
-0.4
-0.3
-0.2
-0.1
0.0
0.1
0.2
0.3
0.4
Deviation from reference blend
PLA
PBAT
TPS
NCC

b)

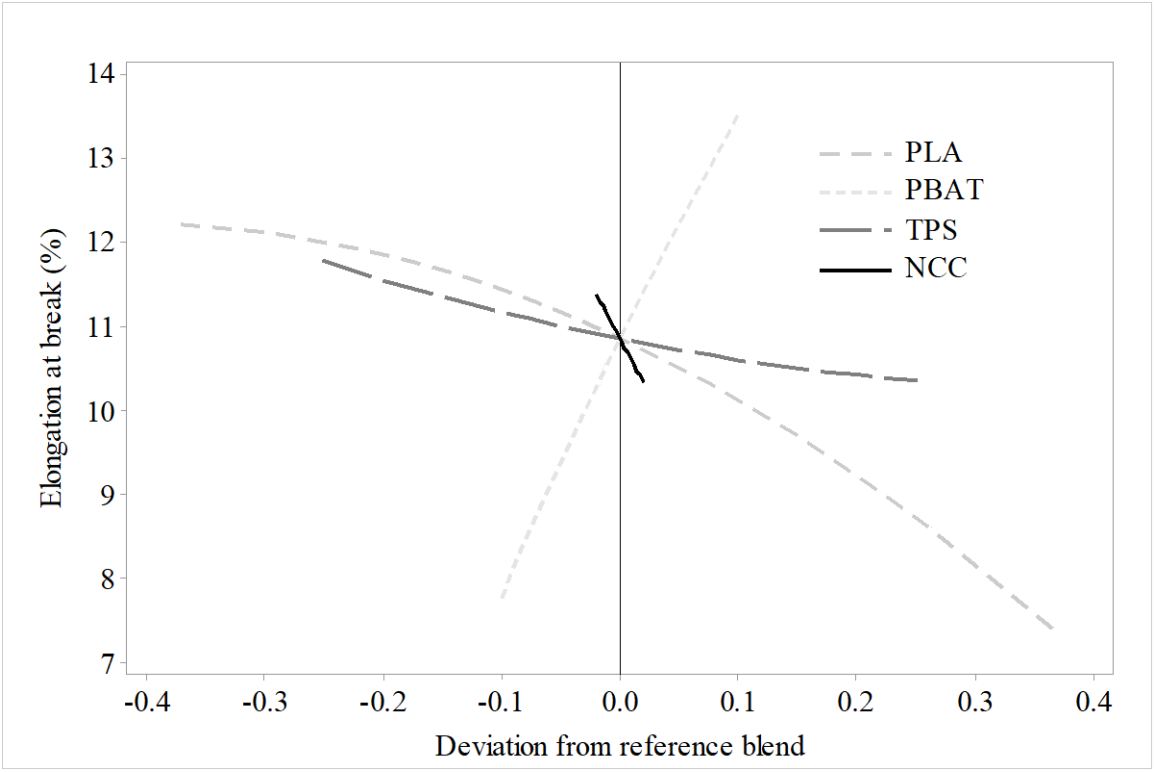
Elongation at break (%)
14
13
12
11
10
9
8
7
-0.4
-0.3
-0.2
-0.1
0.0
0.1
0.2
0.3
0.4
Deviation from reference blend
PLA
PBAT
TPS
NCC

c)

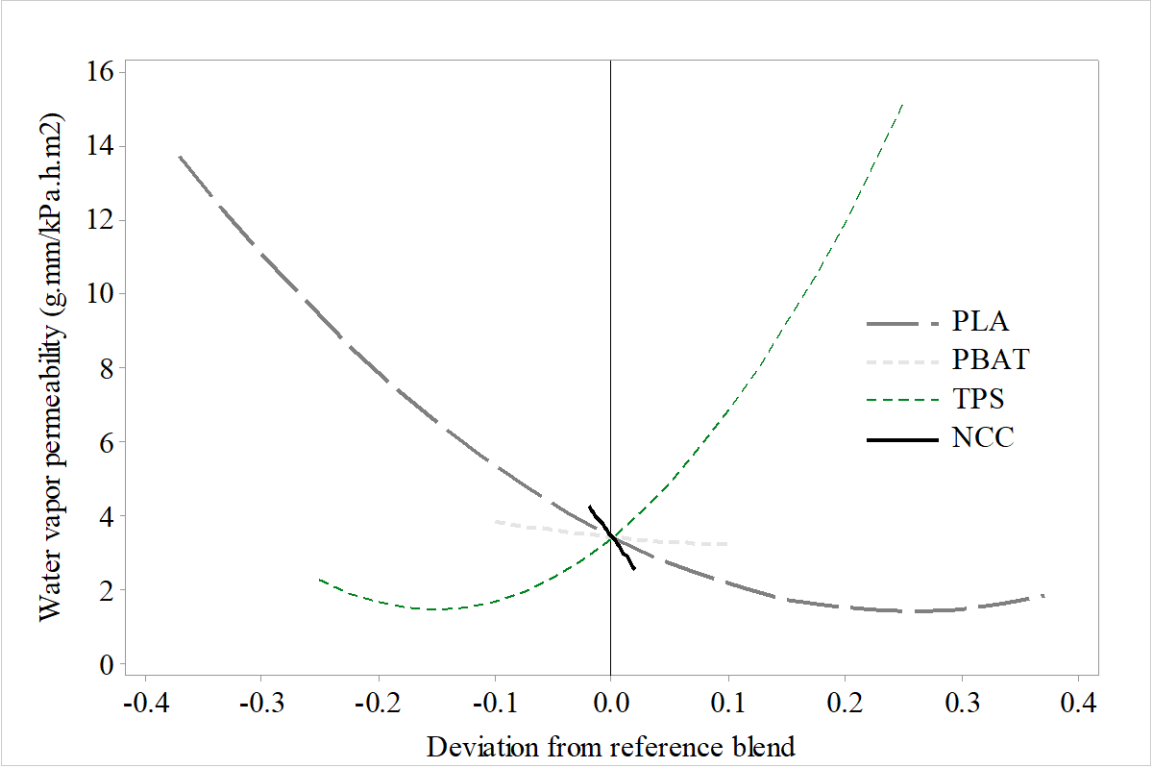

Figure 4.1 Trace plots showing the effect of each component on a) Tensile strength b) Elongation at break c) Water vapor permeability

responses. A trace plot shows the change in response with a change in proportion of each component while keeping all other mixture components in a constant ratio. As one mixture component increases, the proportion of other mixture components decreases while their ratio to one another remains the same. The trace plots for all the responses are shown in Figure 4.1(a-c) and the centroid of the experimental region is chosen as the reference blend. The composition of the reference blend is 62.5% PLA, 10% PBAT, 25% TPS, 2% NCC and 0.5% Joncryl.

The trace plot of TS (Figure 4.1a) showed that the TS of the nanocomposite films were affected by all the components of the mixture. Decrease in TS with addition of PBAT was expected due to lower strength of PBAT compared to PLA. Similarly, TPS addition decreased the TS more significantly compared to PBAT because of lower strength of TPS compared to the

polymers. Addition of NCC increased the TS as the complete dispersion of nanofiller in the polymer matrix facilitates the increase in available reinforcing elements for carrying an applied stress. The coupling between the polymer matrix and the large surface area of the nanofiller optimizes the load transfer to the reinforcement elements, thereby leading to increase in TS.

The trace plot of EB (Figure 4.1b) showed that the EB of the nanocomposite films were influenced by all the mixture components. Addition of NCC led to decrease in EB as the nanofiller reduces the mobility of the polymer chain i.e. confinement of polymer chains and contributes to the higher breaking tendency of the nanocomposite films. Several other studies also showed the decrease in EB with increase in nanofiller content (Ali et al., 2011; Khalil et al., 2017; Tang et al., 2008). Addition of TPS decreased the EB while the PBAT addition increased the EB of the films as expected.

Figure 4.1c shows the trace plot of WVP, which revealed that the addition of PBAT leads to slight increase in WVP because PLA is more hydrophobic in nature compared to PBAT (Shirai et al., 2013; Wang et al., 2016). Addition of TPS increased the WVP of the films. This was expected due to the hydrophilic nature of TPS whereas the polymers PLA and PBAT are hydrophobic. NCC addition decreased the WVP because the complete dispersion of nanofiller in the polymer matrix increases the tortuosity leading to slower diffusion of water vapor through the polymer matrix i.e. reduction of WVP (Azeredo et al., 2010).

4.3.4 Optimization of the films

A contour plot is a two-dimensional plot showing the effect of change in ratios of the components on the responses. As there are 4 components, the contour plot was plotted keeping one factor on hold. Figure 5.2 (a-c) shows the overlaid contour plot of all 3 responses i.e. TS, EB

and WVP generated at 0%, 2% and 4% NCC level. The white region in Figure 4.2 shows the optimum region for the three responses based on the constraints on TS, EB and WVP. As it can be seen, the optimum region keeps changing at various NCC levels. Hence, a multi-response method called desirability was used to optimize the levels of PLA, PBAT, TPS and NCC that yields the responses in the desirable range.

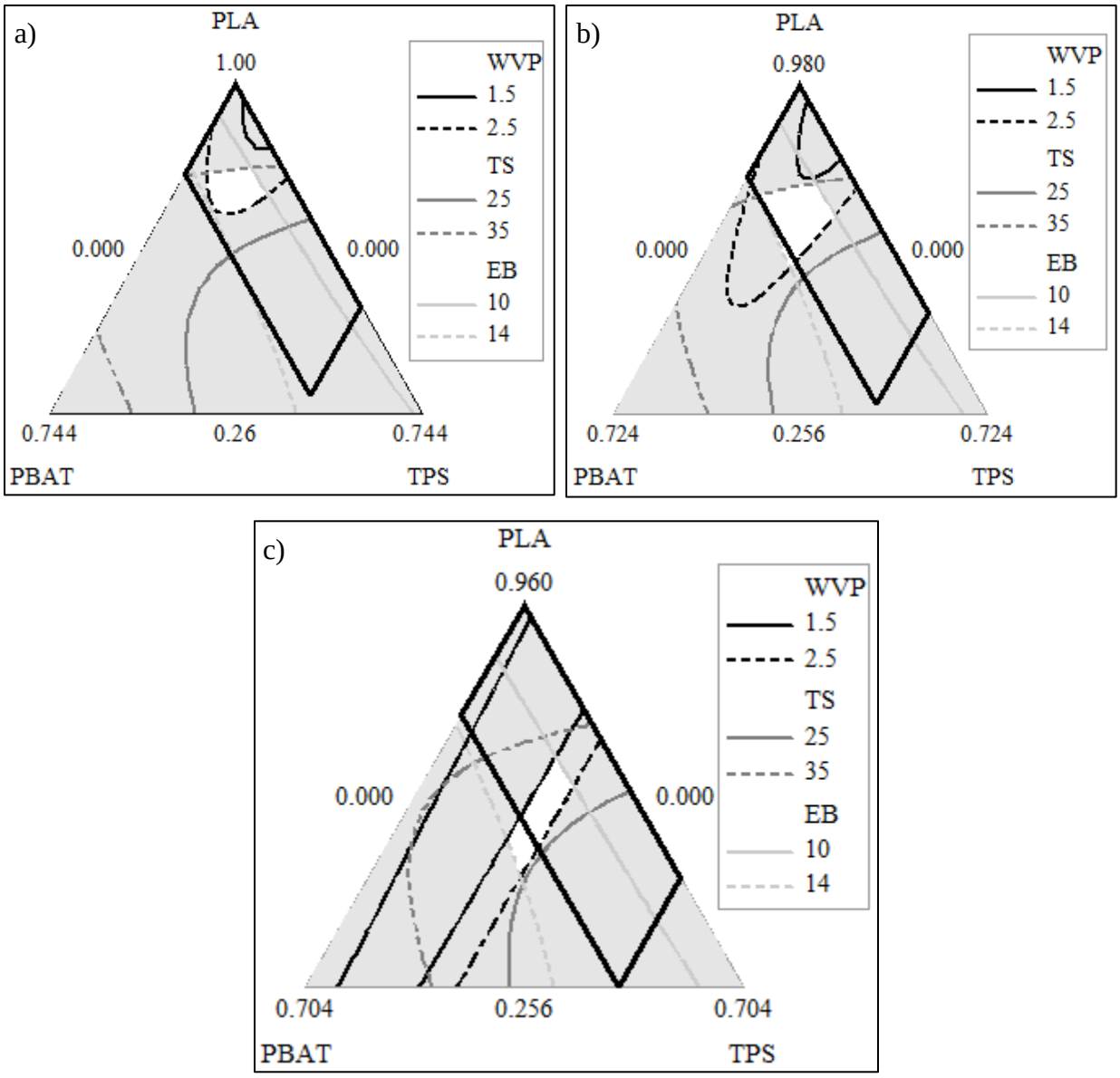

Figure 4.2 Overlaid contour plot showing the optimum region (white area) with desirable responses generated at a) 0% NCC b) 2% NCC c) 4% NCC

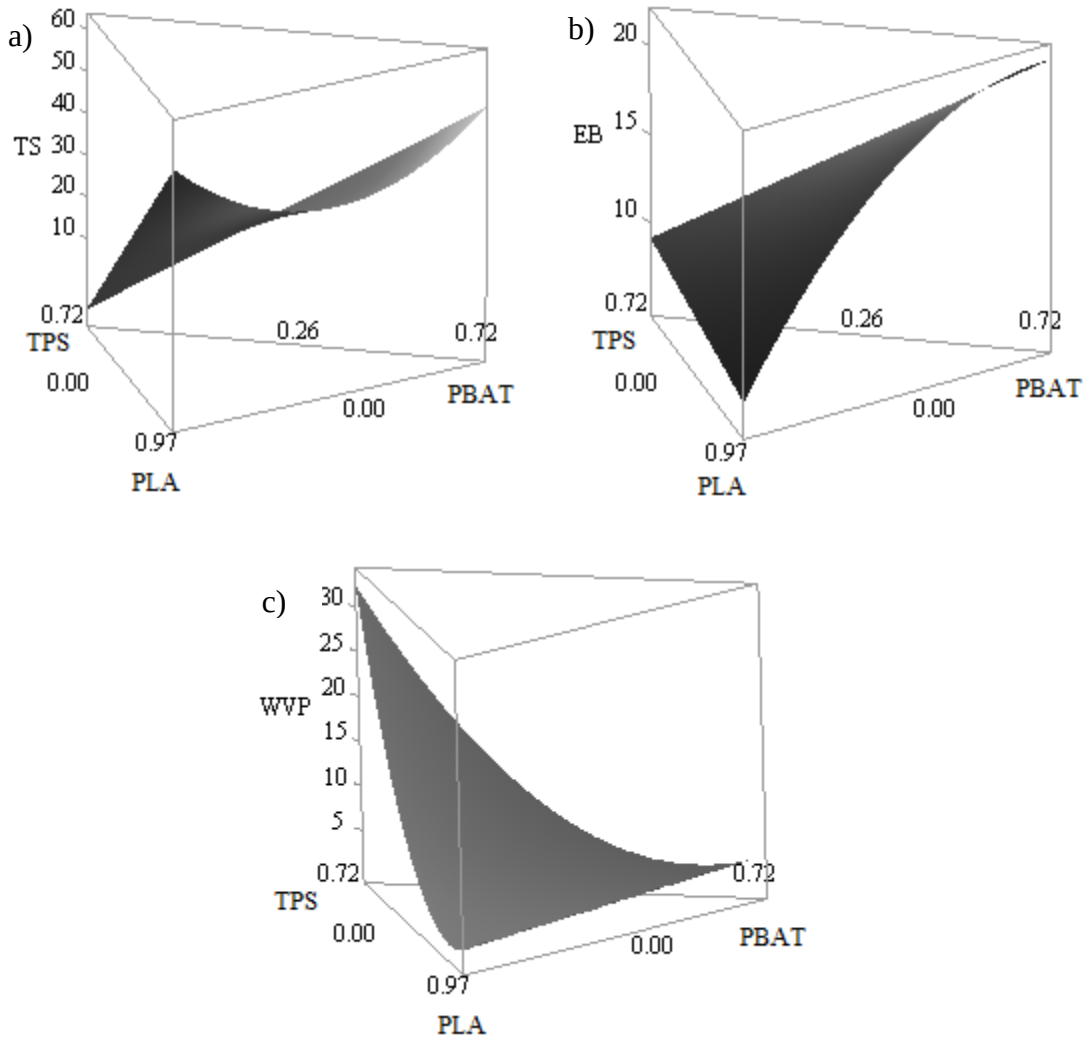

Figure 4.3 Surface plots for a) Tensile strength (MPa) b) Elongation at break (%) c) Water vapor permeability (g.mm/kPa.h.m^2) at 2.6% NCC level

Optimization of the films was done with all these factors in consideration – maximizing TS, EB, biodegradability and minimizing WVP, cost of the films. Maximizing the level of TPS in the mixture maximizes the biodegradability of the films and reduces the cost. The predicted optimum levels of 64.3% PLA, 14.5% PBAT, 18% TPS and 2.6% NCC along with 0.5% Joncryl would yield an optimum film with TS = 29.5 MPa, EB = 12%, WVP = 1.99 g.mm/kPa.h.m^2. A formulation of 72% PLA, 8% PBAT, 20% TPS and 2% NCC in the previous study (Chapter 3) yielded a film with TS = 30.98 MPa, EB = 10.13%, WVP = 2.11 g.mm/kPa.h.m^2 which was a bit

close to the optimum film properties. Hence, this formulation proved as a validation to the optimization study.

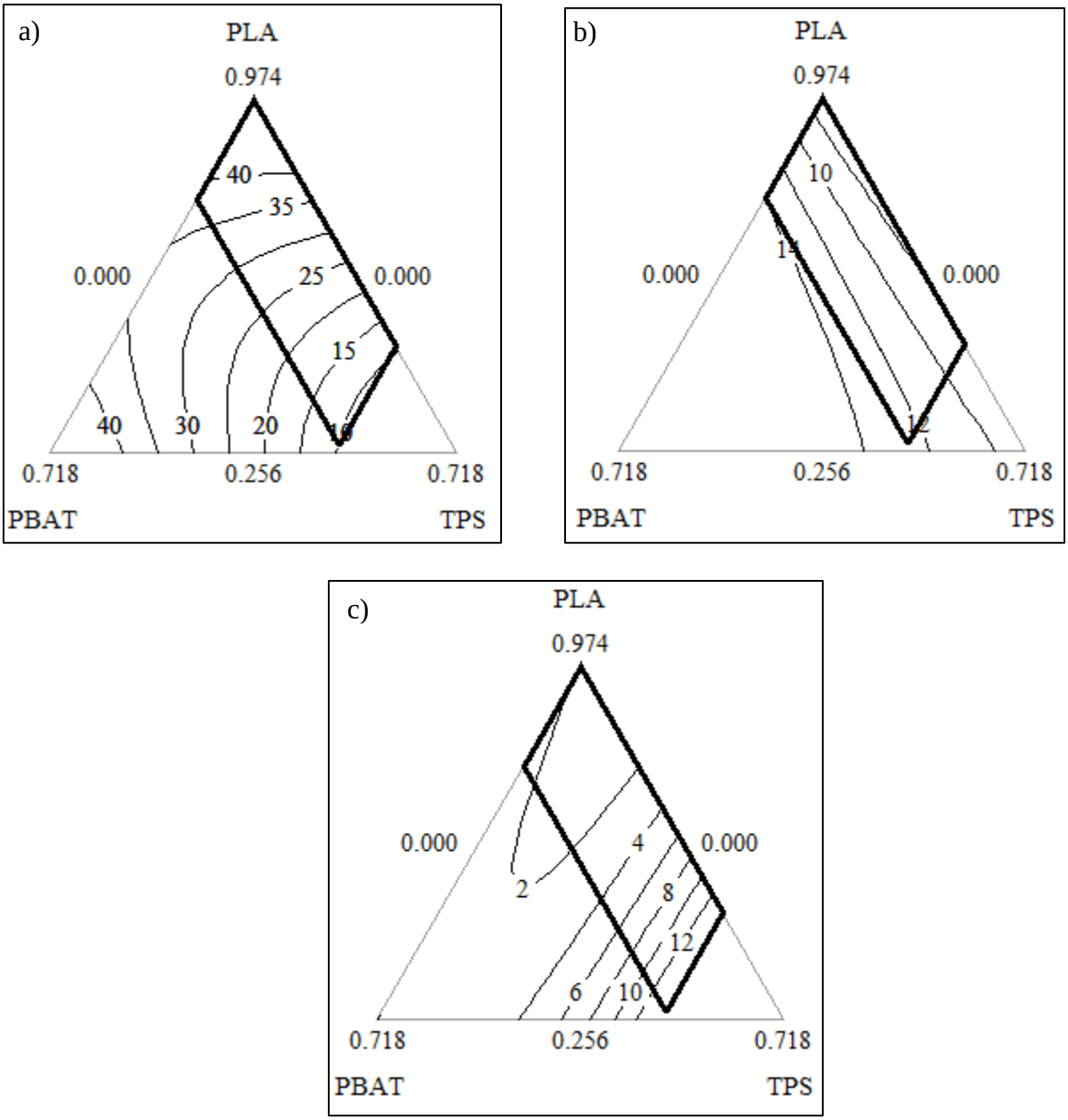

Figure 4.4 Contour plots for a) Tensile strength (MPa) b) Elongation at break (%) c) Water vapor permeability (g.mm/kPa.h.m^2) at 2.6% NCC level

The contour and surface plots of the responses TS, EB and WVP were generated (Figure 4.3, 4.4), by plotting each response to level of three mixture components PLA, PBAT, TPS while

the fourth mixture component NCC level was kept constant at 2.6% i.e. the optimum level obtained in the optimization study to understand the influence of effect of change in ratios of the components on the mechanical and barrier properties of the films.

4.3.5 Comparison with commercial plastics

Table 4.6 Comparison with commercial plastics

Material	Biodegradability in normal conditions	Cost[a]	WVP[b]	Tensile strength[c]	Elongation at break[d]	Reference
PET	None	Moderate	Good	Good	Good	Auras et al., 2005
PP	None	Moderate	Good	Moderate	Good	Ismail, 2002
PE	None	High	Moderate	Moderate	Good	Zhong et al., 2007
PS	None	High	Moderate	Moderate	Poor	Nair et al., 1996
PVC	None	Moderate	Good	Good	Good	Zheng et al., 2007
PA	None	High	Moderate	Good	Good	Yang et al., 1998
PVDC	None	Moderate	Good	Good	Moderate	Shiku et al., 2004
PLA	None	Moderate	Moderate	Good	Poor	Oksman et al., 2003
PLA/PBAT/TPS/NCC	**Moderate**	**Low**	**Moderate**	**Moderate**	**Moderate**	**Current study**

[a]Cost
Low: <5$/kg
Moderate: 5-10$/kg
High: >10$/kg

[b]Test conditions:23°C, 85% RH
Poor: 10-100 g*mm/m^2*day*kPa
Moderate: 1-10 g*mm/m^2*day*kPa
Good: 0.1-1 g*mm/m^2*day*kPa

[c]Tensile strength
Poor: <10 MPa
Moderate: 10-50 MPa
Good: >50 MPa

[d]Elongation at break
Poor: <10%
Moderate: 10-50%
Good: >50%

PET=Poly(ethylene terephthalate), PP=Polypropylene, PE= Polyethylene, PS=Polystyrene, PVC=Poly(vinyl chloride), PA=polyamide, PVDC=Poly(vinylidene chloride)

Table 4.6 shows the comparison of the films developed in the current study with those of the commercial plastics currently used in the industry. The mechanical and barrier properties of the films developed show that the barrier and mechanical properties are in the moderate range. The other advantages of the films developed in this study is the cost and the biodegradability in

normal soil conditions. The cost is less compared to the films used commercially due to addition of starch. Components such as TPS and NCC are completely biodegradable in normal soil conditions. Also, these films are completely biodegradable in composting conditions. Hence, the films developed have a good scope to be used in the food packaging industry.

4.4 Conclusions

Mixture response surface methods was used to investigate the effect of PLA, PBAT, TPS, NCC on the responses WVP, TS and EB. All factors including levels of PLA, PBAT, TPS, NCC influenced the mechanical and barrier properties of the films. Analysis of variance showed that the linear terms and only PLA*PBAT in quadratic terms were significant for TS and EB i.e. p-value < 0.05. In case of WVP, all the linear terms and PLA*TPS, PLA*NCC, PBAT*TPS quadratic terms were significant for WVP. Quadratic models with good predicted R^2 (between 84.3% and 97.59%) were developed for all the responses. TS decreased with addition of PBAT. TPS addition decreased the TS more significantly compared to PBAT due of lower strength of TPS compared to the polymers while the addition of NCC increased the TS. Addition of PBAT improved the EB of the films while NCC and TPS addition decreased the EB. Addition of PBAT lead to slight increase in WVP. TPS addition increased the WVP very significantly while the addition of NCC decreased the WVP of the films. Optimization study was done that could yield films with optimum properties comparable to commercial plastics and maximizing the level of TPS. Films with optimum properties (TS = 29.5 MPa, EB = 12%, WVP = 1.99 g.mm/kPa.h.m^2) were predicted at levels of 64.3% PLA, 14.5% PBAT, 18% TPS and 2.6% NCC along with 0.5% Joncryl.

4.5 References

Ali, S. S., Tang, X., Alavi, S., & Faubion, J. (2011). Structure and physical properties of starch/poly vinyl alcohol/sodium montmorillonite nanocomposite films. Journal of agricultural and food chemistry, 59(23), 12384-12395.

Auras, R. A., Singh, S. P., & Singh, J. J. (2005). Evaluation of oriented poly (lactide) polymers vs. existing PET and oriented PS for fresh food service containers. Packaging technology and science, 18(4), 207-216.

Ayana, B., Suin, S., & Khatua, B. B. (2014). Highly exfoliated eco-friendly thermoplastic starch (TPS)/poly (lactic acid)(PLA)/clay nanocomposites using unmodified nanoclay. Carbohydrate polymers, 110, 430-439.

Azeredo, H. M., Mattoso, L. H. C., Avena-Bustillos, R. J., Filho, G. C., Munford, M. L., Wood, D., & McHugh, T. H. (2010). Nanocellulose reinforced chitosan composite films as affected by nanofiller loading and plasticizer content. Journal of Food Science, 75(1), N1-N7.

Babaee, M., Jonoobi, M., Hamzeh, Y., & Ashori, A. (2015). Biodegradability and mechanical properties of reinforced starch nanocomposites using cellulose nanofibers. Carbohydrate polymers, 132, 1-8.

Brinchi, L., Cotana, F., Fortunati, E., & Kenny, J. M. (2013). Production of nanocrystalline cellulose from lignocellulosic biomass: Technology and applications. Carbohydrate Polymers, 94(1), 154–169.

Campos-Requena, V. H., Rivas, B. L., Pérez, M. A., Garrido-Miranda, K. A., & Pereira, E. D. (2015). Polymer/clay nanocomposite films as active packaging material: Modeling of antimicrobial release. European Polymer Journal, 71, 461-475.

Cox, D. R. (1971). A note on polynomial response functions for mixtures. Biometrika, 58(1), 155-159.

Derringer, G., & Suich, R. (1980). Simultaneous optimization of several response variables. Journal of quality technology, 12(4), 214-219.

Fortunati, E., Armentano, I., Zhou, Q., Iannoni, A., Saino, E., Visai, L., Berglund, L. A., & Kenny, J. M. (2012a). Multifunctional bionanocomposite films of poly(lactic acid),cellulose nanocrystals and silver nanoparticles. Carbohydrate Polymers, 87(2), 1596–1605.

Fortunati, E., Peltzer, M., Armentano, I., Torre, L., Jiménez, A., & Kenny, J. M. (2012b). Effects of modified cellulose nanocrystals on the barrier and migration properties of PLA nano-biocomposites. Carbohydrate Polymers, 90(2), 948–956.

Global bio plastics market to be driven by demand from packaging in North America, 2017. Retrieved from: http://www.plastemart.com/plastic-technical-articles/global-bio-plastics-market-to-be-driven-by-demand-from-packaging-in-north-america/2350.

Ho, K. L. G., Pometto, A. L., & Hinz, P. N. (1999). Effects of temperature and relative humidity on polylactic acid plastic degradation. Journal of environmental polymer degradation, 7(2), 83-92.

Iovino, R., Zullo, R., Rao, M. A., Cassar, L., & Gianfreda, L. (2008). Biodegradation of poly (lactic acid)/starch/coir biocomposites under controlled composting conditions. Polymer Degradation and Stability, 93(1), 147-157.

Ismail, H. (2002). Thermoplastic elastomers based on polypropylene/natural rubber and polypropylene/recycle rubber blends. Polymer Testing, 21(4), 389-395.

Kardar, P., Ebrahimi, M., Bastani, S., & Jalili, M. (2009). Using mixture experimental design to study the effect of multifunctional acrylate monomers on UV cured epoxy acrylate resins. Progress in Organic coatings, 64(1), 74-80.

Khalil, H. A., Tye, Y. Y., Ismail, Z., Leong, J. Y., Saurabh, C. K., Lai, T. K., Chong, E. W., Aditiawati, P., Tahir, P. M. & Dungani, R. (2017). Oil palm shell nanofiller in seaweed-based composite film: Mechanical, physical, and morphological properties. BioResources, 12(3), 5996-6010.

Kumar, M., Mohanty, S., Nayak, S. K., & Parvaiz, M. R. (2010). Effect of glycidyl methacrylate (GMA) on the thermal, mechanical and morphological property of biodegradable PLA/PBAT blend and its nanocomposites. Bioresource technology, 101(21), 8406-8415.

Lin, S. S., Lin, J. C., & Yang, Y. K. (2010). Optimization of mechanical characteristics of short glass fiber and polytetrafluoroethylene reinforced polycarbonate composites via D-optimal mixture design. Polymer-Plastics Technology and Engineering, 49(2), 195-203.

Matos Ruiz, M., Cavaille, J. Y., Dufresne, A., Gerard, J. F. & Graillat, C. (2000). Processing and characterization of new thermoset nanocomposites based on cellulose whiskers. Composite Interfaces, 7(2), 117-131.

Nair, K. C., Diwan, S. M., & Thomas, S. (1996). Tensile properties of short sisal fiber reinforced polystyrene composites. Journal of applied polymer science, 60(9), 1483-1497.

Nayak, S. K. (2010). Biodegradable PBAT/starch nanocomposites. Polymer-Plastics Technology and Engineering, 49(14), 1406-1418.

Ozdemir, M., & Floros, J. D. (2008). Optimization of edible whey protein films containing preservatives for water vapor permeability, water solubility and sensory characteristics. Journal of Food Engineering, 86(2), 215-224.

Rico, M., Rodríguez-Llamazares, S., Barral, L., Bouza, R., & Montero, B. (2016). Processing and characterization of polyols plasticized-starch reinforced with microcrystalline cellulose. Carbohydrate polymers, 149, 83-93.

Rostamiyan, Y., Mashhadzadeh, A. H., & SalmanKhani, A. (2014). Optimization of mechanical properties of epoxy-based hybrid nanocomposite: Effect of using nano silica and high-impact polystyrene by mixture design approach. Materials & Design (1980-2015), 56, 1068-1077.

Shiku, Y., Hamaguchi, P. Y., Benjakul, S., Visessanguan, W., & Tanaka, M. (2004). Effect of surimi quality on properties of edible films based on Alaska pollack. Food Chemistry, 86(4), 493-499.

Shirai, M. A., Olivato, J. B., Garcia, P. S., Müller, C. M. O., Grossmann, M. V. E., & Yamashita, F. (2013). Thermoplastic starch/polyester films: effects of extrusion process and poly (lactic acid) addition. Materials Science and Engineering: C, 33(7), 4112-4117.

Shogren, R. L., Doane, W. M., Garlotta, D., Lawton, J. W., & Willett, J. L. (2003). Biodegradation of starch/polylactic acid/poly (hydroxyester-ether) composite bars in soil. Polymer Degradation and Stability, 79(3), 405-411.

Tang, X., Alavi, S., & Herald, T. J. (2008). Barrier and mechanical properties of starch-clay nanocomposite films. Cereal Chemistry, 85(3), 433-439.

Teixeira, E. D. M., Pasquini, D., Curvelo, A. A., Corradini, E., Belgacem, M. N. & Dufresne, A. (2009). Cassava bagasse cellulose nanofibrils reinforced thermo-plastic cassava starch. Carbohydrate Polymers, 78(3), 422–431.

Wacharawichanant, S., Ratchawong, S., Hoysang, P., & Phankokkruad, M. (2017). Morphology and Properties of Poly (Lactic Acid) and Ethylene-Methyl Acrylate Copolymer Blends with Organoclay. In MATEC Web of Conferences (Vol. 130, p. 07006). EDP Sciences.

Wang, L., Ma, W., Gross, R. A., & McCarthy, S. P. (1998). Reactive compatibilization of biodegradable blends of poly (lactic acid) and poly (ε-caprolactone). Polymer Degradation and Stability, 59(1-3), 161-168.

Wang, L. F., Rhim, J. W., & Hong, S. I. (2016). Preparation of poly (lactide)/poly (butylene adipate-co-terephthalate) blend films using a solvent casting method and their food packaging application. LWT-Food Science and Technology, 68, 454-461.

Wang, H., Wei, D., Zheng, A., & Xiao, H. (2015). Soil burial biodegradation of antimicrobial biodegradable PBAT films. Polymer Degradation and Stability, 116, 14-22.

Wiedmann, W., & Strobel, E. (1991). Compounding of thermoplastic starch with twin-screw extruders. Starch - Stärke, 43(4), 138–145.

Yang, F., Ou, Y., & Yu, Z. (1998). Polyamide 6/silica nanocomposites prepared by in situ polymerization. Journal of Applied Polymer Science, 69(2), 355-361.

Yin, H., Chen, Z., Gu, Z., & Han, Y. (2009). Optimization of natural fermentative medium for selenium-enriched yeast by D-optimal mixture design. LWT-Food Science and Technology, 42(1), 327-331.

Zhao, P., Liu, W., Wu, Q., & Ren, J. (2010). Preparation, mechanical, and thermal properties of biodegradable polyesters/poly (lactic acid) blends. Journal of Nanomaterials, 2010, 4.

Zheng, Y. T., Cao, D. R., Wang, D. S., & Chen, J. J. (2007). Study on the interface modification of bagasse fibre and the mechanical properties of its composite with PVC. Composites part A: applied science and manufacturing, 38(1), 20-25.

Zhong, Y., Janes, D., Zheng, Y., Hetzer, M., & De Kee, D. (2007). Mechanical and oxygen barrier properties of organoclay-polyethylene nanocomposite films. Polymer Engineering & Science, 47(7), 1101-1107.

Chapter 5 - Mathematical modeling of mechanical and barrier properties of poly(lactic acid)/poly(butylene adipate-co-terephthalate)/thermoplastic starch based nanocomposites

Abstract

In this study, mathematical modeling was used to investigate the influence of nanofiller nanocrystalline cellulose (NCC) on the mechanical and barrier properties of the polymer matrix consisting of poly(lactic acid) (PLA), poly(butylene adipate-co-terephthalate) (PBAT) and thermoplastic starch (TPS). The modified Halpin-Tsai equation was used to model the elastic modulus of the nanocomposites, while the modified Nielsen equation was used to model the water vapor permeability (WVP) as a function of nanofiller content, geometry, strength and interactions with polymer matrix. The theoretical predictions for modulus from the modified Halpin-Tsai model were close to the experimental results. This model predicted that the increase in aspect ratio and modulus of nanofiller leads to the increase in modulus of the nanocomposites. The experimental results of WVP were close to the theoretical predictions of modified Nielsen's model. This model predicted that the increase in aspect ratio and surface interaction of fillers with the polymer matrix leads to decrease in WVP. The theoretical predictions and experimental values show an increase in modulus and decrease in WVP with increase in nanofiller content. Therefore, these models could be used to understand the influence of more effective fillers on the mechanical and barrier properties of the nanocomposites.

5.1 Introduction

The desirable properties and low cost of petroleum-based plastics is widely increasing their use in food and non-food packaging. However, these non-renewable petroleum-based plastic packaging contribute to environmental toxicity and waste disposal problems. Renewable and bio-based plastics can be used to replace non-renewable petroleum-based resources. Poly(lactic acid) (PLA), one of the widely growing material in the market (Global bioplastic markets, 2017) is renewable and bio-based with a range of desirable properties including biodegradability in composting conditions, high strength and high modulus (Wacharawichanant et al., 2017). However, PLA based films are brittle i.e. low % elongation at break. PLA can be blended with other flexible polymers such as poly(butylene adipate-co-terephthalate) (PBAT) and compatibilizer Joncryl ADR 4368C to improve the elongation (Kumar et al., 2010). However, the degradation of PLA and PBAT is slow in ambient soil conditions due to slow rate of hydrolysis of these polymers at low temperatures and moisture content (Ho et al., 1999; Shogren et al., 2003; Wang et al., 2015). Due to high cost of polymers PLA and PBAT, it can be blended with starch to make it cost-effective. Starch is a widely available and naturally occurring biodegradable polymer and hence can be considered as an economically viable alternative (Ayana et al., 2014). Native starch can be converted into thermoplastic starch (TPS) using thermo-mechanical treatment in the presence of plasticizers such as water, glycerol, sorbitol etc. (Wiedmann & Strobel, 1991). Addition of TPS also increases the rate of biodegradation of PLA in all conditions (Akrami et al., 2016; Iovino et al., 2008) as the various microorganisms can easily use starch as an energy source.

However, TPS based packaging have some limitations due to its high hydrophilic nature and weak mechanical properties (Babaee et al., 2015; Rico et al., 2016; Teixeira et al., 2009).

One of the promising methods to address this limitation is the use of nanofiller to improve the mechanical and barrier properties of bioplastics (Fortunati et al., 2012b). Nanocrystalline cellulose (NCC) has gained a lot of attention because of their durability and high biodegradability (Brinchi et al., 2013). NCC is composed of generally rod-shaped of about 5-10 nm in width and 100-200 nm in length (Fortunati et al., 2012a). They have a very high aspect ratio (length/diameter) and a large surface area (Matos Ruiz et al., 2000). They also have an exceptionally high tensile modulus (~130 GPa) relative to that of PLA (~50 MPa) and a great number of other fillers (Dufresne, 2013). These factors contribute to the reinforcement at low level of nanofiller. The complete dispersion of nanofiller in the polymer matrix hinders the diffusion pathway of the permeant (water vapor, gas etc.) through the nanocomposites thereby increasing the effective length of diffusion. This leads to increase in increasing the barrier properties of the nanocomposites, which indirectly contributes to higher shelf life of the food. The degree of reduction is greatly dependent on the geometrical characteristics of the nanofillers i.e. shape, aspect ratio (length to thickness ratio), orientation of nanofiller in polymer nanocomposites etc. Hence, there have been several attempts to estimate the barrier properties of the nanocomposites using mathematical models and compare them to the experimental results (Alavi et al., 2014; DeRocher et al., 2005; Picard et al., 2007; Swannack et al., 2005; Takahashi et al., 2006).

The most widely used model is the simple model developed by Nielsen (1967) that estimates the relative permeability of the polymer nanocomposites based on the tortuous path traversed by the permeant. The model assumed that the nanofillers are dispersed uniformly and completely exfoliated with preferred orientation of nanofiller ($\Theta = 0^o$). However, this model assumed that the orientation of nanofiller is perpendicular to the direction of diffusion ($\Theta = 0^o$).

Here Θ refers to the angle between the sheet normal unit vectors and the direction of preferred orientation of the nanofiller as shown in Figure 4.1. The ideal case of $\Theta = 0^o$ is not achieved in most of the cases. Hence, Bharadwaj (2001) modified it to include the orientation of nanofiller using the order parameter S defined below

$$S = \frac{3cos^2\theta - 1}{2}$$

a) b) c)

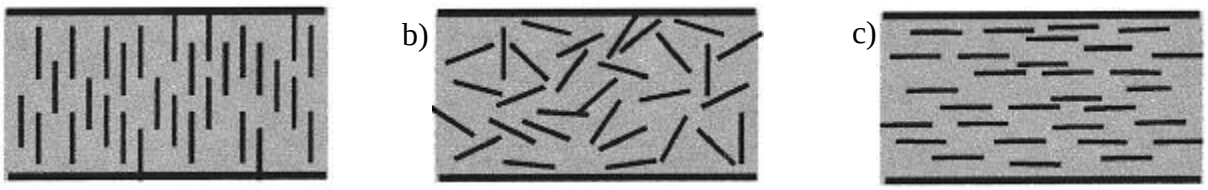

Figure 5.1 Various orientation of nanofiller a) S = -1/2 i.e. Θ = 90º (perpendicular orientation) b) S = 0 (random orientation) c) S = 1 i.e. Θ = 0º (perfect orientation)

Many similar simple models based on aspect ratio and volume fraction of nanofiller have been widely used to estimate the barrier properties of the nanocomposites (Alavi et al., 2014; Cussler et al., 1988; Fredrickson & Bicerano, 1999; Liu et al., 2008; Minelli et al., 2011; Moggridge et al., 2003; Sorrentino et al., 2006).

Modeling can also be used to predict the mechanical properties of the nanocomposite films. Ahmed & Jones, 1990 developed a model to estimate the tensile or elastic modulus of the nanocomposites. They developed a quadratic polynomial equation for spherical shaped nanofillers based on the volume fraction (V_f) and used another term aspect ratio (A) for non-spherical nanofiller. However, the model developed by Ahmed & Jones, 1990 was valid only for low volume fraction of nanofiller. The most widely used model for the mechanical properties of the nanocomposites is Halpin-Tsai model (Affdl & Kardos, 1976; Halpin, 1969; Peterson & Oksman, 2006; Rao, 2007; Ray et al., 2003).

In this work, PLA/PBAT/TPS/NCC nanocomposites were prepared using twin-screw melt extrusion. The purpose of this research is to understand the effect of NCC on the barrier and mechanical properties of the films using mathematical modeling.

5.2 Experimental

5.2.1 Model development for mechanical properties

Wu et al. (2004) modified the Halpin-Tsai model to consider the shape difference between the fiber-like filler and plate-like filler phase and introduced the term MRF (Modulus reduction factor).

$$\frac{E_n}{E_p} = \frac{1 + (MRF * \xi * n * V_f)}{1 - (n * V_f)}$$

$$\xi = 2A$$

$$n = \frac{\left(E_f / E_p\right) - 1}{\left(E_f / E_p\right) + (2 * \xi)}$$

where E_f, E_n and E_p are the tensile or elastic modulus of the filler, nanocomposites and pure polymer matrix respectively, ξ = Shape factor based on geometry of filler, A = Aspect ratio of filler, V_f = Volume fraction of filler and MRF = Modulus reduction factor.

MRF is a composite constant that reflects deviation of filler aspect ratio due to shape effects, dispersion of filler and surface interactions with polymer matrix. It is estimated by fitting the theoretical predictions with the experimental results. This model has been widely used to describe the mechanical properties of the nanocomposites (Alavi et al., 2014; Petersson & Oksman, 2006; Wu et al., 2004) and was used in this study.

5.2.2 Model development for barrier properties

Modified Nielsen's model has been widely used to describe the barrier properties of the nanocomposites (Alavi et al., 2014; Gusev & Lusti, 2001; Lu & Mai, 2007; Yano et al., 1997) and is used in this study to predict the WVP of the nanocomposites.

$$\frac{P_n}{P_p} = (1 + \left(\frac{A * V_f * (S + \frac{1}{2})}{3} \right))^{-1}$$

where P_n and P_p are the permeability coefficients of the nanocomposites and pure polymer matrix respectively, A = Aspect ratio of filler, V_f = Volume fraction of filler, S = order parameter (Figure 4.1).

5.2.3 Materials

High amylose corn starch Hylon V (~55% amylose content) was supplied by Ingredion. Poly(lactic acid), PLA4032D (Density: 1.25 g/cc, Average molecular weight: 100,000 g/mol), was purchased from Natureworks and Poly(butylene adipate-co-terephthalate), Ecoflex® F Blend C1200 (Density: 1.25 g/cc, Average molecular weight: 145,000 g/mol) and Joncryl ADR 4368C were obtained from BASF. Plasticizer sorbitol was purchased from Sigma-aldrich and nanocrystalline cellulose (NCC) was purchased from University of Maine.

5.2.4 Synthesis of thermoplastic starch (TPS)

Thermoplastic starch (TPS) was prepared by mixing dry starch (64%) with sorbitol (36%) using a corotating lab-scale twin screw extruder (Micro-18, American Leistritz, Somerville, NJ, USA). The extruder has a six head configuration, screw diameter of 18 mm and length-diameter ratio of 30:1. The barrel temperatures of the heads used for extrusion were 100-140-140-140-

140-140 ^{o}C. The extrudate was then ground using a Wiley mill (Model 4, Thomas-Wiley Co., Philadelphia, PA) for further use.

5.2.5 Melt blending

All the materials were dried at 80^{o} C for 8 hours in an air oven to remove moisture. The nanocomposites were melt blended using a laboratory-scale co-rotating twin screw extruder (Micro-18, American Leistritz, Somerville, NJ). The barrel temperatures of the heads used for extrusion were 100-180-180-180-180-180 ^{o}C. The extrudates were ground using a Wiley mill (Model 4, Thomas-Wiley Co., Philadelphia, PA) for further use. Sample designations and the relevant sample formulations are shown in Table 5.1. PLA to PBAT ratio of 9:1 was used based on the previous study (Chapter 2) which showed an increase in elongation of PLA with addition of 10% PBAT.

Table 5.1 Sample designations and relevant sample components

Formulation	(PLA-PBAT)* (%)	TPS (%)	Joncryl** (%)	NCC** (%)
80%(PLA-PBAT)/20%TPS	80	20	0.5	0
80%(PLA-PBAT)/20%TPS/1%NCC	80	20	0.5	1
80%(PLA-PBAT)/20%TPS/2%NCC	80	20	0.5	2
60%(PLA-PBAT)/40%TPS	60	40	0.5	0
60%(PLA-PBAT)/40%TPS/1%NCC	60	40	0.5	1
60%(PLA-PBAT)/40%TPS/2%NCC	60	40	0.5	2

*(PLA-PBAT) contains 9:1 ratio of PLA:PBAT
**The weight of Joncryl and NCC was based on polymer basis

5.2.6 Film preparation

Hot press (Model 3889, Carver Inc., Wabash, IN) with process parameter of force of 2100 lb and temperature of hot plates at 180ºC (top and bottom) was used to make the films of thickness of about 200 microns. The hot sample was preheated at 180°C for 5 min and then further pressed for 5 minutes using the hotpress.

5.2.7 Mechanical properties

Mechanical properties of the films were measured using Instron testing machine (Model 4465, Canton, MA, USA) based on standard ASTM D882 method. Films were cut into 1.3 cm wide and 10 cm long strips and conditioned at 23º C and 50% RH for two days before testing. The measurements were reported as the average of five samples.

5.2.8 Water vapor permeability

Water vapor permeability (WVP) was determined gravimetrically according to the standard method E96-00 (ASTM 2000). The films were fixed on top of test cells containing a desiccant (silica gel). Test cells were placed in a relative humidity chamber with controlled temperature and relative humidity (25º C and 85% RH). After steady-state conditions were reached, the weight of the test cells was measured every 24 hours over a five-day period. The slope of each line was calculated by linear regression (R^2>0.99), and the water vapor transmission rate (WVTR) was calculated from the slope of the straight line (W/t) divided by the transfer area (A):

$$\text{WVTR} = \frac{(\frac{W}{t})}{a} \text{ g/h.m}^2$$

where W = change in weight (g), t = time (h) and a = area of transfer (m^2)

WVP was then calculated from WVP using the equation given below

$$\text{WVP} = \frac{WVTR * t}{\Delta P} \text{ g*mm/kPa.h.m}^2$$

where t = film thickness (mm) and ΔP = pressure difference across the films (kPa).

The measurements were reported as the average of two samples.

5.2.9 Statistical analysis

Data was analyzed using SAS studio analysis software. Statistical significance of differences was calculated using Tukey's range test, $P < 0.05$.

5.3 Results and discussion

5.3.1 Mechanical properties

Table 5.2 Mechanical properties of PLA/PBAT/TPS nanocomposites

Formulation	Tensile Strength (MPa)	Modulus (MPa)	Elongation at break (%)
80%(PLA-PBAT)/20%TPS	25.46 ± 2.05[a]	525.82 ± 30.22[a]	10.09 ± 0.49[a]
80%(PLA-PBAT)/20%TPS/1%NCC	28.85 ± 1.69[ab]	672.12 ± 39.04[b]	10.15 ± 0.69[a]
80%(PLA-PBAT)/20%TPS/2%NCC	30.98 ± 1.32[b]	782.88 ± 42.81[c]	10.13 ± 1.5[a]
60%(PLA-PBAT)/40%TPS	15.88 ± 0.97[c]	336.1 ± 21.95[d]	10.19 ± 1.11[a]
60%(PLA-PBAT)/40%TPS/1%NCC	17.53 ± 0.74[cd]	433.04 ± 24.45[e]	10.52 ± 0.89[a]
60%(PLA-PBAT)/40%TPS/2%NCC	20.54 ± 0.95[d]	525.08 ± 13.86[a]	10.02 ± 1.45[a]

Different superscripts within the same column indicate significant difference ($P<0.05$) between treatments.

Table 5.2 shows the mechanical properties of the PLA/PBAT/TPS nanocomposites. TPS addition decreased the tensile strength of the films which was expected due to lower strength of TPS compared to the polymers. Addition of nanofiller NCC led to the increase in tensile strength

and modulus. Theoretically, the complete dispersion of nanofiller in the polymer matrix facilitates the increase in available reinforcing elements for carrying an applied stress. The coupling between the polymer matrix and the large surface area of the nanofiller optimizes the load transfer to the reinforcement elements, thereby leading to increase in tensile strength. Conversely, elongation at break did not exhibit any improvement. This was expected as nanofiller reduces the mobility of the polymer chains i.e. confinement of polymer chains and contributes to the breaking tendency of the nanocomposite films (Ali et al., 2011; Tang et al., 2008).

5.3.2 Modeling of mechanical properties

5.3.2.1 Comparison of experimental and predicted results

The following values were assumed for the model based on literature. Modulus of nanofiller NCC i.e. E_f was assumed as 130 GPa (Dufresne, 2013; Pirani & Hashaikeh, 2013) and aspect ratio was assumed as 40 (Beck-Candanedo et al., 2005; Reid et al., 2016; Sacui et al., 2014). Figure 5.2 shows the comparison of the theoretical predictions of Halpin-Tsai model and experimental values for Young's modulus in PLA/PBAT/TPS nanocomposites. As seen from the figure, the predicted modulus obtained from Halpin-Tsai equation are higher than that of experimental data. Hence MRF was introduced which considers the shape difference between the fiber-like filler and plate-like filler. It is a composite constant that reflects deviation of filler aspect ratio due to shape effects, dispersion of filler and surface interactions with polymer matrix (Wu et al., 2004). After introducing MRF = 0.5, the theoretical predictions from the model were close to the experimental results. Since the agreement between the theoretical predictions and experimental results is very reasonable, this model can be used to investigate the effect of various parameters on the mechanical properties of the nanocomposites.

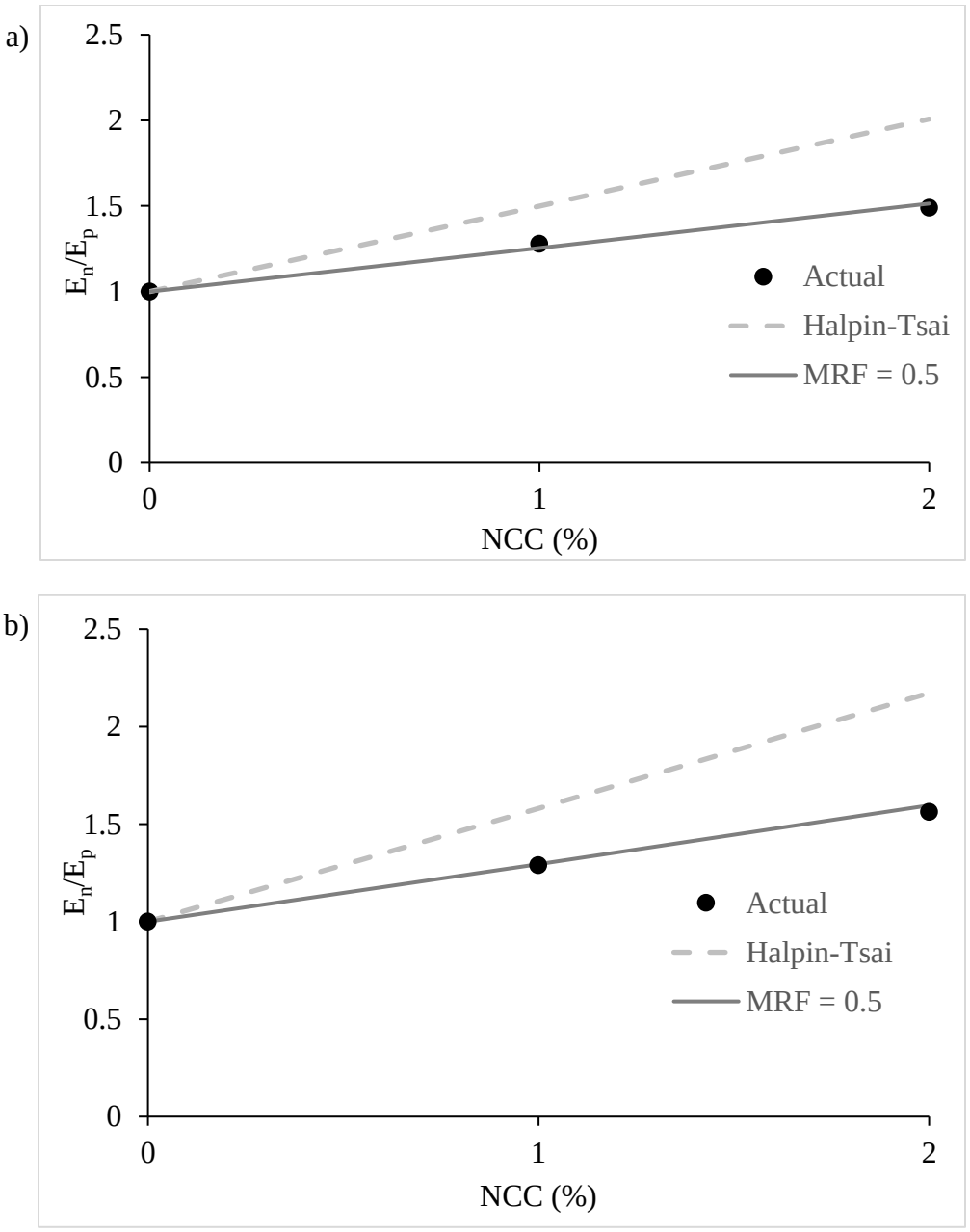

Figure 5.2 Comparison of theoretical predictions with experimental values for Young's modulus in a) PLA/8%PBAT/20%TPS b) PLA/6%PBAT/40%TPS

5.3.2.2 Effect of aspect ratio

The effect of aspect ratio (A) on the modulus of nanocomposites was studied by varying this ratio in the reference system with all the other parameters constant (Figure 5.3). The model predicted the increase in modulus of the nanocomposites with the increase in aspect ratio.

Increase in aspect ratio leads to the increase in surface-area-to-volume ratio. Higher surface-area-to volume ratio leads to further reinforcing mechanism of the nanofillers thereby leading to increase in Young's modulus (Al-Rub et al., 2012). NCC used in this study was derived from trees and wood pulp. NCC can also be produced from various other sources such as algae, tunicate, bacterial, sisal etc. (Araki et al., 2001, Kimura et al., 2005; Revol et al., 1982; Rodriguez et al., 2006) which can yield higher aspect ratio than the one used in the current study. This can lead to better reinforcement of the polymer matrix.

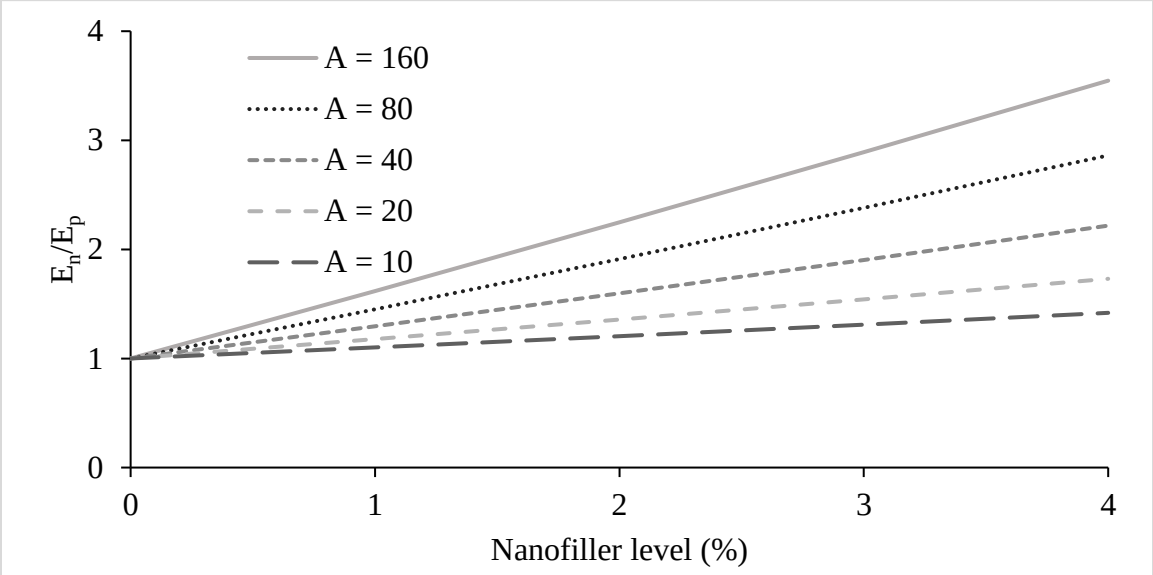

Figure 5.3 Young's modulus of 60%(PLA-PBAT)/40%TPS nanocomposites as a function of aspect ratio

5.3.2.3 Effect of modulus of nanofiller

Figure 5.4 shows the effect of nanofiller modulus (E_f) on the Young's modulus of 60%(PLA-PBAT)/40%TPS nanocomposites. Increase in modulus of nanofiller leads to the increase in modulus of nanocomposites as expected because the dispersion of nanofillers in the polymer matrix facilitates the increase in available reinforcing elements for carrying an applied stress. Hence, using high modulus nanofillers such as graphene (E_f = 1 TPa), carbon nanotubes

(E_f = 1 TPa), montmorillonite (E_f = 250 GPa) etc. can lead to greater increase in the modulus of the nanocomposites (Chen & Evans, 2006; Lee et al., 2008; Wong et al., 1997).

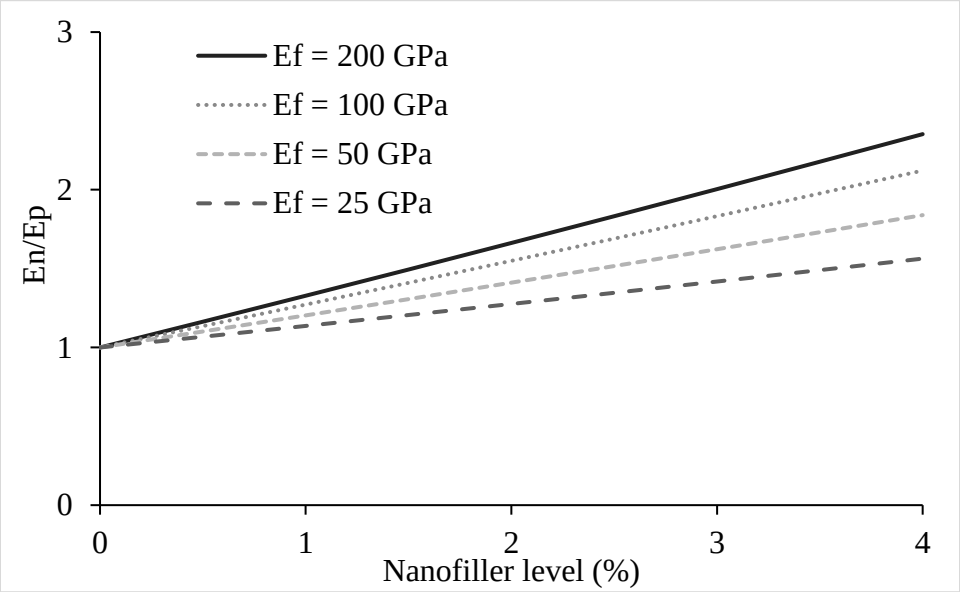

Figure 5.4 Young's modulus of 60%(PLA-PBAT)/40%TPS nanocomposites as a function of modulus of nanofiller

5.3.3 Barrier properties

Table 5.3 Barrier properties of PLA/PBAT/TPS nanocomposites

Formulation	WVP (g.mm/m^2.day.kPa)
80%(PLA-PBAT)/20%TPS	2.44 ± 0.1^a
80%(PLA-PBAT)/20%TPS/1%NCC	2.31 ± 0.04^a
80%(PLA-PBAT)/20%TPS/2%NCC	2.21 ± 0.06^a
60%(PLA-PBAT)/40%TPS	8.32 ± 0.05^b
60%(PLA-PBAT)/40%TPS/1%NCC	7.03 ± 0.03^c
60%(PLA-PBAT)/40%TPS/2%NCC	5.63 ± 0.13^d

Different superscripts within the same column indicate significant difference (P<0.05) between treatments.

Table 5.3 shows the barrier properties of the PLA/PBAT/TPS nanocomposites. TPS addition increased the WVP of the films. This was expected due to the hydrophilic nature of TPS whereas the polymers PLA and PBAT are hydrophobic. The complete dispersion of nanofiller in the polymer matrix increases the tortuosity leading to slower diffusion of water vapor through the polymer matrix i.e. reduction of WVP (Azeredo et al., 2010). Hence, addition of nanofiller NCC decreased the WVP of PLA/PBAT/TPS nanocomposites. Similar reduction of WVP with addition of NCC is observed in chitosan-based films (Khan et al., 2012), mango puree films (Azeredo et al., 2009) and poly(vinyl alcohol) based films (Paralikar et al., 2008).

5.3.4 Modeling of barrier properties

5.3.4.1 Comparison of experimental and predicted results

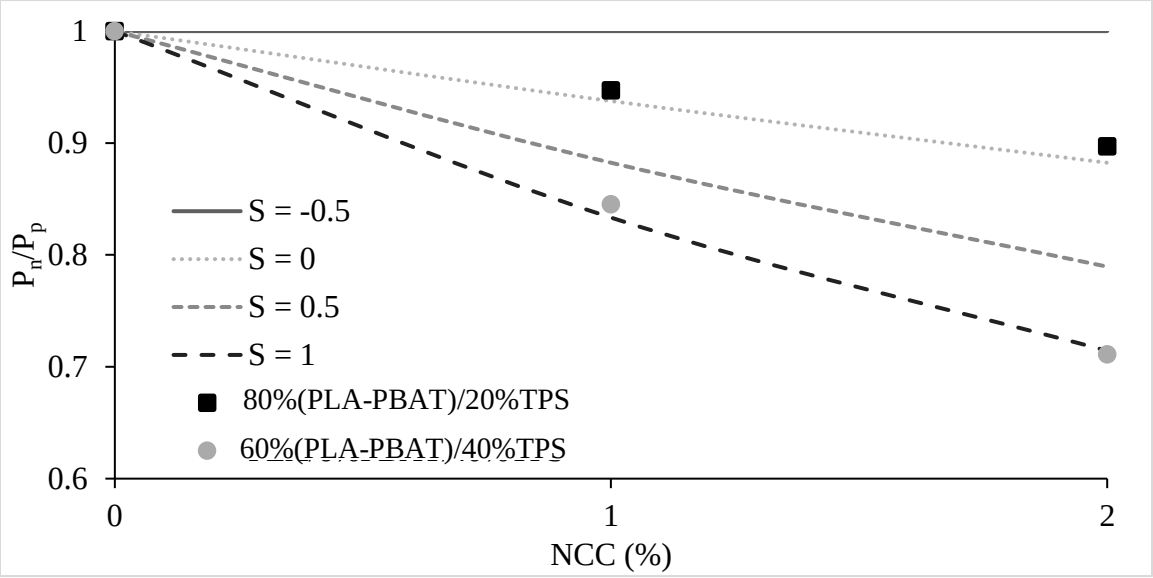

Figure 5.5 Comparison of theoretical predictions with experimental values for WVP in PLA/PBAT/TPS nanocomposites

The aspect ratio of NCC was assumed as 40 based on literature (Beck-Candanedo et al., 2005; Reid et al., 2016; Sacui et al., 2014). The comparison of theoretical predictions with experimental values for WVP in PLA/PBAT/TPS nanocomposites is shown in Figure 5.5.

According to this model, it is observed that WVP of 80%(PLA-PBAT)/20%TPS follows well with random orientation of nanofiller (S = 0) whereas the WVP of 60%(PLA-PBAT)/40%TPS works well with perfect orientation of nanofiller (S = 1). Greater orientation of the nanofiller at higher starch level indicates greater interaction between the nanofiller and starch which led to higher reduction of WVP. Processing techniques can also make a difference in the interactions between the nanofiller and polymer thereby affecting the barrier properties. Since the agreement between the theoretical predictions and experimental results is very reasonable, the model can be used to investigate the effect of various parameters on the barrier properties of the nanocomposites.

5.3.4.2 Effect of aspect ratio

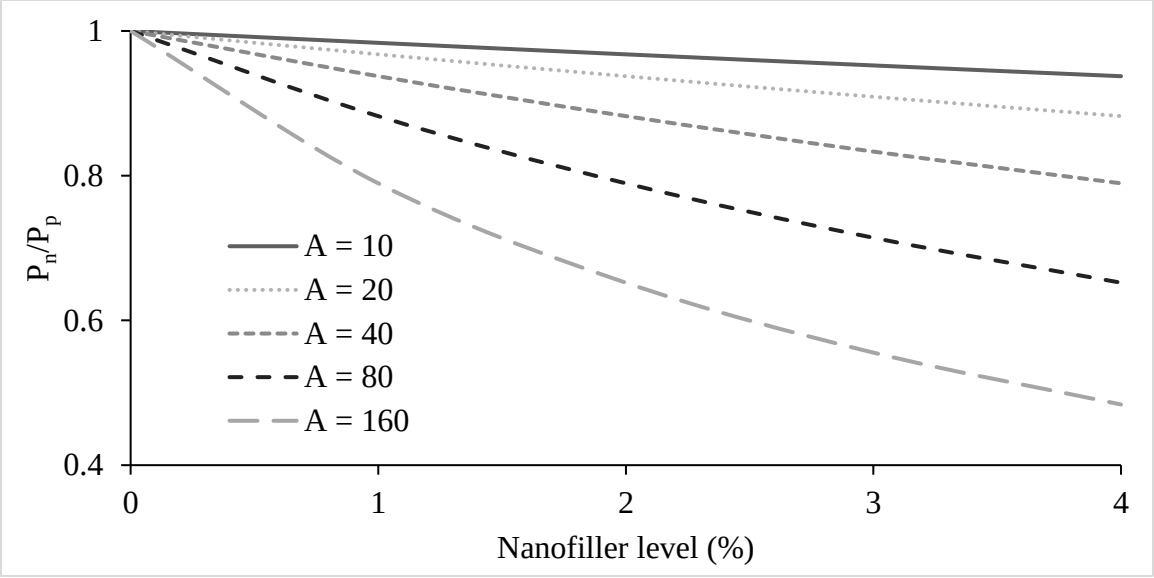

Figure 5.6 Relative permeability of PLA/PBAT/TPS nanocomposites as a function of aspect ratio

The effect of aspect ratio (A) on the WVP of nanocomposites was studied by varying this ratio in the reference system assuming random orientation of nanofiller (Figure 5.6). WVP of the nanocomposites decreased with the increase in aspect ratio. Increase in aspect ratio leads to the

increase in tortuosity, thereby leading to decrease in relative permeability. As mentioned earlier, NCC can also be produced from various other sources such as algae, tunicate, bacterial, sisal etc. which can yield higher aspect ratio than the one used in the current study. This can lead to greater tortuosity, thereby decreasing the WVP of the films.

5.4 Conclusions

In this study, the effect of nanocrystalline cellulose on the mechanical and barrier properties of PLA/PBAT/TPS films was evaluated using mathematical modeling. TPS addition decreased the mechanical properties of the films. Addition of NCC increased the mechanical properties of PLA/PBAT/TPS films. The modified Halpin-Tsai equation was used to model the elastic modulus of the nanocomposites, while the modified Nielsen equation was used to model the water vapor permeability (WVP) as a function of nanofiller content, geometry, strength and interactions with polymer matrix. The theoretical predictions for modulus from the modified Halpin-Tsai model were close to the experimental results. This model predicted that the increase in aspect ratio and modulus of nanofiller leads to the increase in modulus of the nanocomposites. TPS addition led to increase in WVP of the films while the addition of NCC decreased the WVP of PLA/PBAT/TPS nanocomposite films. The experimental results of WVP were close to the theoretical predictions of modified Nielsen's model. This model predicted that the increase in aspect ratio and surface interaction of fillers with the polymer matrix leads to decrease in WVP. The theoretical predictions and experimental values show an increase in modulus and decrease in WVP with increase in nanofiller content. Therefore, these models could be used to understand the influence of more effective fillers on the mechanical and barrier properties of the nanocomposites.

5.5 References

Affdl, J. C., & Kardos, J. L. (1976). The Halpin-Tsai equations: a review. Polymer Engineering & Science, 16(5), 344-352.

Ahmed, S., & Jones, F. R. (1990). A review of particulate reinforcement theories for polymer composites. Journal of Materials Science, 25(12), 4933-4942.

Alavi, S., Thomas, S., Sandeep, K. P., Kalarikkal, N., Varghese, J., & Yaragalla, S. (Eds.). (2014). Polymers for packaging applications. CRC Press.

Ali, S. S., Tang, X., Alavi, S., & Faubion, J. (2011). Structure and physical properties of starch/poly vinyl alcohol/sodium montmorillonite nanocomposite films. Journal of agricultural and food chemistry, 59(23), 12384-12395.

Al-Rub, R. K. A., Ashour, A. I., & Tyson, B. M. (2012). On the aspect ratio effect of multi-walled carbon nanotube reinforcements on the mechanical properties of cementitious nanocomposites. Construction and building materials, 35, 647-655.

Araki, J., Wada, M., & Kuga, S. (2001). Steric stabilization of a cellulose microcrystal suspension by poly (ethylene glycol) grafting. Langmuir, 17(1), 21-27.

Ayana, B., Suin, S., & Khatua, B. B. (2014). Highly exfoliated eco-friendly thermoplastic starch (TPS)/poly (lactic acid)(PLA)/clay nanocomposites using unmodified nanoclay. Carbohydrate polymers, 110, 430-439.

Azeredo, H. M., Mattoso, L. H. C., Wood, D., Williams, T. G., Avena-Bustillos, R. J., & McHugh, T. H. (2009). Nanocomposite edible films from mango puree reinforced with cellulose nanofibers. Journal of food science, 74(5), N31-N35.

Azeredo, H. M., Mattoso, L. H. C., Avena-Bustillos, R. J., Filho, G. C., Munford, M. L., Wood, D., & McHugh, T. H. (2010). Nanocellulose reinforced chitosan composite films as affected by nanofiller loading and plasticizer content. Journal of Food Science, 75(1), N1-N7.

Babaee, M., Jonoobi, M., Hamzeh, Y., & Ashori, A. (2015). Biodegradability and mechanical properties of reinforced starch nanocomposites using cellulose nanofibers. Carbohydrate polymers, 132, 1-8.

Beck-Candanedo, S., Roman, M., & Gray, D. G. (2005). Effect of reaction conditions on the properties and behavior of wood cellulose nanocrystal suspensions. Biomacromolecules, 6(2), 1048-1054.

Bharadwaj, R. K. (2001). Modeling the barrier properties of polymer-layered silicate nanocomposites. Macromolecules, 34(26), 9189-9192.

Brinchi, L., Cotana, F., Fortunati, E., & Kenny, J. M. (2013). Production of nanocrystalline cellulose from lignocellulosic biomass: Technology and applications. Carbohydrate Polymers, 94(1), 154–169.

Chen, B., & Evans, J. R. (2006). Elastic moduli of clay platelets. Scripta materialia, 54(9), 1581-1585.

Cussler, E. L., Hughes, S. E., Ward III, W. J., & Aris, R. (1988). Barrier membranes. Journal of Membrane Science, 38(2), 161-174.

DeRocher, J. P., Gettelfinger, B. T., Wang, J., Nuxoll, E. E., & Cussler, E. L. (2005). Barrier membranes with different sizes of aligned flakes. Journal of membrane science, 254(1-2), 21-30.

de Rodriguez, N. L. G., Thielemans, W., & Dufresne, A. (2006). Sisal cellulose whiskers reinforced polyvinyl acetate nanocomposites. Cellulose, 13(3), 261-270.

Dufresne, A. (2013). Nanocellulose: a new ageless bionanomaterial. Materials Today, 16(6),

220-227.

ElAmin, A. 2005. Common plastics packaging chemical linked to cancer. FoodProductionDaily e-newsletter (May 31, 2005). Retrieved from https://www.foodnavigator.com/Article/2005/05/31/Common-plastics-packaging-chemical-linked-to-cancer

Fortunati, E., Armentano, I., Zhou, Q., Iannoni, A., Saino, E., Visai, L., Berglund, L. A., & Kenny, J. M. (2012a). Multifunctional bionanocomposite films of poly(lactic acid),cellulose nanocrystals and silver nanoparticles. Carbohydrate Polymers, 87(2), 1596–1605.

Fortunati, E., Peltzer, M., Armentano, I., Torre, L., Jiménez, A., & Kenny, J. M. (2012b). Effects of modified cellulose nanocrystals on the barrier and migration properties of PLA nano-biocomposites. Carbohydrate Polymers, 90(2), 948–956.

Fredrickson, G. H. & Bicerano, J. (1999). Barrier properties of oriented disk composites. The Journal of chemical physics, 110(4), 2181-2188.

Global bio plastics market to be driven by demand from packaging in North America, 2017. Retrieved from: http://www.plastemart.com/plastic-technical-articles/global-bio-plastics-market-to-be-driven-by-demand-from-packaging-in-north-america/2350

Gusev, A. A., & Lusti, H. R. (2001). Rational design of nanocomposites for barrier applications. Advanced Materials, 13(21), 1641-1643.

Halpin, J. C. (1969). Stiffness and expansion estimates for oriented short fiber composites. Journal of Composite Materials, 3(4), 732-734.

Ho, K. L. G., Pometto, A. L., & Hinz, P. N. (1999). Effects of temperature and relative humidity on polylactic acid plastic degradation. Journal of environmental polymer degradation, 7(2), 83-92.

Iovino, R., Zullo, R., Rao, M. A., Cassar, L., & Gianfreda, L. (2008). Biodegradation of poly (lactic acid)/starch/coir biocomposites under controlled composting conditions. Polymer Degradation and Stability, 93(1), 147-157.

Khan, A., Khan, R. A., Salmieri, S., Le Tien, C., Riedl, B., Bouchard, J., Chauve, G., Tan, V., Kamal, M. R & Lacroix, M. (2012). Mechanical and barrier properties of nanocrystalline cellulose reinforced chitosan based nanocomposite films. Carbohydrate polymers, 90(4), 1601-1608.

Kimura, F., Kimura, T., Tamura, M., Hirai, A., Ikuno, M., & Horii, F. (2005). Magnetic alignment of the chiral nematic phase of a cellulose microfibril suspension. Langmuir, 21(5), 2034-2037.

Kumar, M., Mohanty, S., Nayak, S. K., & Parvaiz, M. R. (2010). Effect of glycidyl methacrylate (GMA) on the thermal, mechanical and morphological property of biodegradable PLA/PBAT blend and its nanocomposites. Bioresource technology, 101(21), 8406-8415.

Lee, C., Wei, X., Kysar, J. W., & Hone, J. (2008). Measurement of the elastic properties and intrinsic strength of monolayer graphene. science, 321(5887), 385-388.

Liu, W., Hoa, S. V. & Pugh, M. (2008). Water uptake of epoxy–clay nanocomposites: Model development. Composites Science and Technology, 68(1), 156-163.

Lu, C., & Mai, Y. W. (2007). Permeability modelling of polymer-layered silicate nanocomposites. Composites Science and Technology, 67(14), 2895-2902.

Matos Ruiz, M., Cavaille, J. Y., Dufresne, A., Gerard, J. F. & Graillat, C. (2000). Processing and characterization of new thermoset nanocomposites based on cellulose whiskers. Composite Interfaces, 7(2), 117-131.

Minelli, M., Baschetti, M. G., & Doghieri, F. (2011). A comprehensive model for mass transport properties in nanocomposites. Journal of membrane science, 381(1-2), 10-20.

Moggridge, G. D., Lape, N. K., Yang, C. & Cussler, E. L. (2003). Barrier films using flakes and reactive additives. Progress in organic coatings, 46(4), 231-240.

Nayak, S. K. (2010). Biodegradable PBAT/starch nanocomposites. Polymer-Plastics Technology and Engineering, 49(14), 1406-1418.

Nielsen, L. E. (1967). Models for the permeability of filled polymer systems. Journal of Macromolecular Science Chemistry, 1(5), 929-942.

Paralikar, S. A., Simonsen, J., & Lombardi, J. (2008). Poly (vinyl alcohol)/cellulose nanocrystal barrier membranes. Journal of Membrane Science, 320(1-2), 248-258.

Petersson, L., & Oksman, K. (2006). Biopolymer based nanocomposites: comparing layered silicates and microcrystalline cellulose as nanoreinforcement. Composites Science and Technology, 66(13), 2187-2196.

Picard, E., Vermogen, A., Gérard, J. F., & Espuche, E. (2007). Barrier properties of nylon 6-montmorillonite nanocomposite membranes prepared by melt blending: influence of the clay content and dispersion state: consequences on modelling. Journal of Membrane Science, 292(1-2), 133-144.

Pirani, S., & Hashaikeh, R. (2013). Nanocrystalline cellulose extraction process and utilization of the byproduct for biofuels production. Carbohydrate polymers, 93(1), 357-363.

Rao, Y. (2007). Gelatin–clay nanocomposites of improved properties. Polymer, 48(18), 5369-5375.

Ray, S. S., Yamada, K., Okamoto, M., Fujimoto, Y., Ogami, A., & Ueda, K. (2003). New polylactide/layered silicate nanocomposites. 5. Designing of materials with desired properties. Polymer, 44(21), 6633-6646.

Reid, M. S., Villalobos, M., & Cranston, E. D. (2016). Benchmarking cellulose nanocrystals: from the laboratory to industrial production. Langmuir, 33(7), 1583-1598.

Revol, J. F., Bradford, H., Giasson, J., Marchessault, R. H., & Gray, D. G. (1992). Helicoidal self-ordering of cellulose microfibrils in aqueous suspension. International journal of biological macromolecules, 14(3), 170-172.

Rico, M., Rodríguez-Llamazares, S., Barral, L., Bouza, R., & Montero, B. (2016). Processing and characterization of polyols plasticized-starch reinforced with microcrystalline cellulose. Carbohydrate polymers, 149, 83-93.

Sacui, I. A., Nieuwendaal, R. C., Burnett, D. J., Stranick, S. J., Jorfi, M., Weder, C., Foster, E. J., Olsson, R. T. & Gilman, J. W. (2014). Comparison of the properties of cellulose nanocrystals and cellulose nanofibrils isolated from bacteria, tunicate, and wood processed using acid, enzymatic, mechanical, and oxidative methods. ACS applied materials & interfaces, 6(9), 6127-6138.

Shogren, R. L., Doane, W. M., Garlotta, D., Lawton, J. W., & Willett, J. L. (2003). Biodegradation of starch/polylactic acid/poly (hydroxyester-ether) composite bars in soil. Polymer Degradation and Stability, 79(3), 405-411.

Sorrentino, A., Tortora, M. & Vittoria, V. (2006). Diffusion behavior in polymer–clay nanocomposites. Journal of Polymer Science Part B: Polymer Physics, 44(2), 265-274.

Swannack, C., Cox, C., Liakos, A., & Hirt, D. (2005). A three-dimensional simulation of barrier properties of nanocomposite films. Journal of membrane science, 263(1-2), 47-56.

Takahashi, S., Goldberg, H. A., Feeney, C. A., Karim, D. P., Farrell, M., O'leary, K., & Paul, D. R. (2006). Gas barrier properties of butyl rubber/vermiculite nanocomposite coatings. Polymer, 47(9), 3083-3093.

Tang, X., Alavi, S., & Herald, T. J. (2008). Barrier and mechanical properties of starch-clay nanocomposite films. Cereal Chemistry, 85(3), 433-439.

Teixeira, E. D. M., Pasquini, D., Curvelo, A. A., Corradini, E., Belgacem, M. N. & Dufresne, A. (2009). Cassava bagasse cellulose nanofibrils reinforced thermo-plastic cassava starch. Carbohydrate Polymers, 78(3), 422–431.

Wacharawichanant, S., Ratchawong, S., Hoysang, P., & Phankokkruad, M. (2017). Morphology and Properties of Poly (Lactic Acid) and Ethylene-Methyl Acrylate Copolymer Blends with Organoclay. In MATEC Web of Conferences (Vol. 130, p. 07006). EDP Sciences.

Wang, H., Wei, D., Zheng, A., & Xiao, H. (2015). Soil burial biodegradation of antimicrobial biodegradable PBAT films. Polymer Degradation and Stability, 116, 14-22.

Wiedmann, W., & Strobel, E. (1991). Compounding of thermoplastic starch with twin-screw extruders. Starch - Stärke, 43(4), 138–145.

Wong, E. W., Sheehan, P. E., & Lieber, C. M. (1997). Nanobeam mechanics: elasticity, strength, and toughness of nanorods and nanotubes. science, 277(5334), 1971-1975.

Wu, Y. P., Jia, Q. X., Yu, D. S., & Zhang, L. Q. (2004). Modeling Young's modulus of rubber–clay nanocomposites using composite theories. Polymer Testing, 23(8), 903-909.

Yano, K., Usuki, A., & Okada, A. (1997). Synthesis and properties of polyimide-clay hybrid films. Journal of Polymer Science Part A: Polymer Chemistry, 35(11), 2289-2294.

Chapter 6 - Conclusions and future work

6.1 Conclusions

TEM study showed the aggregation of NCC in the PLA/PBAT polymer matrix due to due to the difference in polarity based on the hydrophilic nature of the nanofiller and hydrophobic nature of the polymers. Hence, NCC did not have any positive impact on the mechanical and barrier properties of the PLA/PBAT nanocomposites. Dispersion of NCC in the polymer matrix improved with the addition of hydrophilic TPS. This resulted in increase in tensile strength (TS) and decrease in water vapor permeability (WVP) with addition of NCC. Significant increase in elongation at break (EB) of PLA from 6.3 to 30.5% with addition of PBAT and Joncryl with a trade-off TS reduction from 51.2 to 47.8 MPa. DSC study showed the increase in crystallization temperature and decrease in crystallinity with addition of Joncryl. However, crystallinity did not have any effect on the mechanical and barrier properties of PLA/PBAT/TPS nanocomposites.

The modified Halpin-Tsai equation was used to model the elastic modulus of the nanocomposites, while the modified Nielsen equation was used to model the WVP as a function of nanofiller content, geometry, strength and interactions with polymer matrix. The experimental results in both cases were close to the theoretical predictions by the models. These models predicted an increase in mechanical and barrier properties with increase in aspect ratio and surface interactions of nanofiller with polymer matrix. Using mixture response surface methods, quadratic models with good predicted R^2 (between 84.3% and 97.59%) were developed for TS, EB and WVP. Optimization study was done that could yield films with optimum properties comparable to commercial plastics and maximizing the level of TPS. Films with optimum

properties (TS = 29.5 MPa, EB = 12%, WVP = 1.99 g.mm/kPa.h.m^2) were predicted at levels of 64.3% PLA, 14.5% PBAT, 18% TPS and 2.6% NCC along with 0.5% Joncryl.

6.2 Future work

There are several researches that can be done to further improve the properties of these nanocomposite films. NCC used in this study was derived from trees and wood pulp. NCC produced from other sources such as algae, tunicate, bacterial, sisal etc. which can yield higher aspect ratio than the one used in the current study can be used as this can lead to better reinforcement of the polymer matrix and greater tortuosity, thereby decreasing the water vapor permeability of the films. Hydrophobic form of NCC i.e. Lignin-coated NCC can be used to study the dispersion mechanism of the hydrophobic nanofiller in the PLA/PBAT/TPS matrix.

Other nanofillers such as graphene can also be used to study as the modulus of graphene is very high compared to that of NCC thereby leading to further increase in mechanical properties. The dispersion and reinforcement mechanism of hydrophobic graphene can be compared with that of Lignin-coated NCC.

Processing techniques can also make a difference in polymer-polymer ad polymer-nanofiller interactions. Other techniques such as solvent blending, blending in a melt mixer can be used to process the nanocomposites and understand the influence of processing technique. Processing conditions i.e. extrusion process parameters can also be varied to produce a range of bio-nanocomposites. Melt pressing was currently used in this study to make the films. Other techniques such as solvent casting, film blowing can be done to understand the influence on mechanical and barrier properties of the nanocomposites.

Melt processability of the blends can be evaluated to study the effect of addition of TPS on the PLA/PBAT blends. The rheology data can be compared to that of conventional polymers like LDPE to study the processability of the films. Melt flow index measurements can also be done as it gives an indirect indication of melt strength that gives the ability to draw the film in various directions (machine direction, traverse direction) and bubble stability. It is required to obtain the optimum properties. Similarly, biodegradability testing can be done in all conditions to evaluate the change in rate of biodegradability of PLA/PBAT blends with addition of TPS, Joncryl and NCC.